The Dissertation Committee for Junjun Liu

certifies that this is the approved version of the following dissertation:

Formation of Ultra-thin Ta-based Cu Diffusion Barrier

with Atomic Layer Deposition

COMMITTEE:

Paul S. Ho, Supervisor

Jang-Hi Im

Jack C. Lee

Llewellyn K. Rabenberg

Ennis T. Ogawa

Formation of Ultra-thin Ta-based Cu Diffusion Barrier with Atomic Layer Deposition

by

Junjun Liu, B.S.; B.A.; M.S.E.

Dissertation

Presented to the Faculty of the Graduate School of

The University of Texas at Austin

in Partial Fulfillment

of the Requirements

for the Degree of

Doctor of Philosophy

The University of Texas at Austin

May 2006

To my wife and my family

For their love and support

Acknowledgements

It could have been just one of those journeys dreamed but never made.

With a happy ending finally in sight, I feel so lucky and enormously grateful, for the opportunities I enjoyed, for the fascinating hand of destiny, for those who have shaped me into who I am, and for those without whose help and support it would have never been possible for me to overcome the material hardships and even survive the tumultuous youthful days. To complete a formal education it has taken far more than intellectual aspirations and capacities.

In retrospection, however, my heart can not help being filled with a heavy sense of loss, for all the youthful dreams I had to give up to reach this place, and for those equally colorful dreams of my friends who were never given a second chance to make them true.

There are a lot of people I ought to give my due gratitude.

First, I would like to thank my loving parents, my caring sister, my lovely wife and niece for their unconditional love and support at all times.

No word of gratitude is sufficient for what I owe to two of my friends whose encouragement and moral support sustained me through the darkest moments.

I am permanently indebted to my supervisor Prof. Paul S. Ho. Prof. Ho takes me into microelectronic materials engineering, shows me his insightful understanding of reliability issues, and provides six years of support and guidance. His admirable example of leadership, excellence and professionalism will benefit me in areas far beyond scientific research.

I am grateful to Prof. Llewellyn Rabenberg for being a considerate reader of my master's report and serving in my committee.

I am grateful to Prof. Jang-Hi Im for being a member of my committee and for proving SiLK™ samples for this work.

I am grateful to Prof. Jack Lee for being a member of my committee and for his wonderful teaching.

I am grateful to Dr. Ennis Ogawa of Texas Instruments Inc. for serving as a committee member and for his valuable suggestions, comments and discussions as a mentor ever since he was a research associate with our group.

I would like to thank Dr. E. Todd Ryan of Advanced Micro Devices and Dr. Andrew J. McKerrow of Texas Instruments for providing low k samples used in this work.

I would also like to thank the talented and nice people in the Laboratory for Interconnect and Packaging at the Microelectronics Research Center for their assistance. Special thanks should go to Dr. Chuan Hu who introduced me into the group, Dr. Peter Abramowitz, who showed me into the world of ultra-high vacuum and XPS, Michael Scharnberg for helping set up the ALD system, Junjing Bao and Hualiang Shi for working the night shifts with me, Nan Lu and Jun Liu for help with CV measurements, Dr. Won-chun Kim for help with the wet chemistry used in this work, Junjing Bao and Won-chong Baek for taking the TEM micrographs, William Ostler and William James in MER facilities for helping put up together the system, and our secretary Jo Ann Smith for always being there to help.

Formation of Ultra-thin Ta-based Cu Diffusion Barrier with Atomic Layer Deposition

Publication No. _____

Junjun Liu, Ph.D.
The University of Texas at Austin, 2006
Supervisor: Paul S. Ho

With *in-situ* x-ray photoelectron spectroscopy (XPS) monitoring of atomic layer deposition (ALD) of Ta-based Cu barriers, this dissertation work is aimed at providing definite information regarding the initial interface formation during ALD barrier growth on low dielectric constant (low k) dielectric surfaces. The ALD nucleation and the substrate effects on ALD growth were investigated on two main types of low k dielectrics using two representative chemistries. *In-situ* surface chemical analysis confirmed the existence of a growth initiation stage controlled mainly by the substrate surface chemistry. $TaCl_5$ precursor can readily nucleate on SiLK™ through formation of charge transfer complexes on surface benzene groups, but has difficulties in nucleating on organosilicate (OSG) low k surfaces which are characterized by inactive surface methyl bonds. In contrast, a distinctively different nucleation and pore penetration behavior was observed with an organometallic precursor Pentakis-Dimethylamino Tantalum (PDMAT). This can be attributed to the low self-decomposition temperature and the higher sticking coefficient of PDMAT on the non-polar OSG surfaces.

Beams of reactive sub-molecular radicals were employed to activate the inactive OSG surfaces. Pure radical beams, amine radicals in particular, were found to be effective in the surface activation. Atomic hydrogen beam were demonstrated to provide an effective technique for surface cleaning, which is essential for chemisorption. Additionally, other applications with radical beams in enhancing ALD barrier processes were examined, such as formation of metallic Ta/dielectric Ta_3N_5 bi-layer stack, and reduction of chlorine and oxygen impurity contents.

As dielectric recovery and pore sealing may become a necessity for integration of ultra-low k porous OSG, the interactions between surface silylation and ALD barrier process were investigated. Tri-alkyl-substituted silylation agents were found to be detrimental to the initiation of the subsequent ALD barrier process. The surface activation with radical beams thus provides an effective, controllable and less destructive approach to improving ALD barrier formation following the surface silylation. On the other hand, as a preliminary attempt, alternative phenyl containing silylation agents were tested on porous OSG films damaged with O_2 plasma for dielectric recovery while retaining the surface reactivity for ALD initiation.

Table of Contents

List of Tables

List of Figures

Chapter 1 Introduction

Moore's law, a predicted doubling of transistor density on integrated circuits devices every 18 months to 24 months, has described well for several decades the technological evolution of the semiconductor industry. [1] The economic forces underlining such a man-made law have so far driven the industry to aggressive dimensional scaling both at the so-called front-end-of-line (FEOL), where transistors lie and back-end-of-line (BEOL), where interconnect metallization makes circuit connections from transistor level to the outside world. At this moment, main semiconductor manufacturers have finished or are finishing their development work on 65nm processing technology and almost ready for mass production. A new two-year cycle of research, development and production has been initiated for 45nm manufacturing processes. [2]-[7]

For the back-end-of-line (BEOL) manufacturing processes, research and development (R&D) work has been focused upon implementing a multi-level interconnect structure, featuring Cu wiring for resistance reduction and novel dielectric materials of low dielectric constant (low k) and ultra low k (ULK) as the insulating material for capacitance reduction. [8]-[14] Both approaches are considered essential to reduce the resistance-capacitance (RC) delay, voltage drop and cross talk in the interconnects. [15]-[18] In this performance and reliability-oriented R&D world, Cu/low k interface has attracted a lot of attention for its critical roles in affecting the electrical performance and the structural integrity of Cu/low k interconnects. [19]-[26]

Cu barriers, as the intermediary layer between Cu and low k, are formed right after dielectric patterning and next to low k dielectric surface. They are meant to prevent

Cu diffusion into the dielectrics and promote interfacial adhesion. How to form the diffusion barriers to provide the desired film properties with precise thickness control down to atomic scale as required by the aggressive dimensional scaling [3] has been the focus of the engineering of the Cu/low k interface.

1.1 Ta-based copper diffusion barriers in Cu/low k interconnects

Each time when the semiconductor industry is challenged to make revolutionary technological transitions in the manufacturing processes, it inevitably involves new materials selection, engineering and integration. The transition from the conventional subtractive Al/SiO_2 interconnect structure to Cu/low k damascene interconnect structure has been no exception. [14], [27]-[32] Since Cu readily diffuses into silicates and silicon substrate, Cu has to be completely encapsulated by diffusion barriers to avoid direct contact with the surrounding low k dielectric.

In a typical dual hard mask dual damascene process flow as shown in Fig. 1-1, a diffusion barrier is deposited prior to Cu metallization and after patterning the embedding low k dielectric. An encapsulating layer is then deposited over chemical-mechanically polished (CMPed) Cu-filled dual damascene trenches to seal the low k dielectric from the lower level Cu. The first diffusion barrier, which can be either conductive or dielectric depending upon whether there is an etchback process or not later on, is usually referred to as diffusion barrier. Typically, this first barrier is metallic and throughout the industry Ta-based barriers have been favored. The second encapsulating barrier, which has to be dielectric, is usually termed as either barrier dielectric or cap layer. The focus of this thesis will be the materials engineering and deposition of the diffusion barrier.

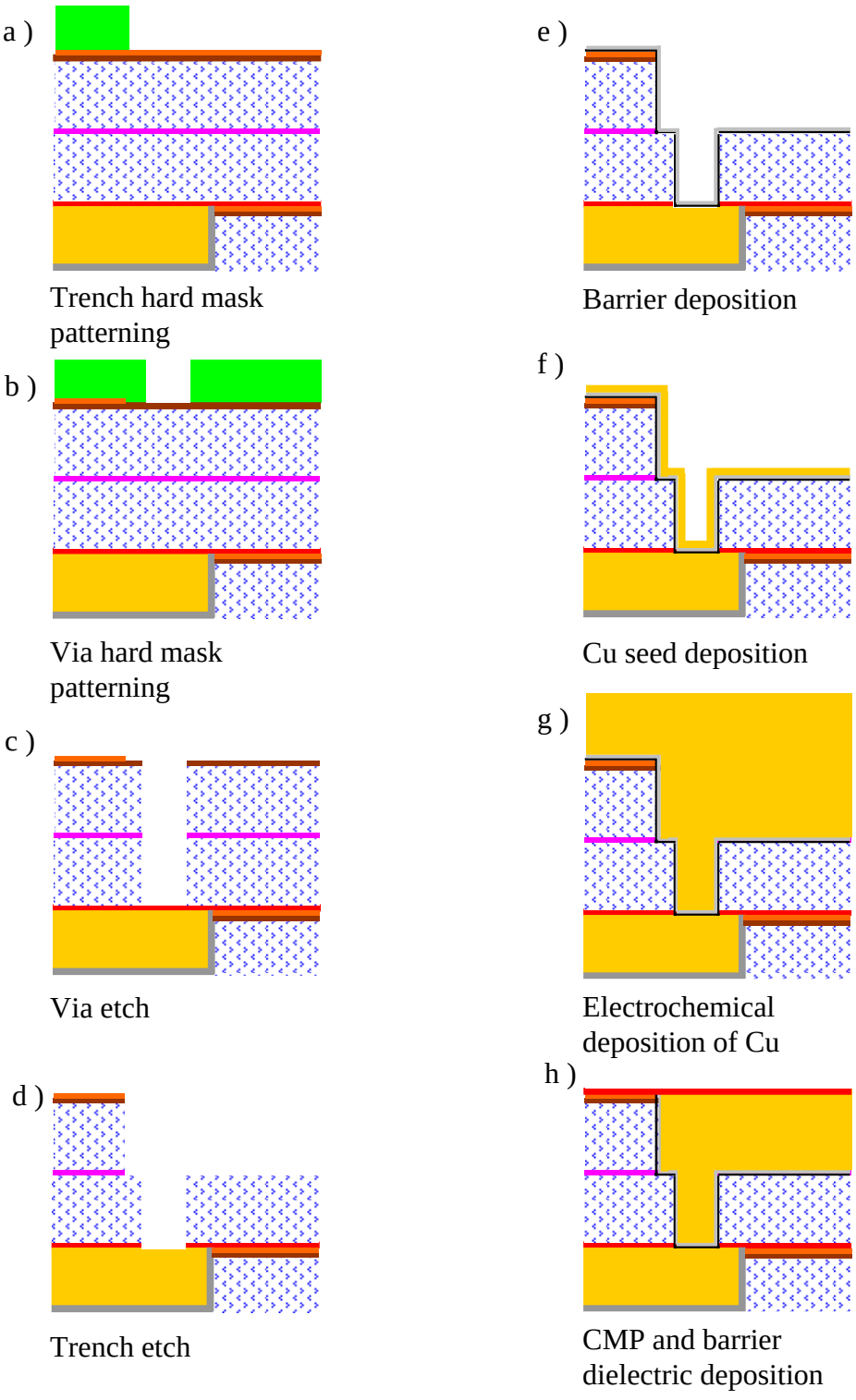

Fig. 1-1 A dual mask dual damascene Cu/low k process flow.

Tantalum and its nitride have been used as diffusion barriers ever since the introduction of Cu wiring. [33]-[39] The selection of Ta and TaN out of a long list of refractory metals, their nitrides, carbides, oxides and silicon nitrides, is based upon considerations over critical materials properties and process compatibility issues, such as its barrier property against Cu diffusion, adhesion to both Cu and low k dielectric, step coverage, contact resistance, conductivity, chemical-mechanical polish (CMP) compatibility, Cu poisoning and so on. [40] Among these concerns, the interface quality, the barrier property against Cu diffusion and the capability for step coverage are indispensable in achieving the dimensional scaling targets with satisfactory reliability. In this regard, Ta/TaN bi-layer stack distinguishes itself among other barrier candidates for the excellent adhesion of TaN to low k and the stable and strong interface between Ta and Cu. [41] On top of that, Ta deposited on TaN base assumes the most conductive body centered cubic (bcc) α Ta phase (~15-30 $\mu\Omega\cdot$cm), which is beneficial to the overall line resistivity. [42]-[45]

In terms of the overall line resistivity or conductivity, a possible better solution is a Ruthenium/TaN stack which has been extensively explored and researched recently.[46]-[49] It has shown potential to eliminate the need for an additional Cu seed layer as the electrode for the subsequent Cu plating. This will possibly enable Cu direct plating and provide more trench volume for Cu inlaid which is critical to achieve an effective Cu resistivity target suitable for further scaling of interconnect dimensions. However, there are seemingly contradictory reports about Ru resistance against Cu diffusion and Ru/Cu interface strength. [50]-[56] As the time-to-market becomes the show stopper for many promising backup technologies in the semiconductor industry, unless

many Ru-related integration issues can be settled soon, a Ta/TaN barrier stack may be extended to future technology nodes.

With the materials selection and materials engineering issues more or less being settled, efforts have been concentrated on exploring deposition techniques of barriers to achieve adequate step coverage at minimal film thickness. Due to the anisotropic nature of the current physical vapor deposition (PVD) techniques and possible shadowing effect of the barrier deposition deep inside a trench or via, non-uniformity in barrier thickness usually results. Shrinking line pitch, increasing aspect ratio, and integration process flows such as a via-first process aggravate the step coverage issue. This becomes more problematic as thinner and thinner barrier thickness is allowed to achieve effective Cu resistivity targets in the future technology generations. A thin PVD barrier was found to be insufficient to provide the desired barrier resistance against Cu diffusion. To mitigate the issue, innovations, such as ionized physical vapor deposition (I-PVD), [57]-[59] barrier first, [60] resputtering [61] and preclean with metal neutral deposition [62],[63] processes, have been adopted to further extend the current sputtering deposition technique to 65nm technology node. Whether these evolutionary process innovations can meet the more stringent requirements posed in 45nm and 32nm technology nodes is not very clear despite some recent optimistic reports. [64]

Looking beyond the PVD processes for conformal deposition, we see that chemical vapor deposition (CVD) techniques are always very conformal to the underlying features. And there are known CVD chemistries for deposition of Ta and TaN using halide precursors or organometallic (MO) precursors. But the low film density of CVD films, high thermal budget and the lack of precise film thickness control have raised

doubts about its extendability to advanced technology nodes. It is with this perspective that atomic layer deposition of Cu barriers has attracted great attention.

1.2 Atomic layer deposition (ALD)

The first known article on atomic layer CVD (ALCVD) appeared in 1965 when a Russian group published a study on forming TiO_2 and GeO_2 in a monolayer by monolayer fashion with a sequential exposure to $TiCl_4/GeCl_4$ and H_2O. [65] The ALCVD concept later evolved to atomic layer epitaxy (ALE) in 70's and found applications in making electroluminescent thin films for flat panel displays. [66]-[68] Its application in depositing microelectronic thin films was then limited, mainly due to its slow growth rate. In late 90's, the need of a deposition technique capable of depositing ultra-thin high quality film on high aspect ratio structures with stringent thickness control helped revive interest in ALD for microelectronics applications. [69]-[73]

In a nutshell, ALD is a variation of CVD with cyclic sequential exposure of a substrate to precursor vapor and reactive gas. An illustration of the process steps in one typical ALD cycle is presented in Fig. 1-2. In the purge steps, any excess of precursor molecules or volatile byproducts except those chemisorbed are removed from the surface, resulting in a reaction kinetics completely controlled by surface reactions. Theoretically, each ALD cycle will produce one uniform and conformal monolayer of the film to be deposited. Repeating the process cycle is believed to enable monolayer by monolayer film growth, providing very fine thickness control. [74]

ALD processes are self-limiting. Given a substrate surface chemistry, at a certain temperature only a fixed number of incoming molecules can be chemisorbed and remain on the underlying surface regardless of the exposure time. This self-limiting

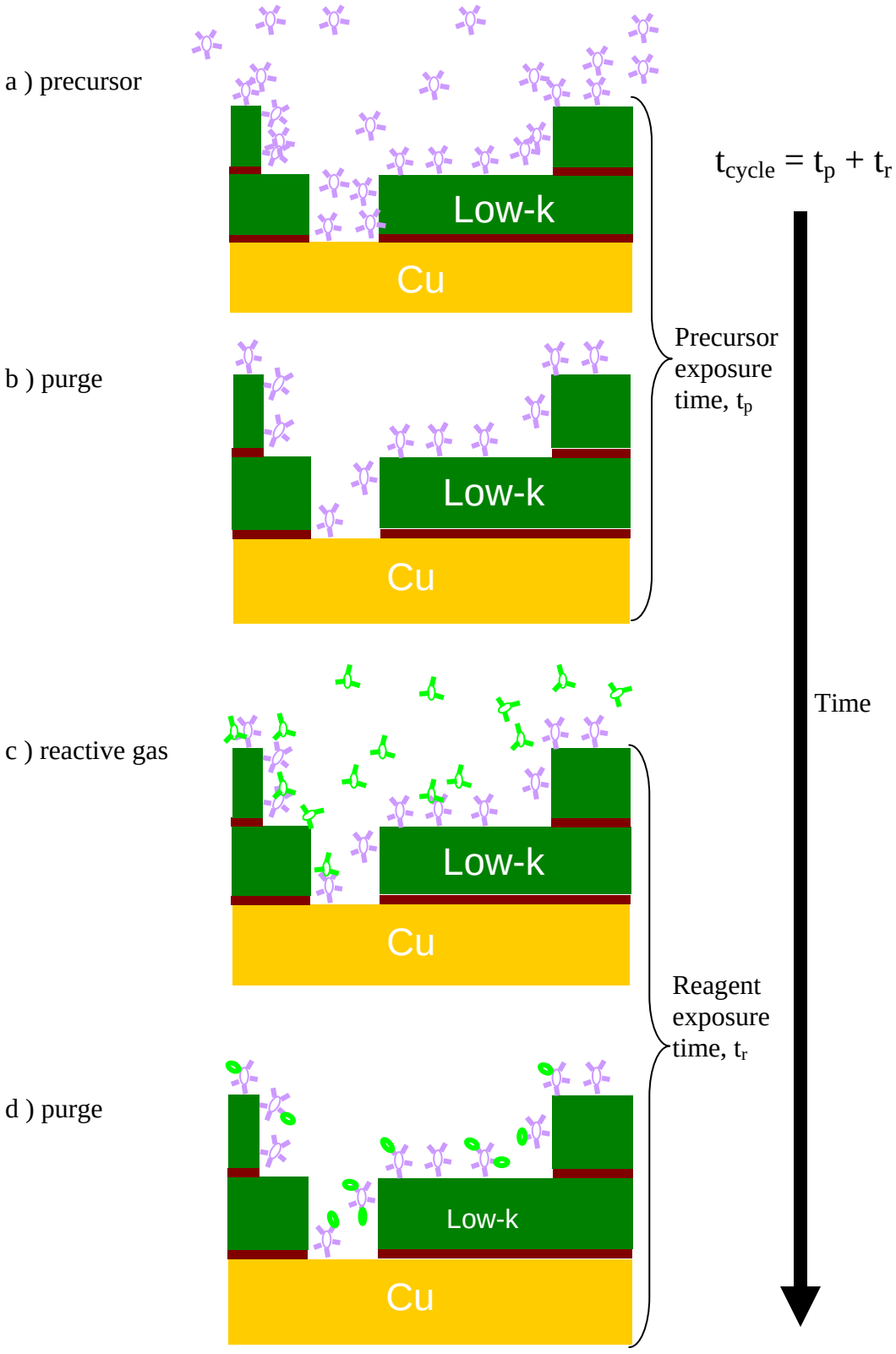

Fig. 1-2 Process steps in one ALD cycle

characteristic gives rise to linear growth rate in an ALD process. It is completely surface chemistry controlled as the whole growth is initiated by the chemisorption of precursor molecules on the substrate surface. The substrate surface chemistry thus determines the ALD nucleation and the subsequent film growth.

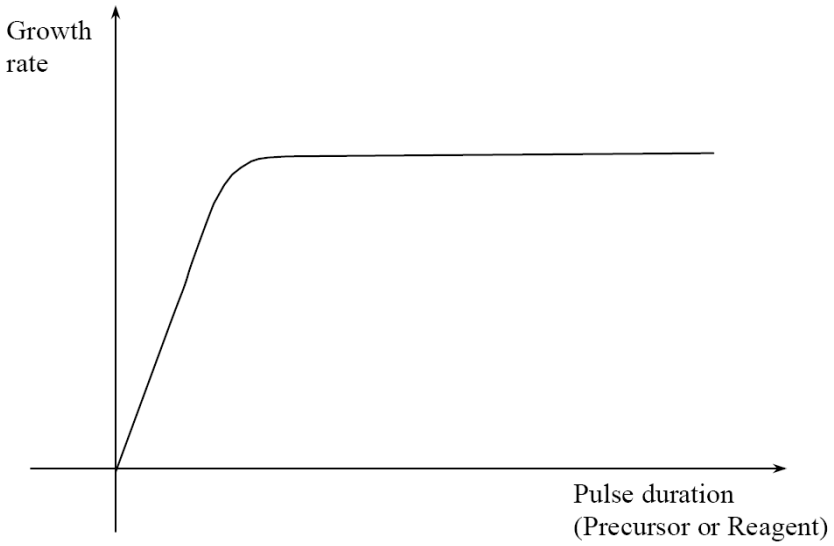

Fig. 1-3 Typical ALD saturation curve

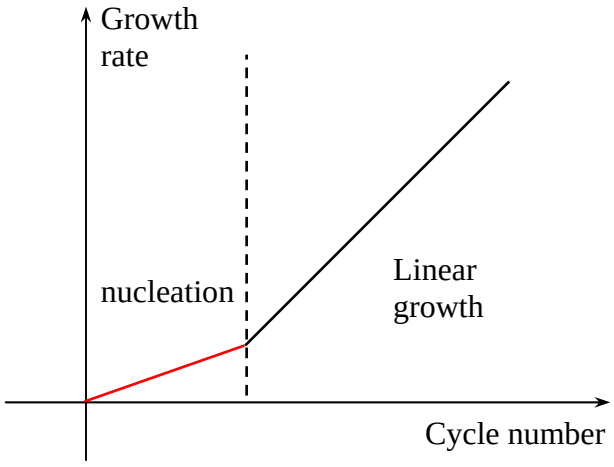

Fig. 1-4 Typical ALD growth curve

The above two characteristics of ALD processes have been used to determine the ALD nature of a thin film deposition process. Fig. 1-3 presents typical ALD saturation curves, where the growth rate varies initially with the pulse time per cycle for precursor exposure or for reactive gas exposure, and then saturates after sufficient exposure time per cycle. Fig. 1-4 presents a typical ALD growth curve where the linear growth region is preceded by a region of lower growth rate. The “incubation” or “nucleation” region is indicative of the substrate surface chemistry effect. It is during this growth region that the incoming precursor molecules are seeing the substrate with a surface chemistry different from what is later on after the substrate has been completely covered with the film to be deposited. A substrate surface chemistry with inadequate chemisorptive sites will definitely have adverse effects on the nucleation process. ALD process on this kind of substrate will require long incubation time before sufficient growth rate can be achieved. In the worst case when the chemisorptive sites are scarcely distributed, it may take very a long period of deposition before the film becomes continuous. Study of this substrate surface chemistry effect on the two main types of low k surfaces and attempts to engineer the substrate surface for better ALD nucleation are the focus of this dissertation.

It has been observed in ALD TiN processes that a metal halide precursor like $TiCl_4$, does not nucleate very well on organosilicate (OSG) type low k dielectric surfaces. [75] It is understandable if we look into the surface chemistry of OSG surfaces. As an attempt to lower the dielectric constant and to achieve hydrophobic surface finish, methyl or other organic side groups are incorporated in the bulk of the materials and on the surface. ALD precursors, Ta-based as well as Ti-based precursors, readily react with

surface silanol groups (Si-OH), replacing the polar O-H bonding with the stronger metal oxide bonding while the terminal organic groups, e.g. $Si-CH_3$, only contain covalent C-H bonds which are significantly more inactive and stable than the O-H bond in Si-O-H. The chemisorption of halide precursor thus only occurs on the surface silanol groups. The surface hydrophobicity of low k dielectrics, which is essential for the process robustness, is expected to be detrimental to the ALD nucleation rate. As we will see in section 1.4, this becomes a serious concern with the possible introduction of a dielectric sealant layer to implement porous low k dielectrics.

There are also a variety of technical difficulties associated with an ALD Ta-based barrier process, including precursor chemistry, reaction energetics, process temperature window, film structure and properties and etc. [76],[77] A commercially viable ALD chemistry requires a thermally stable and volatile precursor that is easy to use and efficient for delivery. The reaction energetics should be able to achieve reasonable growth rate at a temperature compatible with the low k processes, i.e., less than 400°C at most. Also, the precursor should be thermally stable at the process temperature to avoid self-decomposition, which may leave behind undesired impurities.

There are two types of precursor chemistry known for ALD nitride deposition, metal halides reduced by ammonia and metal organic precursors (metal alkyl amides) reduced either by ammonia or hydrogen radical. Among the metal halides, the reaction

$$TaCl_5 + NH_3 \rightarrow Ta_3N_5 + HCl \qquad (1\text{-}1)$$

is a widely investigated chemistry. [78]-[82] The common problems with the halides are long incubation time and slow growth rate. The byproducts HCl or HF in the case of TaF_5 is a concern for Cu corrosion, cross contamination and low k etch. [76],[83]

Three metal alkyl-amides, tert-butylimidotris (diethylamido) tantalum (TBTEDT), [84] pentakis(dimethylamido)tantalum(PDMAT) [85],[86] and more recently tertiaryamylimidotris(dimethylamido)tantalum (TAIMATA) [87],[88] have been extensively studied. The molecular structures of the three MO precursors are given in Fig. 1-5.

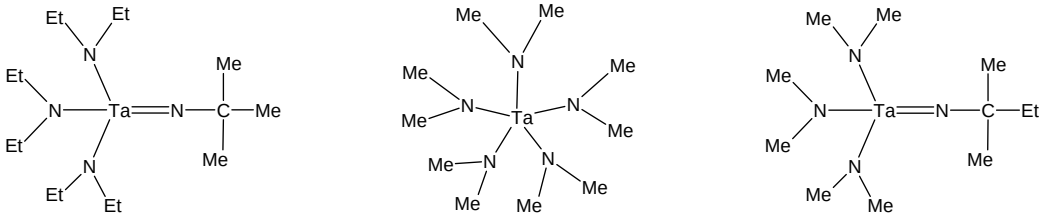

a) TBTEDT b) PDMAT c) TAIMATA

Fig. 1-5 Molecular structure of organometallic Ta precursors

The metal alkyl-amides contain bonds more unstable and reactive than the strong Ta-Cl bonding. One quantum chemical simulation suggests a difference of 1eV per bond between transition metal chloride and its alkylamide. [89] The more favorable reaction energetics and consequently more efficient chemisorption and faster growth rate on most dielectrics have made them better choices for industrial production. But the process window is always a concern with MO precursors since they tend to decompose at more elevated temperatures which are usually used for the sake of faster ALD growth rate. This results in high contents of carbon and hydrogen and makes metal ALD processes nearly impossible.

Another issue is the insufficient reducing power of ammonia as the reactive gas in nitride processes. Metal element in the precursor molecules cannot be reduced by ammonia to its +III valence state for a better microstructure and electrical conductivity. Although the requirement of a conductive TaN layer can be waived as a result of new via-gouging process, [90],[91] a more reactive reagent has been sought extensively to make

the nitride barrier layer more conductive. More reactive methylized hydrazine derivatives were attempted, however, unsuccessfully. [92] Even a second reducing agent, trimethylaluminum (TMA) was added as the catalyst. [93] SiH_4 was also used to form more conductive TaSiN. [82],[94],[95] A very promising process involved the use of a combination of atomic nitrogen and hydrogen species as the reagent together in plasma enhanced ALD process. [96]

The mechanism of mediation by atomic hydrogen species has not yet been well understood. Chemically, it helped remove the chlorine impurity, indicating it facilitated the production of HCl byproduct and somehow reduced the adsorption of HCl on the surface. Thermodynamically, it gives off a lot of heat during reaction, which may be beneficial to the activation of other reactants. The side effect is that excessive hydrogen itself is not a desirable impurity in the deposited film and hydrogenation of polymeric low k surfaces degraded the interfacial strength. [97]

With its superfine control over thickness at atomic scale and superconformal gap filling capacity, atomic layer deposition (ALD) has found wide applications in high quality ultra-thin film deposition on high aspect ratio structures. It is quite natural that ALD was first applied in depositing DRAM cell dielectrics which have the highest aspect ratio, [74],[69]-[73] and high-k gate oxides which are the thinnest and the most critical thin films in a device [74],[97]-[99]. Possible implementation of ALD technique in the actual manufacturing has not met much resistance based on process reasons from the conservatives working on the high volume production lines.

As far as ALD barrier processes are concerned, the industry is not yet committed to any specific film stack, deposition process and integration scheme. ALD

Ta/TaN processes were actively developed as an advanced backup solution. In the meantime, efforts are still concentrated upon innovating, optimizing and extending the existing sputtering processes and exploring other integration schemes, such as PVD Ta flash on ALD TaN, via punch through with simultaneous metal neutral deposition and direct Cu plating on ALD Ru/TaN liner.[64],[91],[100] This has a lot to do with the technical challenges associated with ALD Ta/TaN barrier processes, such as lack of ALD Ta and Cu chemistry, which may require complex tool design to combine different deposition techniques for the metallization process; and integration issues related to the introduction of porous low k materials. In addition, the high thermal budget and long deposition time needed in pure ALD Ta-based barrier processes can be prohibitively costly for multi-level interconnect structures. On the other hand, the biggest advantage of ALD process as a superconformal deposition technique does not matter so much in filling interconnect trenches and vias of which the aspect ratios (AR) are limited close to 2, much less than what is for DRAM cells.

It is not intended here to speculate the right insertion point of ALD as a barrier deposition technique in the BEOL processes. Rather, this work is to investigate the technical issues and challenges facing ALD Ta/TaN barrier process. As the process complexity inevitably increases with aggressive dimensional scaling and new materials integration, any new process has to be examined from an integration point of view before it can be inserted into the process flow. The interactions with and the effects on the other process steps have to be thoroughly evaluated. In this sense, there is no unit process research and development any more; everything is part of an integrated process flow. Keeping the insertion point in mind will help us work on the right issues as the process

steps preceding and following ALD barrier process may differ from one technology node to another, and integration of new materials such as porous ultra low k's may greatly alter the whole process sequence.

1.3 Integration of porous ultra low k dielectrics

For device scaling continuing beyond the 45nm node, the dielectric constant of bulk interlevel dielectrics has to be further reduced to less than 2.1, according to the 2004 updates of the international technology roadmap for semiconductrors (ITRS).[3] To achieve a dielectric constant this low, some degree of porosity has to be incorporated. The incorporation of porosity degrades low k mechanical strength and makes them susceptible to plasma and chemical damage during patterning and metallization. [101]-[109]

The porosity effects together with scaling requirements for finer dimensions and steeper morphology raise significant challenges to the integration of porous low k dielectrics. During damascene patterning, porous ILD is exposed to a series of physical and chemical processes, including plasma etch, ashing, and clean. In a porous medium, these plasma and wet solution processes can induce deep penetration by reactive ions, radicals and etch residues, and cause surface densification, surface roughening, moisture absorption as a result of loss of hydrophobicity, and so on. Besides profile distortion, process induced damage contributes to significant dielectric degradation and increase in the leakage current, posing severe scaling issues for porous dielectrics.[103],[108] The plasma processing damage basically turns the top surface of low k dielectric to a skin layer of densified material similar to SiO_2.[106] If nothing can be done for dielectric recovery, a pessimistic analysis notes that the benefits of using porous low k ILDs will be completely lost at the 32 nm technology node when the damaged surface layers on the

sidewalls exceed a good portion of the whole line width for the dielectric. [110] This will limit the further scaling of the effective dielectric constant of ILD. In addition, porous dielectrics with interconnected pore structures give rise to a lot of reliability concerns associated with the presence of "killer" pores. Statistically, if the nano-scale pores in a thin film are randomly distributed, chances are that they can agglomerate into pores big enough to impact on the material strength and the dielectric strength.[111]-[115] Furthermore, pore tunnels provide easy pathways for chemical penetration and moisture uptake. Even if the surface can be engineered to be hydrophobic, moisture can still infiltrate into the bulk of the dielectric, increasing the dielectric constant and becoming a reliability concern as many material properties degrade at the presence of moisture.[116]-[118]

How to make porous ULKs with small pore size and tight pore size distribution to reduce the fraction of killer pores and achieve satisfactory material and dielectric strength is an important and active area of low k materials engineering. It has attracted most of the attention in ULK materials engineering. For instance, various deposition processes have been attempted for porous low k dielectrics, from xerogel process,[119] templated copolymerization,[120],[121] to the most recent nano-clustering (of silica) (NCS)[122],[123] and molecular-pore stacking (MPS).[124] The advance in ULK solutions will fundamentally improve the outlook of ULK integration. Because the ULK picture is quite murky at this time, more general integration issues related to metallization - in particular, ALD barrier formation on typical low k dielectric surfaces – became the focus of this thesis.

Porous surfaces, in particular, those with big-sized pores and interconnected pore structures, pose severe challenges to metallization, starting with the barrier

formation. It is widely reported that the ALD precursor penetration is the top issue, which necessitates a pore sealing process prior to the ALD deposition.[83], [125]-[127] As ALD allows sufficient time for the diffusion of precursor molecules, chemisorption will occur at every location that is accessible to the precursor. However, this turns out to be a red-herring because so far there is no BEOL compatible ALD metallic Ta process, and what may be deposited inside the pore tunnels is dielectric of a higher k value. Although it may marginally increase k value, no immediate metal deposition causing circuit short would occur. Incomplete barrier coverage on porous low k sidewall can lead to Cu deposition inside the ULK during Cu seed or later Cu electrochemical deposition (ECD) process. A discontinuous or defective PVD Cu seed layer eventually either provides passage for Cu deposition inside the low k or creates weak spots for Cu out-diffusion during electrical stressing.

From a barrier deposition point of view, it is clear that the porous surface can be treated as an aggravated type of surface roughness. For a conformal CVD-type deposition technique, the minimum thickness of deposition for continuous coverage would be at least half of the pore opening size, or 1-2 additional nanometers. However, there is not always such process room available given the stringent scaling and reliability criteria. The need for a “pore sealing” process becomes more imperative because it serves two purposes: first as a hermetic sealing against penetration of moisture and other process residues and contaminants, and then as a planarization layer to provide a smoother surface for metallization.

With the additional but possibly necessary dielectric recovery and pore sealing process inserted into the process flow, ALD barrier process has to be re-evaluated on the

new surface chemistry resulting from such processes. In this study, different pore sealing approaches will be discussed and their impacts on ALD barrier formation will be evaluated.

1.4 Interface engineering

In a larger sense, successful ALD barrier formation on low k and porous ultra low k dielectric surfaces itself is an undertaking that requires a great deal of interface engineering. As mentioned previously, low k dielectric surfaces- in particular, OSG surfaces- are characterized by significant amounts of organic termination and can be very inactive in the precursor chemisorption. For better nucleation and subsequent film growth, the surface has to be activated first before exposure to the precursor. The aggravated surface roughness resulting from the incorporation of porosity needs to be planarized before barrier deposition to ensure defect-free surface coverage. And the film stack has to be fine tuned to meet the requirements on the barrier, interface and conductivity properties with proper thickness control. In fact, since every process step of ALD process is in principle completely controlled by the underlying surface chemistry, vast opportunities exist to engineer the growth at a monolayer level.

To tackle the interface engineering tasks in forming a robust and high performance Cu/low k interface, we first need to acquire the surface chemical information about the interface formation. Based upon understandings of the chemisorption processes involved in ALD barrier and other relevant processes obtained with *in-situ* surface chemical analysis, this dissertation work will continue to examine the possibilities for surface modification, process enhancement and film stack engineering.

To overcome deficiency of chemisorptive sites on a substrate for better nucleation, the substrate surface can be physically or chemically altered to create more chemisorption sites for nucleation. To create a film stack of fine structure, such as superlattices and the Ta/TaN barrier stack, different ALD precursors or reactive agents can be alternated at desired points to fine tune the film stack or even the microstructure to achieve desired film properties. In addition, utilizing the surface functionality groups, porous surfaces can be planarized by adding a self-assembled monolayer.

Conventionally, plasma processes were widely employed for polymeric surface preparation and process enhancement.[75],[126],[128]-[130] With both chemically reactive sub-molecular radicals and energetic ions and neutrals, plasma can form either more reactive moieties on the surface or create more functional groups by chain-grafting. However, poor resistance of low k and ultra low k films against the physical damage caused by plasma has limited its practical use.

To limit plasma induced damage to low k dielectric surfaces, remote plasma or down stream plasma setups have gained favor in low k processing.[131]-[137] By moving the wafer to be processed outside of the plasma chamber, after traveling long distance, only a small number of energetic ions can reach the sample surface, thus the physical damage by energetic ions can be minimized. Simulating this process, this dissertation work has employed a plasma induced ion/atom source outside the process chamber for surface pretreatment and process enhancement. With a boron nitride dielectric aperture in place to block the charged ions, only radicals and neutrals can arrive at the sample surface in order to prevent any physical beam damage, such as surface roughening and/or densification, from occurring. Surface modification has been attempted with amine

radicals (-NHx) and atomic hydrogen beams on OSG low k dielectrics. It is intended to have the surface methyl termination replaced with -NHx moieties, which are much more reactive with the ALD precursor molecules. With increased surface chemisorptive sites, ALD nucleation process and the subsequent film growth can be enhanced. Several aspects of the process enhancement with radical beams have also been investigated, such as the enhancement of the growth using radical beams as the reactive agents and the possible roles of atomic hydrogen in process enhancement. Varying reactive gases or agents in different process stages can assert fine control over the film stack deposited.

Another route for surface modification is through reactions of additional chemical molecules with surface functional groups. This is a route normally taken to form self-assembled monolayers (SAM). By engineering the ad-molecules, surface functionality can be modified from one type of functionality to another. Utilizing this concept, tri-substituted silicon-based agents are proposed to couple, block and tailor the low k surfaces for dielectric recovery and pore sealing.[138]-[141] The silylation agents proposed include chlorosilanes and disilazanes.

The surface silylation of plasma damaged low k surfaces is illustrated in Fig. 1-6. As a result of plasma processing, methyl bonds are depleted from the organosilicate (OSG) based low k surfaces; consequently, large amount of surface silanol groups (Si-OH) are present which can be utilized as the reactive sites to form self-assembled layers. One approach for surface silylation is to use tri-alkyl-substituted disilazanes or chlorosilanes, such as hexamethyldisilazane (HMDS) and trimethyl chlorosilane (TCMS), and so on. While these silylation agents have been confirmed to recover part of the dielectric damage, they are inadequate for surface planarization/pore sealing due to only

monolayer coverage. And they are also detrimental to the subsequent barrier processes with atomic layer deposition (ALD) because the finished surface is terminated with methyl bonds which are inactive in ALD nucleation.[75],[142]

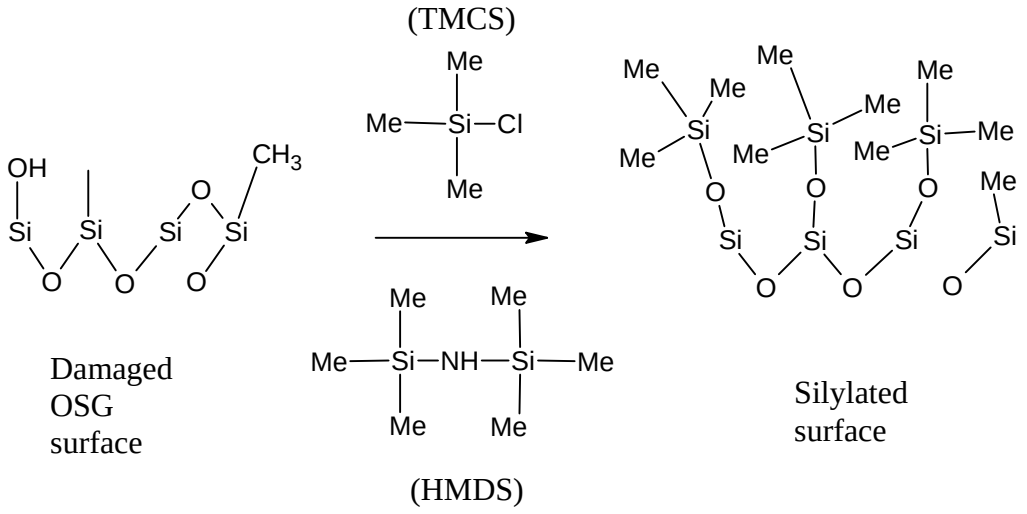

Fig. 1-6 Surface silylation of damaged OSG surface.

If atomic layer deposition (ALD) of Cu barriers is to be inserted into the back-end-of-line (BEOL) process sequence, it will be a process step following the aforementioned low k dielectric recovery and pore sealing processes. Due to its sensitivity to the substrate surface chemistry, strong interactions with the dielectric recovery and pore sealing processes are expected. These interactions have to be considered when developing a dielectric recovery and pore sealing process.

Extensive studies on dielectric recovery, pore sealing, and ALD barrier process have been reported. [138]-[141] However, few of these studies have tried to manage these issues from an integration point of view. Most of them attempted to manage these issues separately. In this dissertation, a novel silylation process has been attempted to tackle these issues from an integration point of view. Based upon the concept of surface

silylation to selectively attack the silanol bonds induced in plasma processing, while at the same time introducing crosslinking bonds for pore sealing and surface planarization, and also attempting to provide surface nucleation sites for ALD barrier process, a two-step silylation process has been proposed: deposition of crosslinked organosilicate sealant layer with alkylsilsesquioxanes for pore sealing and surface planarization, and then followed by a surface finish with phenyl containing tri-substituted silyl agents, such as phenyldimethylchlorosilane (PDMCS) and diphenyltetramethyldisilazane (DPTMDS), for dielectric recovery and to introduce benzene groups at the surface as the ALD nucleation sites and to passivate the surface silanol groups against moisture uptake.

1.5 Organization of the dissertation

The research work contained in this dissertation is to be presented in seven chapters as follows:

Chapter 1 is an introduction to atomic layer deposition of Ta-based Cu barriers on the low k dielectric surfaces and the challenges in this application.

Chapter 2 presents the experimental details: design and construction of an ultra high vacuum (UHV) system for *in-situ* surface chemical analysis of the ALD barrier processes, instrumentation to realize *in-situ* surface pretreatments and process enhancements, setup for surface silylation experiments for dielectric recovery and pore sealing processes, and other techniques necessary for this work.

Chapter 3 summarizes a study of the substrate surface chemistry effects on the ALD nucleation and growth. In this study, the initial chemisorption of precursor molecules is carefully monitored and analyzed. Comparison is made on two main types of low k dielectrics and with two main types of precursor chemistries.

Chapter 4 studies the possibility of surface activation of organosilicate low k surfaces with radical beams. A demonstration with amine (NHx) radical beams is to be presented. Significant growth enhancement has been observed as a direct result of the surface activation.

Chapter 5 investigates other possible process enhancements with radical beams in the ALD barrier processes.

Chapter 6 evaluates a novel surface silylation agent for dielectric recovery and pore sealing process on plasma damaged porous ULK films. The emphasis is the interactions of this process with the subsequent ALD barrier process.

Chapter 7 summarizes the conclusions and plans future work.

Chapter 2: Experimental

2.0 Overview

To obtain *in-situ* surface chemical information necessary in understanding the growth mechanisms of atomic layer deposition of Ta-based Cu barriers, a UHV cluster tool has been constructed, which consists of an ALD process chamber equipped with *in-situ* surface treatment capabilities and an XPS analysis chamber. Calibrated with transmission electron microscopy (TEM) and ellipsometry (EP) measurements, XPS has also been used to monitor the film thickness during film deposition.

To prepare low k surfaces for ALD barrier formation, radical beams, or beams of reactive sub-molecular neutrals are generated in an atom/ion hybrid source and selectively introduced onto the sample surface, in order to simulate the effects of plasma pretreatments of low k dielectric surfaces and plasma enhancements of deposition process in a plasma enhanced ALD (PEALD) process. Exclusion of energetic ions allows focused study of the chemical effects while avoiding severe physical damage to the low k films.

To investigate the interactions between ALD barrier processes and possible additional dielectric recovery and pore sealing processes in the implementation of porous ultra low k, surface silylation experiments have been attempted using wet chemistry.

This chapter presents the experimental details of this dissertation work.

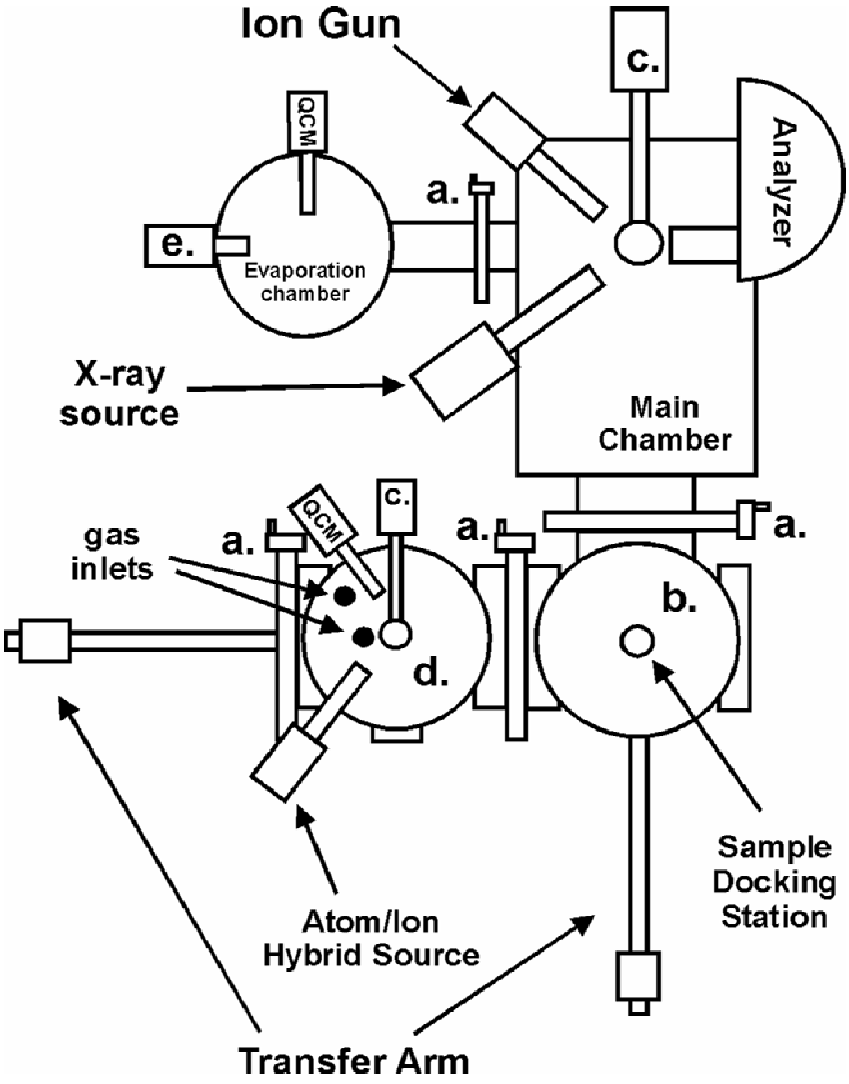

Figure 2-1 UHV system for *in-situ* XPS studies of ALD barrier formation.

a. gate valves;

b. transfer chamber;

c. docking stations;

d. ALD process chamber;

e. evaporator.

2.1 Process Chamber for Atomic Layer Deposition

An ALD process chamber has been added to an existing XPS system in order to enable *in-situ* XPS study of interface formation during barrier layer deposition. Figure 2-1 shows a schematic top view of the whole ultra-high vacuum (UHV) system. Three docking stations and two orthogonal transfer arms are used for sample transfer among the transfer chamber, the ALD process chamber and the XPS analysis chamber without breaking the vacuum. Pictures of the details of the system can be found in Appendix A.

Ultra high vacuum is maintained through differential pumping with turbopumps and ion pumps backed up with mechanical pumps. Base pressures in the three chambers were maintained as follows:

Main analysis	mid-10^{-10} torr
ALD process	Low 10^{-7} torr *
Transfer chamber	mid-10^{-8} torr

The ALD process chamber consists of a UHV chamber, a gas delivery system and an atom/ion hybrid source. As shown in Figure 2-2, argon (Ar), ammonia (NH_3) and hydrogen (H_2) gases are introduced through electropolished stainless steel ¼" tubing from two gas cabinets holding the gas cylinders. Gas selection and flow direction are controlled by three 3-way pneumatic valves, and the flow rates are set using three Mass Flow Controllers (MFC's). Chamber pressure is controlled with a down stream throttle valve adjusting the conductance between the pumps and the chamber. All the pneumatic valves, MFC's and the pressure controllers are controlled through a computer program written with LabVIEW. [143] For the record, details of the instrumentation for the control over the valves, flow controllers and pressure controller are given in Appendix B.

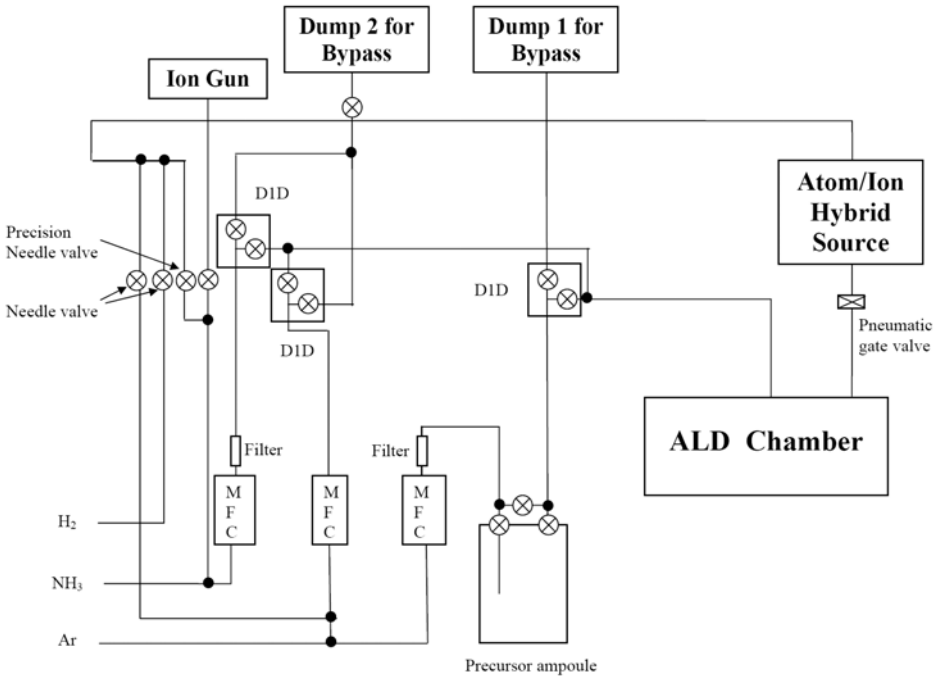

Figure 2-2 Schematic of the gas delivery system.
D1D's are three-way pneumatic valves.

$TaCl_5$ precursor and PDMAT precursor are stored in ampoules specifically designed by ATMI for enhanced precursor delivery. These prototypes were provided by ATMI in support of the project. The precursor ampoule and MFC's are placed in another smaller gas box very close to the process chamber for both safety considerations and minimization of the gas path.

It was a great learning experience designing and building the system from scratch. Many mistakes and mishaps occurred. It was through mistakes, accidents and even disasters that the importance of completely separating the pumping lines for the Ta precursor and the reactive gas was realized. The halide precursor was observed to form yellowish $TaCl_5 \cdot xNH_3$ flakes inside and outside the mechanical pump even though the

$TaCl_5$ precursor and NH_3 were never flown simultaneously in any segment of the gas delivery system. It was thought to be due to incomplete and slow evacuation of the process gases by the mechanical pump.

It is also imperative to maintain a laminar flow pattern and to reduce the transient time needed to switch from one gas to another. The former is to avoid deposition non-uniformity and particle generation on the sample surface. The latter is for better control over the deposition process.

ALD process is supposedly quite independent of precursor delivery. As long as the precursor molecules carried onto the sample surface can over-saturate the surface chemisorptive sites, small fluctuations in the total amount of precursor molecules should not matter. However, turbulence in the gas delivery system can do far more harm than small fluctuations in the gas flow. The pressure surge accompanying the turbulence may disturb the flow pattern so much that the surface chemisorption can no longer be achieved in a predictable way with certain repeatability. The sudden surge in the tubing can also generate a dragging force to carry the solid particles or condensates into the chamber. Turbulence is often caused by pressure imbalance between the bypass gas lines and the delivery line when switching among gases. It would have been more desirable to have three similar turbopumps or dry pumps on the precursor gas line, NH_3 and purge gas line, and the process chamber to keep the pressure balanced among all the gas lines to be switched. In addition, using turbopumps on all the gas lines can greatly reduce the possibility of pump oil back streaming. For economical considerations though, only two turbopumps are used. The precursor gas line is pumped with a mechanical pump only, for precursor condensation can greatly reduce the lifetime of turbopump.

For sample preparation, surface pre-treatments, and process enhancement, an "Osprey" mini atom/ion hybrid source [144] from Oxford Scientific is mounted onto the process chamber and aimed at the sample surface from a distance of about 10 cm at an incident angle of about 40°. A VAT mini pneumatic gate valve is inserted in between to serve as an automated shutter. An illustration of the hybrid source is presented in Figure 2-3. The source uses a magnetron to generate microwaves at a frequency of 2.45GHz. Under an 87mT magnetic field, electrons are forced into Electron Cyclotron Resonance (ECR) at this frequency. Microwave is coupled into the plasma chamber to ignite plasma at a proper gas pressure in the plasma chamber. With ECR enhanced ionization efficiency, the plasma cracks gas molecules more efficiently into ions and other sub-molecular neutral species. The filamentless design of the source makes it an ion or sub-molecular radical source for almost any gas or gas mixture. In particular, it is compatible with the use of those gases which are normally considered dangerous to crack with plasma, such as hydrogen and oxygen.

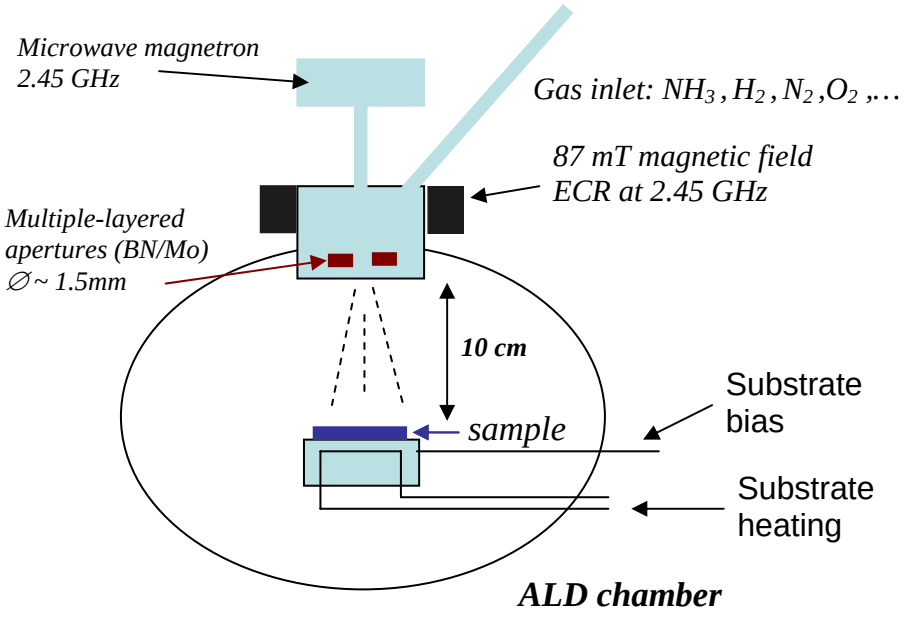

Figure 2-3 Ion/Atom hybrid source

The selection between ions and radicals is achieved through a layered shutter made of boron nitride aperture and molybdenum grids. The dielectric BN aperture can be rapidly charged up by ions, repelling further like-charged ions from entering the aperture. If no accelerating voltage is applied to the Mo grids to extract the ions, only neutral species can exit the source. If a high voltage is applied to the grids, ions with up to 1.5keV can be added to the beam. The plasma chamber is differentially pumped by the introduction chamber pumping system. In the atom mode, only neutral species can leave the aperture and reach the process chamber. In the ion mode, ions of up to 1.5keV kinetic energy can be added to the beam. It is very similar to commercial downstream plasma setups.

In this study, the atom/ion source will be used to generate atomic hydrogen and nitrogen containing species or NH_x radical beams for low k surface pre-treatments and for radical or remote plasma enhanced ALD processes. These enhancements are expected to promote film growth and reduce the reaction temperature, making the process compatible with low k materials (< 400°C).

One caveat of the use of radical beams is the difficulty in calibrating the radical beam intensity. There are simply too many uncertainties involved in deciding the beam intensity at the sample surface. It is affected by the ionization efficiency to ignite the plasma, plasma density, dissociation efficiency of the gas molecules, gas flow rate, aperture size, travel distance, chamber pressure, radical recombination rates and etc. None of these factors is easy to define, control and measure, so the beam intensity has to be measured from the effects at the surface of a certain standard sample. Still, the

reaction rate of a certain type of radicals differs from one surface to another and is affected by many other extrinsic factors such as the temperature and pressure.

Nevertheless, efforts have been devoted to giving an estimation of the radical beam intensity under normal experimental conditions. Instead of using an irrelevant "standard" surface, the reduction of germanium native oxide by atomic hydrogen was used to measure the flux of atomic hydrogen beam generated in the atom/ion hybrid source at a chamber pressure of 1 mtorr. Estimation of amine radical beam intensity can certainly be done following a similar methodology with surface nitridation of elemental germanium or silicon or any metal reactive with amine radicals. However, considering the large uncertainties surrounding the numbers, no additional experiments were performed to quantify the intensities for other radical beams.

Ge native oxide cannot be reduced by molecular hydrogen gas at any temperature lower than 450°C, [145],[146] but was found to be reducible by atomic hydrogen around 300°C. Incidentally, a patent application based on similar observations was filed later by Applied Materials. [147] A nearly oxygen free Ge surface was obtained by cyclic HF cleaning [148] and exposed to excessive atomic hydrogen flux. The cleaned Ge was oxidized again in the loadlock with dry air. The oxide layer was estimated based on the elemental Ge3d and the oxide Ge3d signals. The newly formed GeO_x thin layer was again cleaned *in-situ* with a controlled atomic hydrogen flux. Given the surface density of oxygen atoms on the thin oxide layer, the atomic hydrogen beam intensity can be evaluated. The operational procedure is illustrated in Figure 2-4.

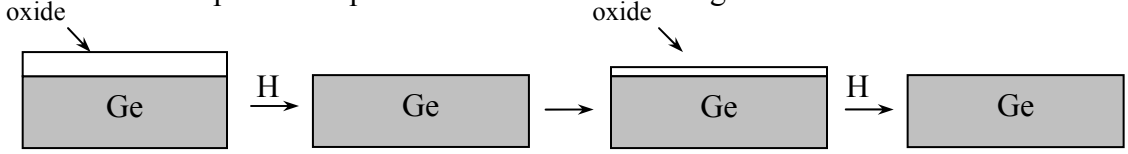

Figure 2-4 Measuring flux of atomic hydrogen beam

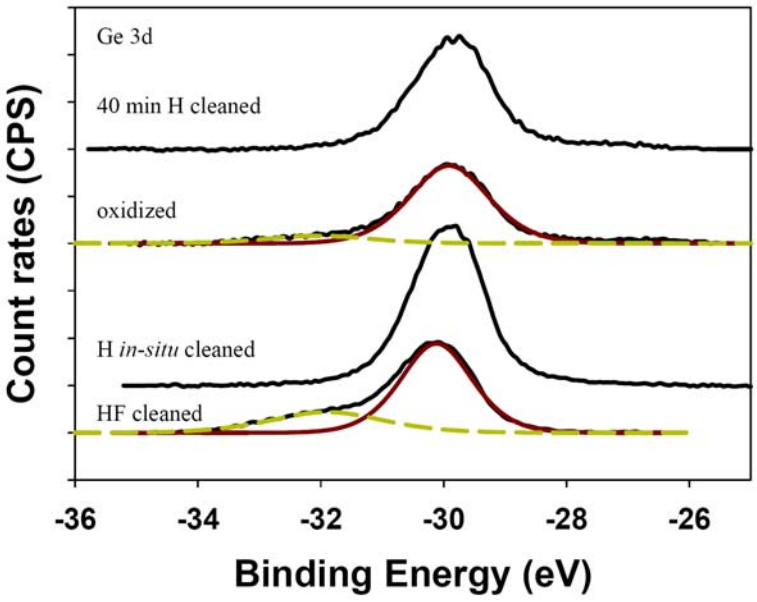

Figure 2-5 Evolution of Ge 3d spectrum on a Ge surface

Figure 2-5 presents the evolution of Ge3d spectrum. The oxide thickness can be deduced to be 4.5Å from a 30% decay of the elemental Ge3d signal in the GeO_x overlayer, assuming an effective attenuation length (EAL) of 2.6nm [149] in GeO_2 for Ge3d photoelectrons escaping from the substrate. The methodology for overlayer thickness evaluation will be described with more details in Section 2.3. With further assumption of a uniform chemical composition of GeO_2 for the newly formed GeO_x overlayer, the surface density of oxygen can be estimated to be:

$$\frac{\rho \cdot N_A}{M} \cdot 4.5\times10^{-8} \times 2 = \frac{4.5\times6.02\times10^{23}\times4.5\times10^{-8}\times2}{104.59} = 2.3\times10^{15}\ /cm^2 \qquad (2\text{-}1)$$

where ρ is the assumed density for GeO_2, M the molecular weight, N_A is Avogadro's number and the factor of 2 comes from two oxygen atoms per molecule.

As each oxygen atom can bond with two hydrogen atoms to form water vapour, the removal of this amount of oxygen atoms suggested the flux of atomic hydrogen beam

to be $4.6\times10^{15}/cm^2$. Since the oxide overlayer could only barely be cleaned with 40 minute atomic hydrogen irradiation, the atomic hydrogen beam intensity is thus roughly estimated to be in the order of 10^{12} atoms/(cm^2·s).

The *in-situ* surface chemical analysis capability, coupled with other optional *in-situ* characterization tools, e.g. quadruple mass spectrometer, in addition to the versatile surface treatment capabilities makes the setup very suitable for more fundamental studies on the mechanisms of thin film growth, plasma damage on porous low k dielectrics and pore sealing with beam or vapor treatments.

2.2 Conditions for atomic layer deposition

In this study, two types of ALD processes were implemented. One is the conventional thermal process, and the other is radical beam assisted ALD process. Both halide ALD chemistry and metal organic ALD chemistry were examined. Regardless of the use of radical beams and the ALD chemistry, temperature profile is the most important condition for a successful and eventless ALD process.

The temperature profile is maintained to achieve satisfactory precursor vapor pressure, good reaction rate, no condensation in the tubing, valves and the chamber wall, and theoretically no self-decomposition. Since the vapor pressure differs from precursor to precursor, different ampoule temperature was used for $TaCl_5$ (0.0002 mmHg at 20°C) and PDMAT (0.002 mmHg at 26°C). [150] 80°C was normally used for $TaCl_5$ ampoule while 30°C was used instead for PDMAT ampoule. It was noted that there was an abrupt increase in the vapor delivery rate of $TaCl_5$ at 75°C.

The two precursors have different thermal stability as well as different vapor pressure. Solid PDMAT starts to decompose at 55°C [150] so the tubing, valves and the

chamber wall were kept at around 50°C. And this thermal instability has been utilized for post-process cleaning by raising the temperature along the precursor path in order to remove any precursor condensates. Whereas $TaCl_5$ is fairly stable up to its melting point at 216°C, so the tubing and the valves were kept at 120°C, which is the highest temperature that the seal in the valves can take, in order to prevent precursor condensation, and the chamber wall was heated up to 200°C to avoid any condensation inside the chamber, the downstream throttle valve and the turbopump.

The substrate temperature was chosen based upon reported processes on Applied Materials tools. [86] Samples were resistively heated to 300-390ºC for $TaCl_5$ processes and 200-250ºC for PDMAT processes by a Molybdenum heating wire underneath the holding plate. This reaction temperature obviously lies in the self-decomposition range of PDMAT, implying there could be a CVD decomposition component.

For electrical insulation purpose, the substrate temperature was not directly read from a thermal couple in the process chamber. Rather, it was calibrated with the correlation between the heating current and the substrate temperature. It was intended as a temporary solution, but turned out to be quite accurate and repeatable in controlling the temperature after being properly calibrated. The substrate temperature was first calibrated with a thermal couple attached on the sample surface and a thermal couple attached to the back of the sample supporting plate in a vacuum similar to the process condition. The temperature at the sample surface was observed to be about 30ºC higher than the reading at the backside of the sample supporting plate. This has to do with the remote location of the backside thermal couple from the heating filament. Every time during sample

outgassing, the substrate temperature measured with the backside thermal couple was correlated to the heating current at three temperatures, and a heating current was then linearly extrapolated to achieve the desired process temperature on the sample surface. Unavoidably, the resulting temperature uncertainty is still as high as ±20°C.

The flow rates for all the three gases were maintained at 100 sccm. The gas upper stream pressures at the regulators were adjusted occasionally in order to compensate for the conductance difference due to the presence of gas filters on the ammonia and carrier gas lines and inside the precursor ampoule. The pressure was set to be 5-6 psi for NH_3 and 10-12 psi for Argon. This is to help reduce the response time of the downstream throttle valve by regulating the gas pressure at the inlet to the process chamber. The chamber pressure was usually maintained at 20 mtorr for all the process steps in the thermal ALD process.

When radical enhanced ALD process is to be implemented, the process sequence in each ALD cycle becomes

Purge$\rightarrow$ Precursor $\rightarrow$ Purge $\rightarrow$ Evacuation $\rightarrow$ Radical beam irradiation

To avoid cross-contamination in the plasma chamber, an evacuation step about 5 second long was inserted prior to the opening of the mini gate valve. And during the radical beam irradiation step, as the plasma can only strike when the downstream chamber pressure is in the mtorr range, the chamber pressure was kept at 1.0 mtorr.

In radical beam processes or pre-treatments, atomic hydrogen beam was obtained by cracking hydrogen gas molecules, and an amine radical beam was generated by cracking ammonia gas molecules. In radical enhanced ALD processes, atomic hydrogen or amine radical beams were introduced to take the place of ammonia gas as

the reagent in the ALD processes. During these processes, the pressure at the differentially pumped plasma chamber was maintained as close to 1.0 mtorr as possible prior to striking plasma merely for process control purpose.

Pulse time conditions were determined with saturation curves as shown in figure 1-3. Varying the precursor pulse time from 2 seconds to 17 seconds, samples after deposition of 80 ALD cycles were transferred for XPS analysis. The ratio of XPS Ta4f signal characteristic of the layer deposited to Si2p signal from the substrate is indicative of the amount of deposition. The ratios were plotted against the pulse time. The resulting curve is presented in Figure 2-6. It is clear that the $TaCl_5$ pulse time has to be at least 14 seconds to reach saturation, or to achieve maximum chemisorption at each cycle. The slow response can be attributed to the low precursor delivery rate due to low carrier gas flow rate, low ampoule temperature and possibly the long travel distance.

For economical considerations, excessive ammonia was used for reaction with the chemisorbed precursor molecules. The second saturation curve was not examined. Typical process conditions were 14 seconds of precursor, 4 seconds of purging, 4 seconds of ammonia and then 3 seconds of purging in each ALD cycle.

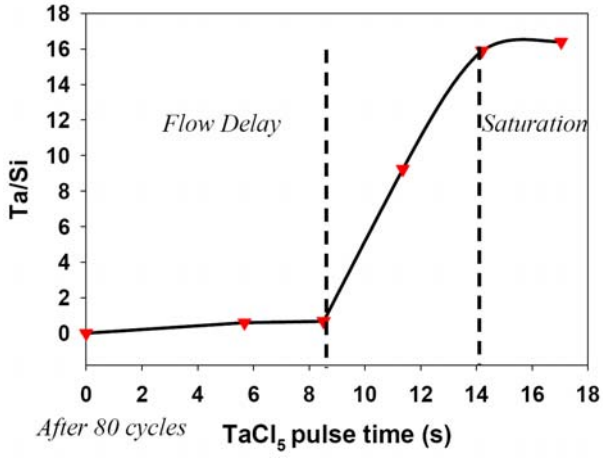

Figure 2-6 Saturation curve for $TaCl_5$ ALD process

The experimental conditions for various ALD processes are summarized below.

Table 2-1: Typical ALD process conditions

	TaCl5	PDMAT
Reaction temperature	300-390 °C	200-250 °C
Ampoule temperature	80°C	30°C
Tubing & valve temperature	120°C	50°C
Flow rates	100 sccm	
Process pressure	20 mtorr	
Pulse time (precursor, purge, ammonia, purge)	14s,4s,4s,3s	

2.3 *In-situ* X-ray Photoelectron Spectroscopy (XPS)

X-ray photoelectron spectroscopy is a powerful surface characterization tool widely used in both surface physics and surface chemistry. It is capable of monitoring the chemical states as well as stoichiometric analysis for the chemical composition, and provides fingerprint information of the chemical bonding environment inside a material.

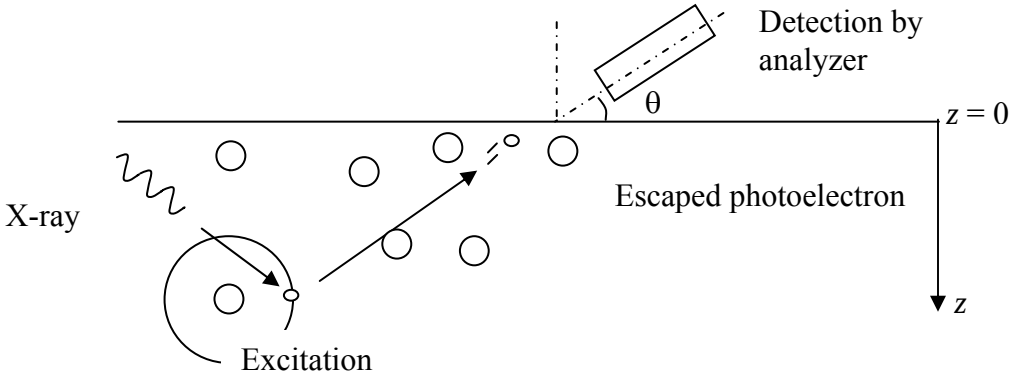

Figure 2-7 Core level X-ray Photoelectron Spectroscopy.

In an x-ray photoemission process, as illustrated in Figure 2-7, core level electrons absorb incoming x-ray photons, acquire more than sufficient energy to break the binding from the nuclei, and either directly escape from the sample surface or result in secondary excited electrons and Auger electrons through other electron-material

interactions. The escaped photoelectrons are collected and differentiated in terms of the acquired kinetic energy.

The detected binding energy of the core level electrons has to do with the nucleus-electron binding, initial and final energy states of the atoms, attenuation on the escape path and the local chemical bonding environment. The nucleus-electron binding gives rise to the fingerprint binding energies for core level electrons excited from the binding environment of different types of atoms. The integrated area under a core level photoelectron peak reflects the amount of the specific atoms providing the characteristic binding energy to the photoelectrons within the sampled region, with the proportionality constant being the atomic sensitivity tabulated in most handbooks for XPS. [151] The local chemical bonding possibly is the smallest factor affecting the binding energy, but the small "chemical" shifts caused by this factor attract most of the attention, because they provide significant information on the complex chemical states of atoms in a material. Characteristic chemical shifts can be used to identify the chemical states of atoms. For example, the binding energy of $Ta4f_{7/2}$ electrons in Ta_2O_5 shifts by 5.0 eV to higher binding energy from what is in elemental Ta, and the binding energy of O1s electrons in Ta_2O_5 shifts by 2.8 eV to lower binding energy from what is in SiO_2.

The surface sensitivity of XPS arises from the short electron inelastic mean free path (IMFP). Depending upon the kinetic energy of the excited photoelectrons, IMFPs (λ) for most core level electrons of interest, such as carbon 1s, nitrogen 1s, oxygen 1s, silicon 2p, and tantalum 4f, range from 10 to 50Å in the dense Ta-based barrier materials. [152] Because the reduction rate of the number of photoelectrons at any depth due to electron-material interactions depends on the number of the photoelectrons at that depth, an

exponential extenuation model is usually assumed for escaping photoelectrons while still in the sampled materials.

The depth from where significant amount of photoelectrons can escape to the analyzer varies with the detection angle θ, as seen in Figure 2-7. Measurements taken at a glancing angle θ~18° or 30° collect photoelectrons - 95% of which have escaped within a sampling depth of $3\lambda\sin\theta \sim 3\lambda/4–3\lambda/2$ from the surface, containing mostly surface specific information. Measurements taken at the normal angle θ~90° collect photoelectrons - 95% of which have escaped within a sampling depth of 3λ, showing mixed information of surface and bulk properties.

More importantly, XPS analysis is non-destructive in most cases and can be easily incorporated into UHV systems, making it a good tool for *in-situ* process monitoring and surface characterization. In this study, by connecting the ALD process chamber and the XPS system together via a UHV transfer chamber, the evolution of the surface chemistry was tracked with XPS analysis *in-situ* throughout the deposition processes, providing the very much needed information to understand the ALD growth mechanisms and engineer the surface chemistry for interface improvements.

2.3.1 Basic analysis techniques

Details about the XPS system in our lab can be found in P. Abramowitz's dissertation. [129] It is a Leybold system with a nonmonochromatized dual anode (Mg Kα and Al Kα) x-ray gun and a concentric hemispherical energy analyzer. The x-ray gun is mounted about 64.5° from the analyzer.

In this study, the Al Kα line with excitation energy of 1486.6 eV is used. At a pass energy of 38.45 eV, the nominal energy resolution is estimated to be 0.9 to 1.0 eV.

[151] Another inherent issue for XPS analysis is surface charging and peak broadening on insulators, such as the dielectrics investigated in this study. The energy scale of an XPS spectrum can be well calibrated by conductive metal samples with known binding energies. [151] However, the depletion of electrons from a dielectric surface can leave the surface positively charged, causing unpredictable shifts of the whole spectrum, and worse yet, different shifts for different characteristic spectra due to differential charging. The charging effects can be very misleading when interpreting spectra on insulator samples.

Fortunately, in the previous studies, [129],[153] no significant charging effect was observed. Given that the sample thickness was usually only 1 kÅ thick and the substrate intentionally chosen to be heavily doped silicon, the testing samples were very leaky at storing charges. As long as similar sample specifications were followed, it was not necessary to use a low energy electron flood gun to neutralize the surface charge. Observed energy shifts due to the charging effect were always less than 4 eV, even though occasionally some low k films used were about 300 nm thick and the substrate was only normally doped. This is because those films under study are highly porous, so even leakier against charge built-up.

For energy referencing, the energy scale was first calibrated with Au $4f_{7/2}$ (~ - 84.00 ± 0.01 eV) and Cu $2p_{3/2}$ (~ - 932.66 ± 0.02 eV). On low k dielectrics, the energy scale was calibrated with known peak positions for carbon 1s in different materials as long as the carbon peak remained visible. On organosilicate samples, the primary aliphatic carbon peak was matched to -285.0 eV [151] while on SiLK™ [154] samples, the primary aromatic carbon peak was matched to -284.8 eV. [155] When the substrate carbon signals became much too distorted with tantalum nitride coverage, metal oxide peak was

chosen for energy referencing instead. The de-convoluted O1s peak for tantalum oxide was matched to -530.7eV, a well documented and confirmed binding energy value. [156]

Since different reference peaks have been adopted during the spectral evolution, the plentiful chemical shift information would unavoidably be compromised to some extent. Nevertheless, as will be seen in the later part of the dissertation, this method did not add too much artifacts to the spectra, and the spectral evolution observed can still be meaningfully interpreted.

Shirley background subtraction, [157] which assumes that background photoelectron intensity at any energy is due to the secondary electron emission and is linearly proportional to all the electrons with higher kinetic energies, was adopted for background correction whenever applicable. Otherwise, linear background subtraction was used instead. For example, Shirley subtraction for C1s spectra in SiLK™ resulted in large artifacts which are believed to be caused by the wide energy range of the spectrum and the presence of π-π^* shake-ups (-290~-292 eV) [151],[155],[158] far away from the primary peak.

After background subtraction, the integrated area of each spectrum was divided by the corresponding atomic sensitivity, yielding the atomic concentration. Relative concentrations were then calculated by normalizing each concentration to the sum of all the contents. Atomic concentrations were usually calculated with atomic sensitivities provided by D. Briggs and M. P. Seah. [151] The atomic sensitivities used in this dissertation are Ta4f (2.4), N1s (0.42), C1s (0.25), Si2p (0.27) and Si2s (0.26). However, calibration measurements on very thick thermal dioxide and tantalum oxide did not give the right silicon to oxygen and tantalum to oxygen ratios if a reference sensitivity value

0.66 for O1s was used. Instead, 0.90 was found to be a more suitable sensitivity number. As a result, throughout this work, the new calibrated value 0.90 has been used as the atomic sensitivity for O1s.

Because the ionization cross-sections for hydrogen and helium with X-ray photons are very small, [159] XPS is not sensitive to these two light elements. Therefore, all stoichiometric analysis has excluded hydrogen, which is actually abundantly present in the low k dielectrics.

The actual peak shape is neither Gaussian nor Lorentzian, but a convolution of Lorentzian natural line shape with an instrument-dependent exponential response function of the detector. Software PeakFit [160] and CasaXPS [161] have been used to de-convolute the spectra. In PeakFit, Voigt peak shape was used to fit the data, while in CasaXPS Gaussian-Lorentzian product was used with a weight factor around 50-60%.

2.3.2 Overlayer thickness evaluation

XPS signal intensity or the integrated area of a specific XPS peak corresponds to a sum of all the photoelectrons emitting from different depths of the sample. Assuming an exponential decay model for the photoelectrons on their way out, in a coordinate system shown in Fig. 2-7, the total XPS signal intensity can be written as

$$I = A \cdot M \cdot S \cdot I_0 \cdot \int_0^{\infty} c(z) \exp\left(-\frac{z}{\lambda \sin\theta}\right) dz \qquad (2\text{-}2)$$

where A is the analyzed area, M is a geometric factor which is a function of the x-ray incident angle and the photoelectron exit angle, S is the excitation probability or cross-section for electrons in a specific energy level, I_0 is the x-ray intensity, $c(z)$ is the atomic concentration at a certain depth z, λ is the mean free path for electrons excited from this depth z and θ is the photoelectron exit angle with respect to the sample surface.

For a thin overlayer on a substrate, photoelectrons from an element only present in the overlayer and photoelectrons from an element characteristic of the substrate will have XPS signal intensities as follows:

$$\begin{aligned} I^O &= A \cdot M \cdot S \cdot I_0 \cdot \int_0^d c(z) \exp\left(-\frac{z}{\lambda_O \sin\theta}\right) dz \\ &= A \cdot M \cdot S \cdot I_0 \cdot c \cdot \lambda_O \sin\theta \cdot \left(1 - \exp\left(-\frac{d}{\lambda_O \sin\theta}\right)\right) \\ &= I_O^{\infty} \cdot \left(1 - \exp\left(-\frac{d}{\lambda_O \sin\theta}\right)\right) \end{aligned} \tag{2-3}$$

$$\begin{aligned} I^S &= A \cdot M \cdot S \cdot I_0 \cdot \int_d^{\infty} c(z) \exp\left(-\frac{z}{\lambda_S \sin\theta}\right) dz \\ &= A \cdot M \cdot S \cdot I_0 \cdot c \cdot \lambda_S \sin\theta \cdot \exp\left(-\frac{d}{\lambda_S \sin\theta}\right) \\ &= I_S^{\infty} \cdot \exp\left(-\frac{d}{\lambda_S \sin\theta}\right) \end{aligned} \tag{2-4}$$

$$\frac{I^O}{I^S} = \frac{\lambda_O}{\lambda_S} \cdot \frac{1 - \exp\left(-\frac{d}{\lambda_O \sin\theta}\right)}{\exp\left(-\frac{d}{\lambda_S \sin\theta}\right)} \tag{2-5}$$

All these three formulas can be used to deduce the overlayer thickness. For simplicity and convenience, formula 2-4 is most commonly used since the overlayer morphology is usually not so well controlled that the mean free path obtained on a very thick (infinitely thick) overlayer may not be a good description of the decay of photoelectrons in a much thinner film, and it is not always practical to grow a very thick overlayer for *in-situ* XPS measurements. On top of that, the use of two mean free paths will certainly introduce larger experimental error. Using formula 2-4, the ratio between the substrate photoelectron signals with a thin overlayer coverage and without can be directly related to the overlayer thickness. The only parameter needs determining is the

mean free path, which can either be theoretically predicted or experimentally calibrated with other physical characterization techniques, such as transmission electron microscopy and ellipsometry. Experimental calibration is always preferred since many parameters required for the theoretic prediction are not readily available.

2.3.3 Growth curve monitoring

In-situ thickness monitoring in ALD processes was reportedly possible with quartz crystal microbalance (QCM). [162]-[164] Initially, this metrology was followed in this study to establish the ALD process conditions [165],[166] until it was realized that the QCM sensor was of completely different surface chemistry and completely different reaction temperature. The data obtained from QCM can still provide a good monitor of the pulse-by-pulse nature of ALD processes. But as a thickness measurement metrology, it simply requires too much calibration and involves too many uncertainties.

The *in-situ* XPS capability of the system constructed in this work provides another means for thickness monitoring. Assuming a simple exponential decay model [151] of a substrate XPS signal intensity in a uniform overlayer, the thickness of the overlayer can be easily estimated after the effective attenuation length (EAL) or inelastic mean free path (IMFP) of the substrate photoelectrons inside the overlayer is known. There is an EAL database provided by the National Institute of Standards and Technologies (NIST). [149] And other databases and references of other equivalent parameters, such as inelastic mean free paths (IMFP), also exist. [152] However, the theoretical predictions are bound by many oversimplified assumptions and the experimental measurements on the same type of overlayer of interest are not always available. So it is always suggested that calibration with other physical measurements of the overlayer have to be done first to

obtain a reasonable estimation of the attenuation length. Transmission electron microscopy (TEM) and ellipsometry are two commonly used calibration techniques. [167]

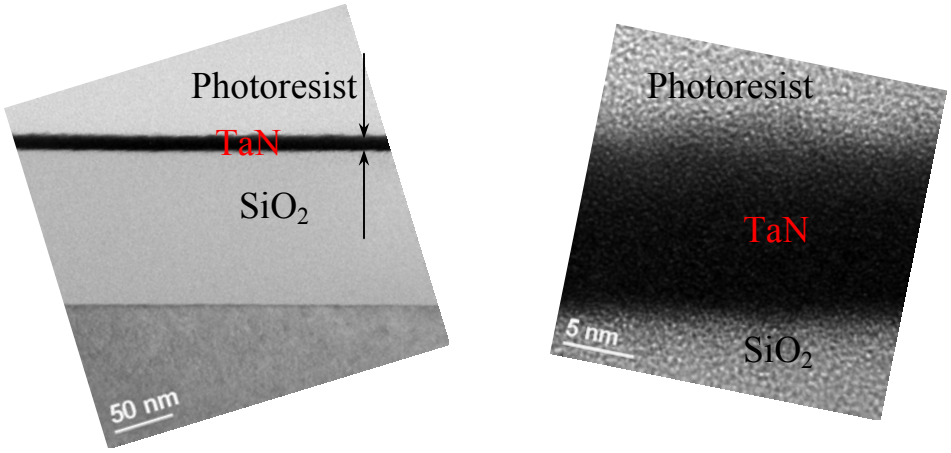

Figure 2-8 TEM thickness measurements (Courtesy of Junjing Bao)

In this work, calibration was done with cross-section TEM and ellipsometric measurements of a very thin tantalum nitride layer deposited with ALD on SiO_2 substrate. The oxide thickness was first accurately measured with a Rudolph ellipsometry tool to be 1006 Å. This thickness was then used to calibrate the TEM scale in the micrograph presented in Figure 2-8. The barrier thickness was found to be 11.2 nm when the SiO_2 substrate was measured to be 1250 Å. Therefore the actual ALD tantalum nitride thickness is $\frac{11.2}{1250}\cdot 1006 = 9.0nm$. The overestimation of the film thickness in TEM micrograph can be attributed to improper sample tilting or inaccurate ion milling with focused ion beam (FIB). The corresponding decay of Si2p photoelectron intensity at an exit angle normal to the sample surface is from 17016 counts per second (cps) on thick SiO_2 substrate to 1309 cps on the overlayer of tantalum nitride. The effective attenuation length of Si2p photoelectron in the dense ALD tantalum nitride overlayer can be evaluated using the following model:

$$\frac{I^{overlayer}}{I^{\infty}} = exp\left(-\frac{d}{\lambda sin\,\theta}\right) = exp\left(-\frac{d}{\lambda sin\,90^{\circ}}\right) \quad (2\text{-}6)$$

$$\lambda = \frac{d}{ln\left(I^{\infty}\right) - ln\left(I^{overlayer}\right)} = \frac{9.0}{ln\left(\frac{17016}{1309}\right)} = 3.5nm \quad (2\text{-}7)$$

This estimation is to be used through this work for overlayer thickness evaluation. It is larger than a theoretical prediction of an IMFP about 2.2 nm by the use of TPP-2M equation developed by Tanuma *et al.* [152] and an EAL about 1.8 nm obtained from a NIST database of EAL's based on TPP-2M estimation. But this value is smaller than another empirical estimation of an IMFP about 4.9 nm following Seah *et al.*'s formula. [168] Given the fact that IMFP's usually underestimate the role of the elastic scattering in reducing the free path, the result in this study can be considered in reasonable agreement with the other studies.

It has to be realized, however, that overlayer thickness evaluation with XPS is not free of limitations and artifacts. The overlayer has to be homogeneous in both physical density and chemical composition through the thickness. More importantly, the film coverage has to be uniform in the area to be analyzed. In an island growth mode, which is in fact very common at very low coverage, the XPS evaluation is more or less an averaged thickness, since the substrate signal is attenuated differently from area to area. Even in the island growth, when assuming some simplified surface profile, information about the island coverage can be obtained from the exponential decay of the substrate photoelectron signal at various exit angles. [168],[169]

2.4 Wet chemistry for surface silylation

Surface silylation was attempted with wet chemistry, first as an alternative way to modify the low k surface, then as a path-finding work for future work on dielectric recovery and surface planarization of plasma-patterned porous low k dielectric surfaces.

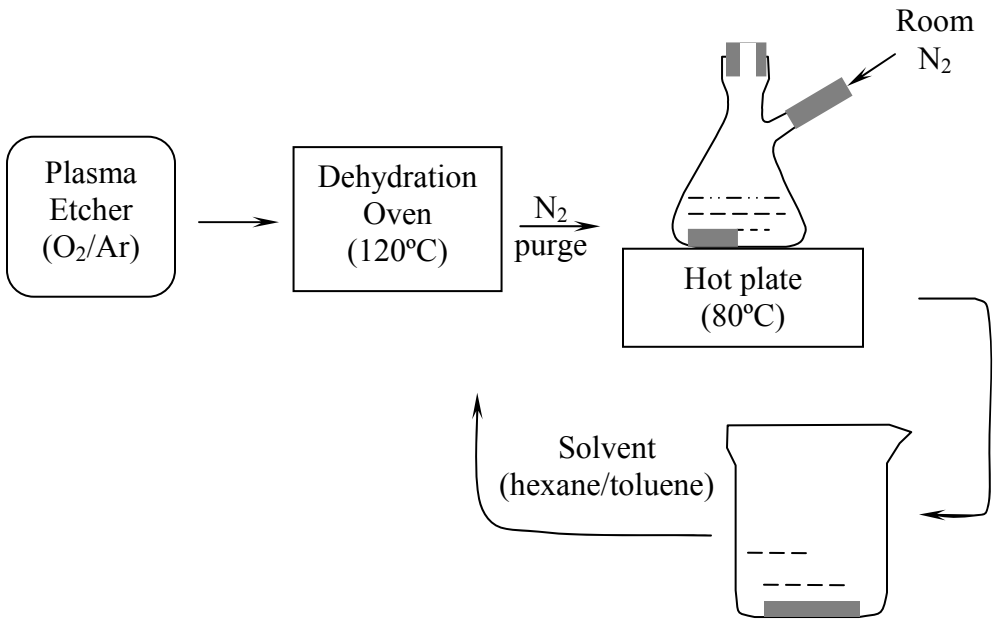

Figure 2-9 Procedures for surface silylation of plasma damaged porous low k dielectrics.

An illustration of the experimental procedures is presented in Figure 2-9. Porous OSG low k films were first subjected to a surface damaging plasma process, which was intended to simulate the possible etch/ashing processes used in actual manufacturing. Since it is a common practice to use carbon fluoride gases balanced with argon for etching and oxygen gas in ashing, an argon/oxygen mixture was used to simulate the two process conditions with varying gas ratios, power level and treatment time in a reactive ion etch (RIE) chamber in the cleanroom.

After plasma treatments, the damaged samples were baked at 120°C in a vacuum chamber for dehydration. They were cooled down to 80°C and brought back to atmospheric pressure under nitrogen purge prior to silylation. All these precautions were taken to prevent moisture uptake, as the silylation agents themselves are very sensitive to moisture. Slight amount of moisture present in the sample or in the local reaction ambient may take the place of the reactive silanol groups on the damaged low k surfaces to react with the silylation agents first.

The actual silylation experiments were done under the direction of Dr. Woon-chun Kim. Silylation agents and their corresponding solvents were obtained from Sigma-Aldrich and Gelest. The silylation agents were stored in small, sealed, amber serum bottles and applied with single use syringes at the time of use to prevent moisture absorption. Most of the silylation experiments were performed at 80°C on a hot plate under constant nitrogen purge. Dehydrated samples were immersed into a silylation agent stirred with a mini stirring bar for a time period from one hour to one day. The samples were then removed from the agent and rinsed with a corresponding solvent to remove the residue. For example, hexane was used for alkyl-substituted disilazanes and chlorosilanes, and toluene was used for phenyl-containing disilazanes and chlorosilanes. Silylated samples were then baked at high temperature (200°C) again to evaporate the solvent.

Various characterization measurements were then performed to evaluate the effects of surface silylation with different agents. Change in the film chemistry was examined with infra-red (IR) absorption spectra using a Nicolet Magna-IR 560 spectrometer. Fourier transform IR (FTIR) spectra were collected on the pristine film, films after plasma processes, after silylation, and after additional high temperature anneal.

For correlation, the surface energies of the films were measured with the contact angle measurements, using three liquids, polar liquid de-ionized (DI) water, glycerol, and non-polar liquid diiodomethane. The polar and dispersive terms of the surface energy were obtained by applying Young-Dupré equation. [170]

For electrical characterization, about 1 μm thick Al(Cu) dots were patterned on these films by shadow masked sputtering. The backside of the films was also coated with about 0.3 μm thick Al(Cu) to improve electrical contact. The dielectric constant and the leakage current were measured on these metal-insulator-semiconductor (MOS) capacitors through capacitance-voltage and leakage current-voltage sweeps. Because these are MOS capacitors, large sweep voltage had to be used to reach the flat band voltage. The dielectric constant was deduced from the flat band capacitance.

To check the compatibility with ALD barrier process, identical ALD deposition processes were carried out on films silylated with different agents and the deposition was examined with *in-situ* XPS.

In addition, cross-section TEM was used to evaluate the pore sealing effects.

2.5 Sample information and preparation

Various organosilicates and SiLK™ low k dielectrics were used in this work. For clarity, information for the samples studied was tabulated in Table 2-2 below.

XPS samples were normaly cleaned with acetone, isopropyl alcohol (IPA) and de-ionized (DI) water [175] followed by outgassing at 350°C for at least 4 hours at low 10^{-7} torr. As the effect of solvent residues on the real substrate surface chemistry became a concern, this procedure was no longer followed. For a reason which will be discussed further in Chapter 4 regarding the roles of atomic hydrogen, OSG films in this work were

no longer cleaned with solvents and DI water; instead, they were simply kept in a clean and dry ambient, cleaned of particles with dry nitrogen blow prior to being loaded into the loadlock, outgassed as previously described and then *in-situ* cleaned with atomic hydrogen. Even for SiLK™ films, which are susceptible to surface hydrogenation and not suitable for atomic hydrogen surface cleaning, the solvent and DI water clean steps were skipped for fear of the artifacts on the substrate surface chemistry. In this case, only high temperature outgassing in high vacuum was used for surface cleaning.

Table 2-2: Sample information

Category	Films	Properties
Oxide	PECVD SiO_2 (SiH_4 and TEOS chemistry)	Dense films
Organosilicates	Black Diamond™ [171]	
	SOD porous OSG	Mean pore size ~ 3 nm, interconnected pore structure
	CVD porous OSG	Mean pore size ~ 1 nm
SiLK™	Dense SiLK™	
	Porous SiLK™	Mean pore size ~ 8.6 nm [172]-[173]
	SiLK™ Y resin	Mean pore size ~ 1.5 nm [174]

Notes: TEOS (tetraethoxysilane) and SOD (spin-on deposition)

Chapter 3: Substrate Surface Chemistry Effect

3.0 Overview

In an ALD process, the substrate can only be seen by the incoming precursor molecules before complete film coverage has formed. Consequently, the substrate surface chemistry effect only manifests in the initial chemisorption of the precursor molecules. Despite the critical role of the initiation process in ALD deposition, studies of the initial growth so far are insufficient. The initial formation of the interface was examined either indirectly by extrapolation from the growth rate in later linear growth region [83],[176] or *ex-situ* with surface sensitive techniques. [75] Growth curve extrapolation has illustrated the difference in growth behavior at the ALD initiation process and the later linear growth region, and how the incubation time changes with the substrate. *Ex-situ* examination with time-of-flight secondary ion mass spectrometer (ToF-SIMS) provided valuable information about the effects of the substrate surface chemistry on the ALD nucleation process, but it could not provide information about the evolution of the surface chemistry and also suffered from possible surface contamination due to the exposure of the deposited films to the air. Lack of *in-situ* surface chemical characterization information caused the previous studies to be either indirect or inconclusive.

This work, for the first time to the author's best knowledge, provides *in-situ* surface chemical information during the initiation of ALD Ta-based barrier processes. It enables understanding of the initial chemisorption process in general and the effects of the substrate surface chemistry in particular. The results obtained on SiO_2, SiLK™, and organosilicate films are to be presented and discussed in this chapter, highlighting the need of surface activation of OSG surfaces before ALD deposition.

3.1 SiO_2

1000Å SiO_2 films were deposited with plasma enhanced chemical vapor deposition (PECVD) processes with either SiH_4 or TEOS chemistry. These dense oxide films were mainly used to establish ALD process conditions. After an *in-situ* atomic hydrogen cleaning process which will be discussed later in Chapter 4, atomic layer deposition of tantalum nitride barrier was implemented with success.

The following graph in Figure 3-1 presents the evolution of the surface chemistry from clean substrate, to that after 80 cycle ALD deposition and that after 200 cycles. As tantalum and nitrogen signals increased, the substrate silicon and oxygen signals decreased, indicating the formation of a tantalum nitride overlayer on the substrate.

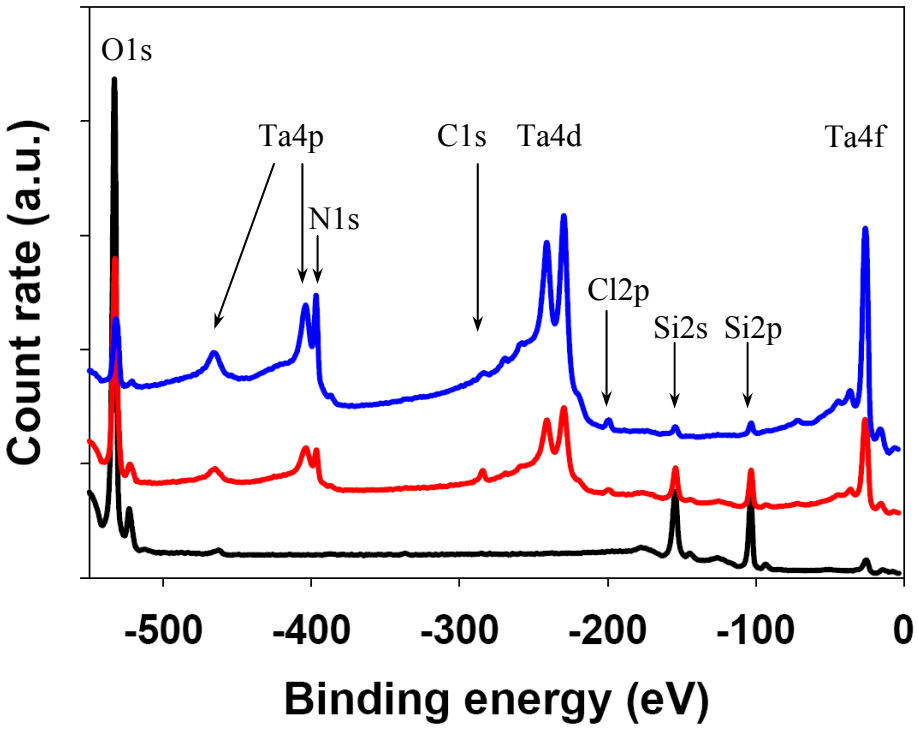

Figure 3-1 Evolution of SiO_2 surface chemistry. From the lowest curve to the top curve, XPS survey curves on clean SiO_2, after 80 ALD cycles and 200 ALD cycles.

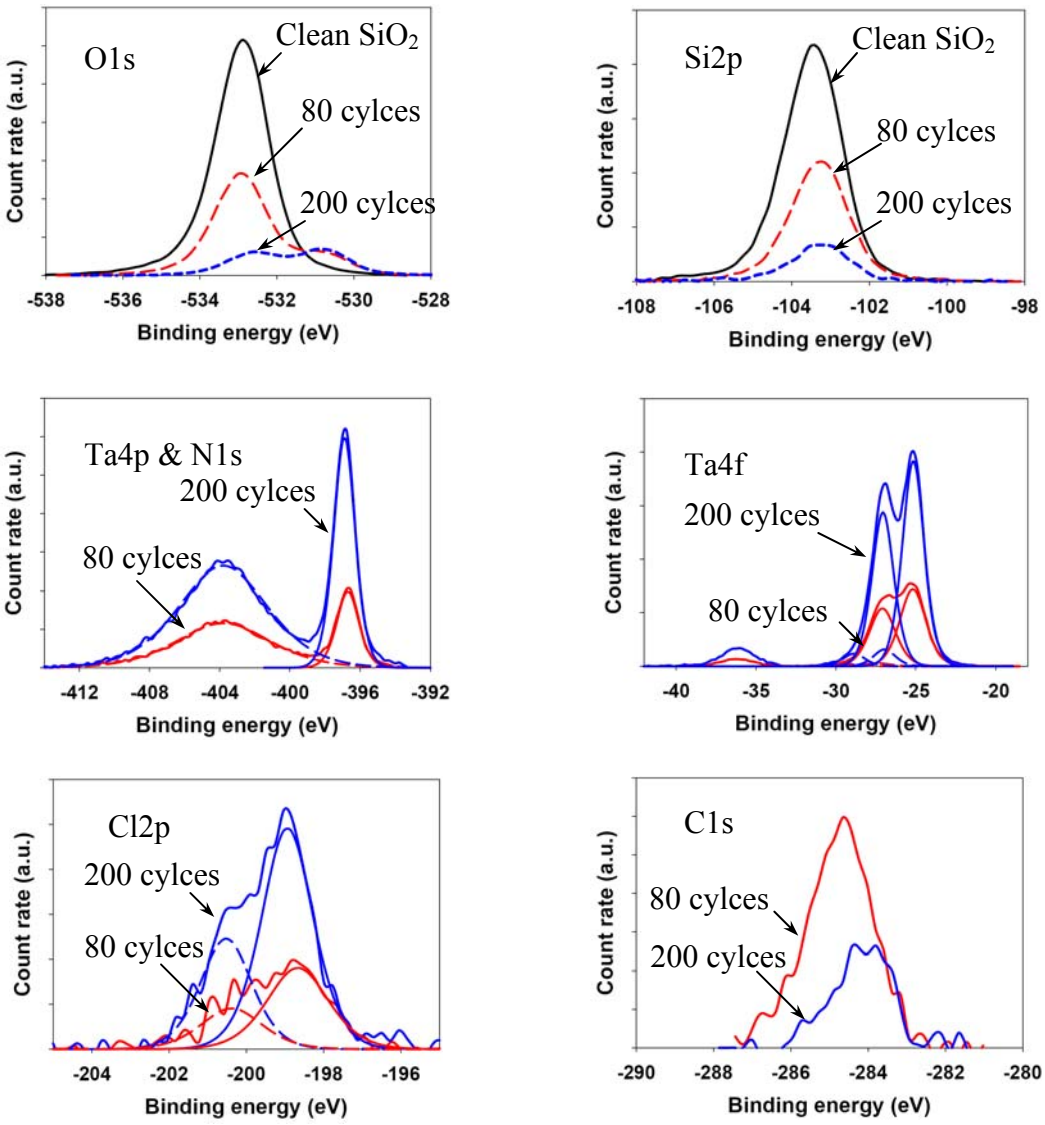

Figure 3-2 Details of the evolution of SiO_2 surface chemistry. Black, red and blue curves are XPS spectra obtained on clean SiO_2, SiO_2 surface after 80 ALD cycles and that after 200 ALD cycles, respectively.

Details of the surface chemistry are examined in Figure 3-2. As more ALD cycles were deposited onto the substrate, the spectra displayed chemical shifts indicating reaction with oxygen to form Ta-O bonding and reaction with ammonia to form Ta-N bonding: development of a secondary oxygen peak in O1s at -530.7 eV [156] and appearance of metal nitride peak in N1s at -397.0 eV, [156] in correlation with the

appearance of tantalum oxide (-26.9 eV) and dielectric tantalum nitride (-25.2 eV) peaks for Ta $4f_{7/2}$. Extrapolating the oxide content to the start of ALD cycles in Figure 3-3, there was oxide formation from the very beginning of the process, suggesting the initial chemisorption was through the formation of Si-O-Ta bond.

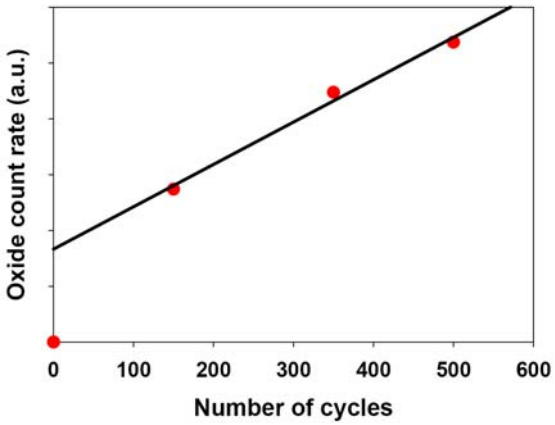

Figure 3-3 Extrapolation of tantalum oxide during ALD process on SiO_2

There were indications of slight carbon contamination and chlorine residues. The carbon contamination is actually of trace amount, most likely due to pump oil vapor condensed in the three way valve controlling the precursor gasline. Further deconvolution of the Cl2p spectra suggested that the chlorine residues were in a single chemical state, for the deconvoluted two peaks had similar full width at half maximum intensity (FWHM) and a theoretical relative ratio between $2p_{1/2}$ and $2p_{3/2}$ 1:2. The binding energy of $Cl2p_{3/2}$ was located at -198.9 eV, which suggested a metal chloride bonding. [156]

To clarify the origins of the undesired impurities which were not supposed to exist in an ideal chloride ALD tantalum nitride process, angle dependent XPS analysis was performed on the sample with 200 cycle ALD deposition. The signal intensities of a "surface" scan at 30° to the sample surface and a "bulk" scan normal to the surface are plotted in Figure 3-4. It can be concluded that tantalum nitride was formed, and that

carbon impurities were incorporated during the film deposition since the C to Ta atomic ratio remained almost unchanged from 0.11 at the surface scan to 0.15 at the bulk scan. Oxygen was also gradually incorporated during the process, as suggested from a nearly unchanged O-Ta to Ta-N bond ratio which showed a slight increase from 0.42 at the bulk scan to 0.50 at the surface scan. Oxygen in O-Ta bonding was used for comparison instead due to failure in deconvolution of Ta-O and Ta-Cl, of which the chemical shift difference is too small to resolve meaningfully.

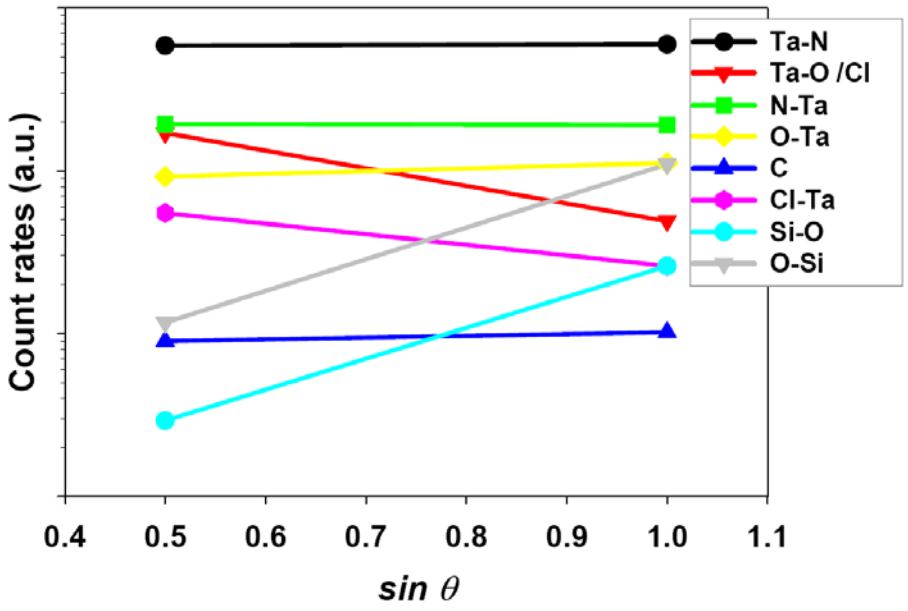

Figure 3-4 Angle dependent XPS results of signal intensities after 200 ALD cycles.

In contrast, chlorine content was rich at the surface, as indicated by a remarkable rise in the atomic ratio between Cl and Ta in Ta-N bonding from 0.14 at the bulk scan to 0.30 at the surface scan. Together with the information obtained in deconvoluting Cl2p spectra (Fig. 3-2) and the fact that chlorine content increased with the number of cycles (Fig. 3-1 and 3-5), we can conclude that the chlorine impurities at our process temperatures above 300ºC were not inherently present due to re-adsorption of HCl byproduct [76],[77],[86] but primarily due to incomplete reaction of $TaCl_5$ at each cycle

and possibly some embedded Ta-Cl bonds which were not reduced by NH_3 due to a possible steric hindrance effect. [76]

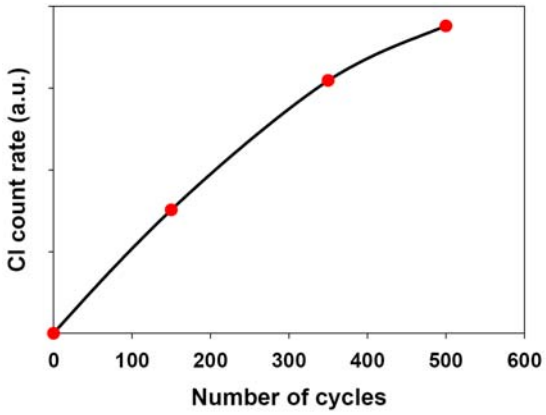

Figure 3-5 Increase of chlorine content with process cycles

Stoichiometric analysis found Ta to N ratio for atoms in Ta-N bonding to be 0.57, which is close to what is in the known dielectric for tantalum nitride, Ta_3N_5. In good agreement, 4-point probe measurement of the sheet resistance was out of scale on this sample too. It is further supported by the high $Ta4f_{7/2}$ binding energy at -25.2 eV. The binding energy is way higher than -22.4 eV for $Ta4f_{7/2}$ in PVD Ta(N) studied previously, [129],[153],[165] suggesting a much stronger nucleus-electron binding in the ALD film. Although the core level binding energy is not a direct measure of the binding exerted on the outer shell electrons by the nucleus, there is supposed to be strong correlation between the two binding forces because the disturbance on the core level binding energy is actually caused by a change in the outer shell electron configuration in forming the chemical bonding with other atoms. As a metal ion loses more free moving conduction electrons to tight binding ionic bonds, escaping core level photoelectrons are experiencing less repelling force from the outer shell electrons. The large positive Ta4f chemical shift in ALD Ta_3N_5 suggested much fewer conduction electrons in the material,

or in other words, more dielectric character than the conductive PVD Ta(N) and elemental Ta films.

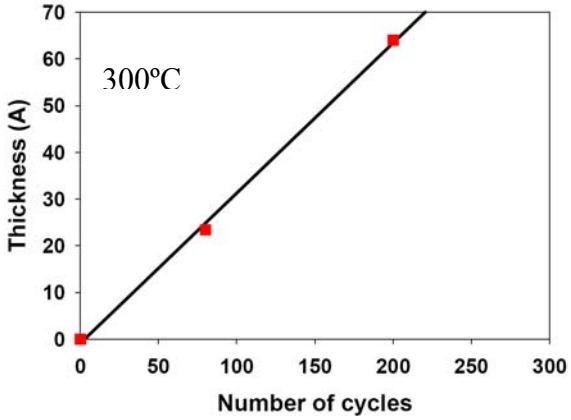

Figure 3-6 ALD growth curve on *in-situ* cleaned SiO_2 substrate

Looking at the growth curve as a whole in Fig. 3-6, there is barely a nucleation region present. No data point was collected beyond 200 cycles, as the weak substrate Si2p signal could no longer be used to calculate the overlayer thickness beyond a certain thickness. The absence of the nucleation process was in fact expected as the *in-situ* surface cleaning with atomic hydrogen beam had exposed reactive surface silanol groups, and these silanol groups were as reactive as the amine terminal groups later present on ALD Ta_3N_5 growing surface. The growth rate was estimated to be about 0.32Å/cycle, which is about 30% higher than normally reported growth rate 0.24 Å/cycle for $TaCl_5$ and NH_3 chemistry. [76],[77] This discrepancy could be attributed to either overestimation of XPS effective attenuation length (EAL) or difference of the experimental conditions, in particular, the substrate temperature and the pulse time for precursor.

3.2 SiLK™ films

SiLK™ and its porous versions, such as porous SiLK™, SiLK Y resin are highly cross-linked polyphenylene thermosets synthesized by the DOW Chemical

Company. [154], [172]-[174] The SiLK™ polymer surfaces contain primarily aromatic carbon with a small amount of ether bonds (C-O-C) [155] as verified by deconvolution of C1s spectrum obtained on a pristine dense SiLK™ film in Figure 3-7. It is made up of a sharp primary peak at about -284.8eV, an ether carbon peak at -286.3eV and π-π^* shake-ups between -290eV and -292eV characteristic of aromatic ring structures. A very small amount of oxygen is present only in the form of ether bonds resulting from the cross-linking processes. Considering the small percentage of oxygen (< 2 at. %), [155] and the inactive nature of ether bonds, study has been naturally focused upon reactions between carbon in the substrate and incoming precursor molecules.

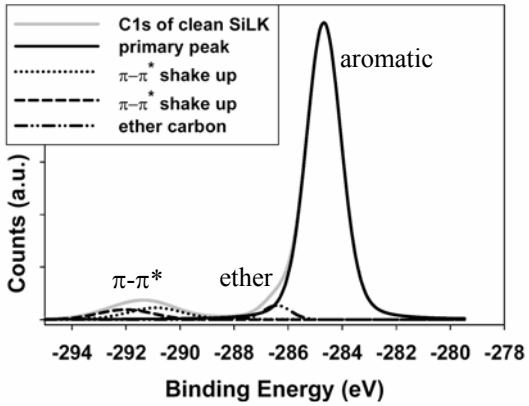

Figure 3-7 Deconvolution of C1s in SiLK™

The evolution of the surface chemistry with ALD deposition is presented in Figure 3-8. ALD tantalum nitride process was found to nucleate readily on SiLK™ films despite the absence of any secondary "carbide" peak throughout the film deposition. Examination of oxide content as shown in Figure 3-9 indicated that oxidation did not play a role in the initial chemisorption of the precursor. Oxygen was simply gradually incorporated into the film most likely due to oxygen impurities in the process gases, in particular, ammonia.

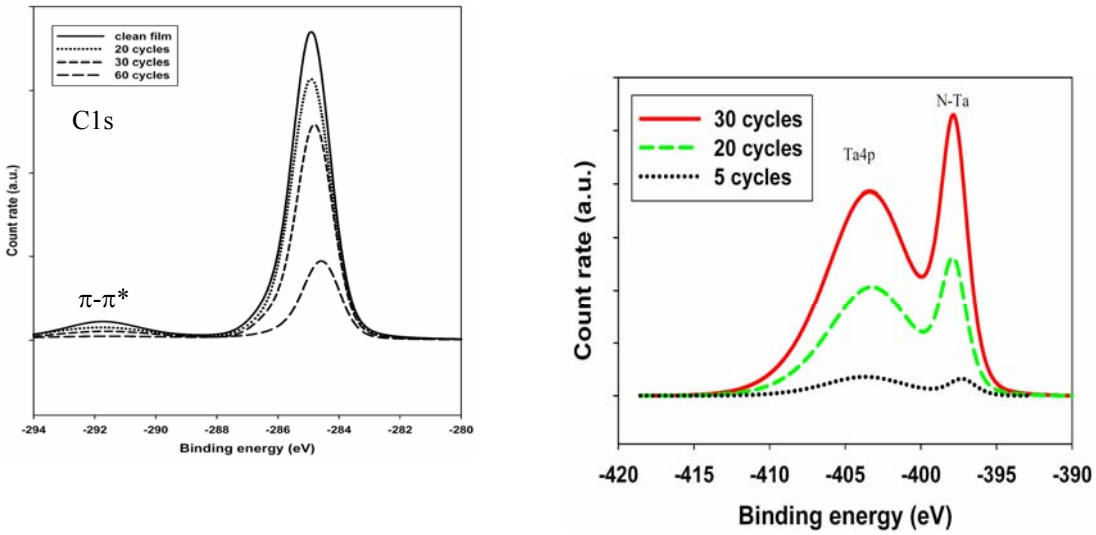

Figure 3-8 Evolution of C1s and N1s during ALD deposition on SiLK™

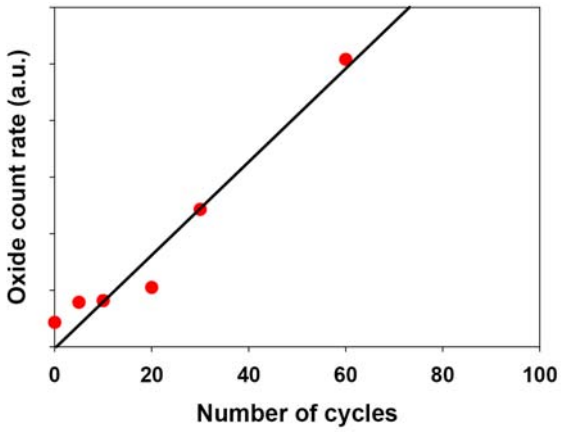

Figure 3-9 Oxide extrapolation during ALD deposition on SiLK™

In Figure 3-8, the π-π* shakeups decreased with Ta deposition but without the immediate appearance of a secondary "carbide"-like peak around -283eV. In fact, no "carbide"-like peak was ever observed at any Ta_3N_5 coverage. All peaks simply decreased in intensity with increasing Ta coverage. It suggested that there was no "strong

chemistry" between $TaCl_5$ molecules and carbon atoms during the initial chemisorption. There is no known substitution reaction between short-chain saturated alkanes and $TaCl_5$ due to the strong covalent C-H bonding (~ 400 kJ/mol or 4.3 eV/bond). [177] Then the observed strong chemisorption must be due to a certain "weak chemistry" between the intact benzene rings and $TaCl_5$ molecules.

Formation of charge transfer complexes by transition metal atoms on aromatic polymers observed and discussed previously in M. Scharnberg's thesis on PVD Ta and Ta(N) processes [165] provides such a mild coordination mechanism. Charge transfer complexes or electron-donor-electron-acceptor complexes provide intermolecular binding through partial electronic charge transfer from π electrons of the donor moieties to unoccupied d orbitals of the acceptor moieties. It is a well documented reaction mechanism between transition metals and aromatics. [178]-[180] Such a coordination of a Ta atom on a benzene ring is illustrated in Figure 3-10.

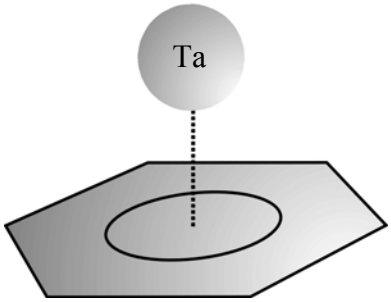

Figure 3-10 Coordination of Ta 5d orbitals with π-electrons on the benzene ring.

During e-beam evaporation of Ta on SiLK™ in UHV (metallic Ta process) and nitrogen ambient (metallic Ta(N) process), the evolution of C1s spectrum with increasing Ta coverage were presented in Figure 3-11. As expected from the polyphenylene structure, C1s spectrum on the pristine film showed a sharp primary peak at about -284.8

eV, an ether carbon peak at -286.3eV and π-π^* shake-ups between -290eV and -292eV which are characteristic of aromatic ring structures. The main aromatic carbon peak decreased with increasing Ta coverage. As the π-π^* shake-ups also decreased and finally disappeared at higher coverages, a secondary peak gradually developed around -283.0eV, corresponding to a handbook binding energy value for tantalum carbide. The disappearance of the π-π^* shake-ups and the appearance of a carbide peak were normally interpreted as an indication of dramatic disruption of the benzene rings and subsequent reaction of Ta with the aliphatic carbon. [181]-[183]

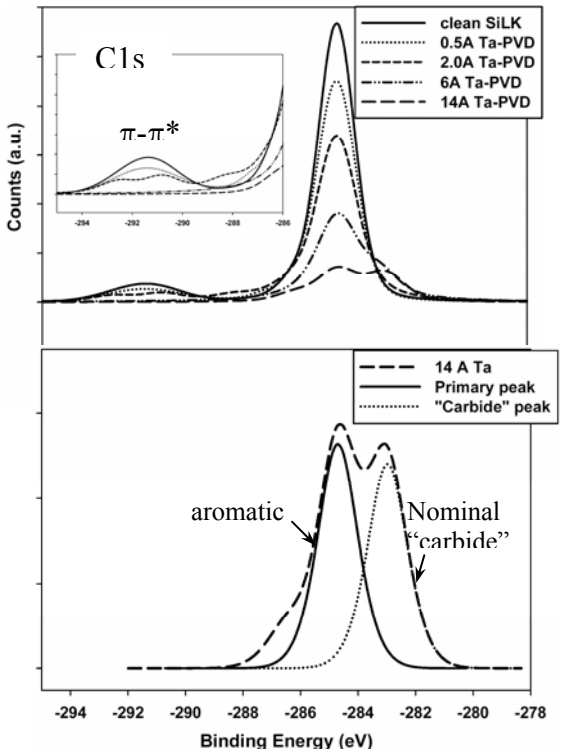

Figure 3-11 Details of C1s evolution during e-beam depositions on SiLK™

However, careful examination of the C1s spectra at very low Ta coverage presented here allows a different interpretation. It would be more reasonable for the

reactions to be interpreted as the formation of charge transfer complexes through a coordination of Ta 5d orbitals with the π-electrons of the aromatic rings of SiLK™.

As shown in the inset of Fig. 3-11, with 0.5Å Ta deposition, the shake-up satellites shifted to slightly lower binding energies of -292.0 eV and -290.7 eV, and the counts in the valley between the satellites and the primary peak increased. The primary peak and ether peak remained unchanged. This observation favors the formation of charge transfer complexes over the carbide formation. The partial transfer of the π-electrons on the benzene rings disturbed the original electronic structure of the benzene rings. With more coordination of the π-electrons to the unoccupied Ta5d orbitals, fewer delocalised π-electrons can form bonding π state; consequently, lower intensity in the π-π* shakeups results from transitions from the highest occupied molecular orbitals (HOMO)- bonding π states to the lowest unoccupied molecular orbitals (LUMO)- antibonding π* states, and less electron density associated with the carbon atoms on the benzene rings increases the binding energy of the photoelectrons to higher than that of the aliphatic carbon (-285eV). If real Ta-C bonds were formed by breaking up the aromatic rings, the shake-up satellites should simply decrease in intensity and eventually disappear, while at the same time formation of a carbide peak on the low binding energy side of the primary peak should be observed around -283eV. Only after 4Å Ta coverage, did a secondary peak at -283.3eV start to develop. Results from molecular orbital calculation [179] revealed that with additional consideration of interactions among coordinated metal atoms, the formation of charge transfer complexes can result in a similar binding energy shift of about 1.8eV from the primary peak position without the assumption of carbide formation.

Similar C1s evolution was observed during e-beam Ta(N) process. Evolution of N1s spectra indicated that nitride did not form upon the arrival of Ta atoms on the surface. The amount of nitride appeared appreciable only after significant amount of Ta deposition (~4 Å). [165]

The observation also illustrated the difficulties in forming a nitride interface on low k dielectrics in general. Because of the strong reactivity of Ta with the low k substrate, the reactions resulted in an unavoidable interface layer of dielectric oxide or carbide prior to the formation of the more desirable conductive nitride layer. [129],[153],[165],[181],[184],[185]

In contrast with PVD Ta and Ta(N) processes, the ALD process saw nitride formed right away on SiLK™ as indicated by the evolution of N1s spectra in Fig. 3-8. It is understandable since nitride formation is the only available reaction pathway for $TaCl_5$ chemisorbed on the low k surface.

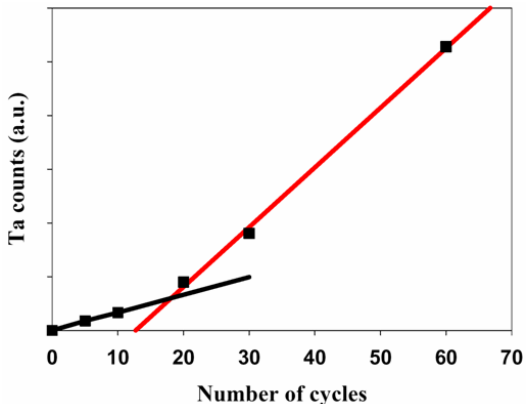

Figure 3-12 Growth of ALD tantalum nitride on SiLK™

With formation of charge transfer complexes with the benzene rings on the substrate, ALD tantalum nitride process was found to nucleate readily on SiLK™ films. A complete ALD Ta_3N_5 growth on SiLK™ film is plotted in Fig. 3-12. It is evident that

an initial transient growth region existed, where part or all of the incoming precursor molecules adsorbed directly onto SiLK™ dielectric surface until forming complete "monolayer" coverage. Subsequent reaction cycles occurred on the newly formed nitride surface, increasing the rate of ALD formation of tantalum nitride. A linear growth behavior was observed as a result of a constant surface chemistry in the subsequent reaction cycles.

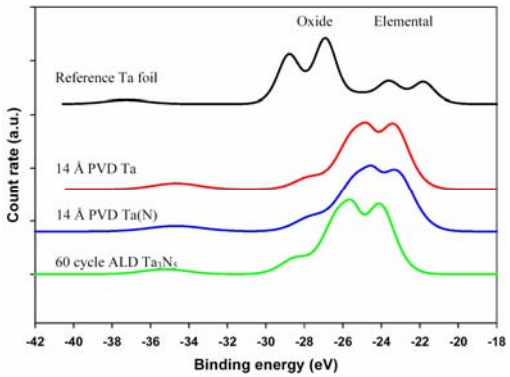

Figure 3-13 Comparison of Ta chemical states in PVD and ALD processes on SiLK™

Again, the nitride formed with ALD was found to be dielectric. To illustrate, Ta4f spectra obtained on thicker barrier films deposited with the three deposition processes are shown in Fig. 3-13 where Ta4f spectrum from a tantalum foil is also included as a reference. The elemental $Ta4f_{7/2}$ has a binding energy at -21.9eV and the peak corresponding to oxide $Ta4f_{7/2}$ is located at -26.9eV. The binding energy of Ta-N bonds in ALD nitride was found again to be about 1eV higher than that of Ta-N bonds in PVD nitride. Stronger binding energy of the core electrons indicates fewer conduction electrons existing in the outermost shell. Higher electrical resistivity was expected. The binding energies of $Ta4f_{7/2}$ electrons in PVD Ta and Ta(N) were very close and about 1eV higher than that in the bulk metallic bcc Ta. The difference in the binding energy of the Ta4f photoelectrons in Fig. 3-13 is an indirect indication of the difference in the

electrical conductivity. It correlated well with the reports [186]-[188] that PVD Ta thin films usually are tetragonal β-Ta, different from the bcc α-phase in the bulk metal. The two phases have very different electrical resistivity, 170-210 μΩ·cm for β-Ta and 20-30 μΩ·cm for α-Ta. The conductivity of PVD Ta(N) decreases with increasing nitrogen incorporation. A low nitrogen phase Ta_2N [189] and a stoichiometric face-centered-cubic (fcc) TaN reportedly have a resistivity of 200-300 μΩ·cm. [188]

Four probe sheet resistance measurements were also performed on samples with thicker barrier deposition to verify the results of the photoemission measurements. Good agreement was found in that the sheet resistance of the ALD nitride film was out of scale, while the sheet resistance for the other PVD barriers was still measurable, in the order of kΩ/□. Stoichiometric analysis with XPS of thicker ALD nitride film found the N/Ta ratio is about 1.6, close to the ratio of the known dielectric phase of tantalum nitride, Ta_3N_5.

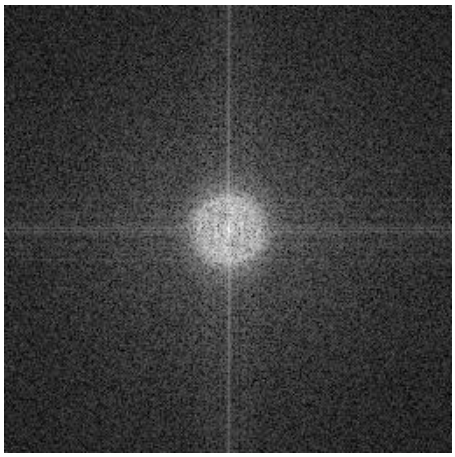

Figure 3-14 Fourier transform of TEM cross-section image of ALD Ta_3N_5 on SiO_2 (Courtesy of Junjing Bao)

Glancing angle x-ray diffraction of a thicker ALD nitride film did not show any crystalline structure. Certainly, this could be due to the weak signals resulting from very thin thickness of the film, which is only a little more than 10 nanometers. Yet it

correlated very well with the Fourier transformed micrograph of a TEM cross section of ALD Ta_3N_5 on SiO_2, which is presented in Figure 3-14. There is no bright spot in this reciprocal space, suggesting no lattice structure or crystalline structure in the real space.

The decay of C1s photoelectrons from the low k substrate in the barrier overlayer provides significant information about the interface and the barrier growth morphology. It is normally evaluated with XPS uptake curves, which are widely used to investigate the thin film growth morphology, to see if the deposited film grows in a layer by layer mode or coalesces into 3-dimensional clusters. [190]-[194]

Signal-time of deposition curve, so called "Uptake" curve, describes the change in adsorbate and substrate XPS intensities with coverage. The area covered by adsobates increases linearly with deposition time or effective film thickness until a full monolayer is formed. At that point, there will be a break in the curve. Ta4f photoelectron intensity was found to be a good measurement of the deposition amount. Up to several nanometers, it is almost linearly proportional to the nominal thickness measured by quartz crystal monitor. The ratio of the overlayer Ta4f and the substrate C1s signals was plotted against Ta4f intensity to get the uptake curve.

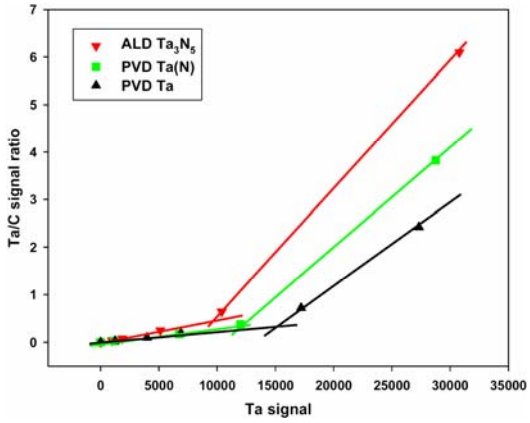

Figure 3-15. Comparison of interfaces formed with PVD and ALD Ta-based barriers on SiLK™

Three uptake curves are compared in Figure 3-15. Taking the transition points as a measurement of the end of the interfacial region, it was found that the interface thickness for the three barriers was equivalent to 3Å, 4Å and 6Å for ALD Ta_3N_5, PVD Ta(N) and PVD Ta, respectively. At the same Ta coverage, the substrate C1s photoelectrons decayed fastest in ALD Ta_3N_5, slowest in PVD Ta, suggesting that the density of the films deposited increase with N incorporation and ALD Ta_3N_5 has the densest structure.

Since ALD Ta_3N_5 could form continuous "monolayer" coverage with only half of the mount of Ta that was needed with PVD Ta, the additional Ta atoms deposited in PVD Ta must have either gone deep into the low k or formed small clusters prior to a continuous layer. Comparing the deconvoluted C1s spectra at 14 Å during PVD Ta in Fig. 3-11, it becomes clear that at similar Ta coverage, there were more interactions between Ta and carbon in PVD Ta process, as indicated by the ratio of the "carbide"-like peak and the primary peak. This suggests an intermixing interface, most likely due to Ta diffusion into SiLK™. Reduced interface thickness together with less interaction among coordinated Ta atoms in the presence of NH_3 [195] can be explained as a result of suppressed Ta diffusion. Absence of any "carbide"-like peak during ALD Ta_3N_5 and the sharp interface indicates limited diffusion of $TaCl_5$ molecules in SiLK™. This can be attributed to less chemical potential difference driving the diffusion in PVD and ALD tantalum nitride processes.

In summary, formation of charge transfer complexes was found to provide better interpretation of the reactions leading to the interface formation during PVD Ta and Ta(N) and ALD Ta_3N_5 on SiLK™ low k surfaces. It is a convenient explanation for the

ready nucleation of $TaCl_5$ precursor on SiLK™. Comparison of the barriers deposited in the three processes revealed that PVD Ta and PVD Ta(N) have similar electrical conductivity while ALD Ta_3N_5 is dielectric. Comparison of the growth morphology indicated good interface of all three barriers on SiLK™. The interface thickness was found to decrease in the order of PVD Ta, Ta(N) and ALD Ta_3N_5, suggesting reduced intermixing region between the barrier molecules and the low k substrate for the ALD process. The absence of "carbide" formation throughout the whole film growth and much less metal-substrate intermixing suggested that a very sharp interface was formed in the ALD process. Despite its dielectric nature which may affect the overall Cu conductivity, in future technology nodes where Cu displacement by barrier thickness becomes a major concern, the sharp interface of ALD Ta_3N_5 with the low k dielectric and its excellent barrier property as suggested by the dense structure still make it a top candidate for ultra-thin Cu diffusion barrier.

3.3 Organosilicates

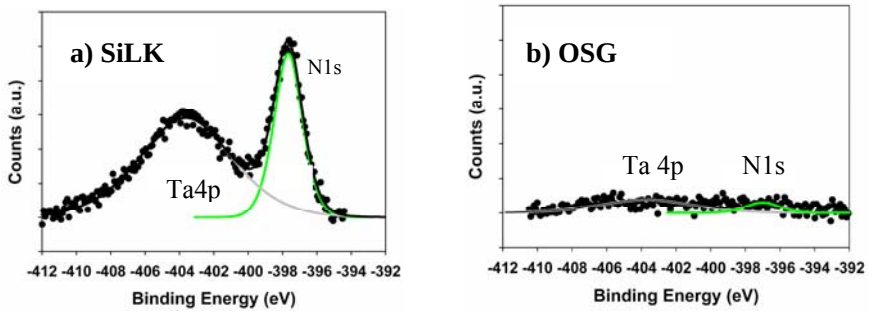

Figure 3-16. Ta4p and N1s spectra on a) porous OSG and b) SiLK™after 80 ALD cycles.

ALD nucleation was found to be distinctively different on organosilicate low k films. After 80 identical ALD cycles, only a small amount of tantalum nitride was formed on a dense OSG film, even less was formed on a porous OSG film, in contrast to the

ready formation of Ta_3N_5 on the SiLK™ film. Because the dense OSG film contains nitrogen in the pristine film, for clarity, only spectra obtained on the porous OSG and SiLK™ are shown in Figure 3-16. There was nearly no well developed Ta4p and N1s peaks on the porous OSG film whereas the corresponding peaks were prominent on the SiLK™ film after identical ALD processes.

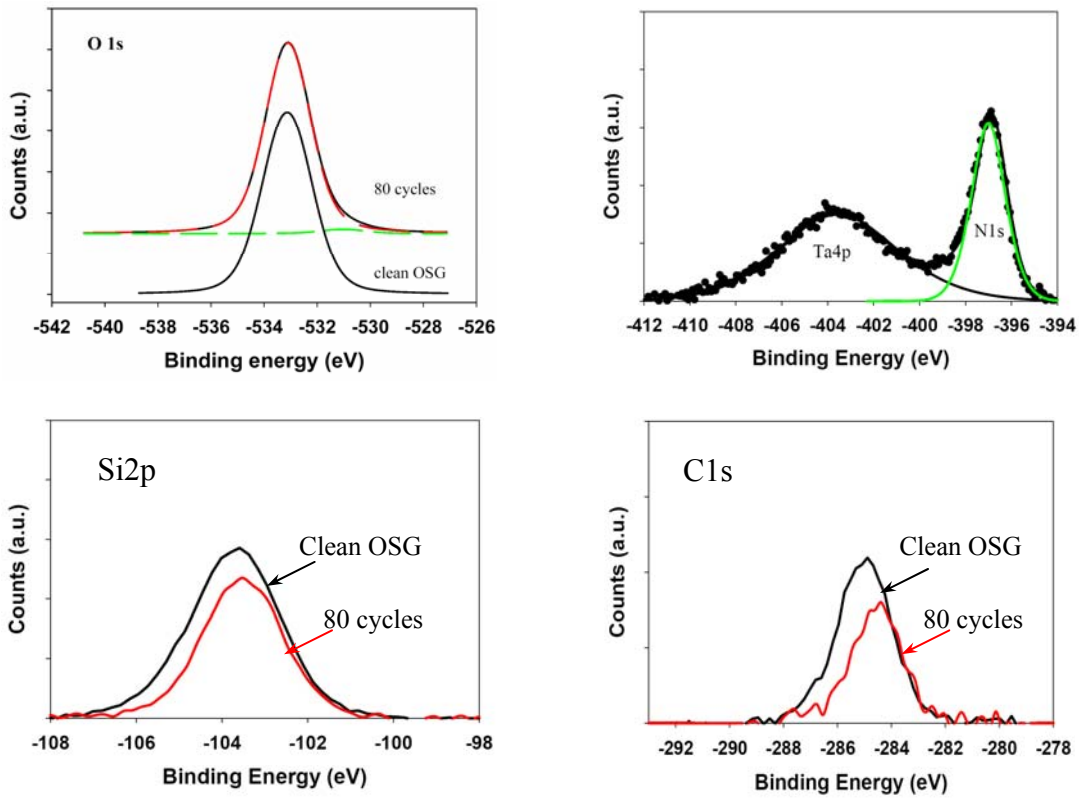

Figure 3-17 Evolution of the surface chemistry on an OSG film

The chemisorption mechanism was studied with the XPS spectra obtained on these films with low overlayer coverage. On the porous OSG film of a mean pore size about 1nm, after 80 ALD cycles a small metal oxide peak developed at -530.6eV while no appreciable changes were seen in Si2p and C1s spectra, suggesting the only possible reaction mechanism is the formation of Ta-O bonding. The Si2p, C1s and O1s spectra were compared in Figure 3-17. The inactivity of the OSG surfaces for $TaCl_5$ nucleation is

likely due to insufficient silanol (Si-OH) terminal bonds on the surface. This correlates well with the observation that the contact angle of water on the porous OSQ was larger than 90º. Even if there were some silanol bonds present on the dense OSG films, the long outgassing and preheating could have annealed the dangling silanol bonds under vacuum where silanol groups (Si-OH) condensed to form siloxane bonds (Si-O-Si).

3.4 Nucleation of PDMAT on organosilicates

Besides the substrate surface chemistry, ALD nucleation process is naturally dependent upon our choice of the precursor. Metallic organic precursors are designed to have reactive ligands that are easy to break. Consequently, better reaction energetics with the surface reactive groups, on the substrate and on the nitride surface alike, is expected for PDMAT ALD nitride process. Indeed, compared with 0.24 Å/cycle the reported growth rate for $TaCl_5$ ALD nitride process above 300ºC, [77] PDMAT ALD nitride process was reported to have achieved a growth rate 0.6-0.8 Å/cycle depending on the process temperature. [77],[86],[196]

The fast nucleation and growth rate of PDMAT ALD tantalum nitride has generated interests in the pathways for its nucleation. In addition to the formation of Si-O-Ta bonding with the surface silanol groups, is it possible for PDMAT precursor to attack the abundant $Si-CH_3$ terminal groups? This has been examined with *in-situ* XPS analysis of the evolving chemical states of the elements.

Presented in Figure 3-18 is a PDMAT ALD tantalum nitride deposition on the porous hydrophobic OSG on which water has a contact angle close to 90° and where $TaCl_5$ could hardly chemisorb as seen in Figure 3-16. Significant deposition was observed after 200 cycles. More surprisingly, although the main part of the growth curve

is linear, when extrapolated to the beginning of the deposition, there is significant deposition in the initial 10 cycles. It suggests another reaction mechanism for nucleation different from oxidation as in the formation of Si-O-Ta bonds with the substrate surface silanol groups, and nitridation as in the formation of N-Ta bonds with the amine groups on the growing nitride surface.

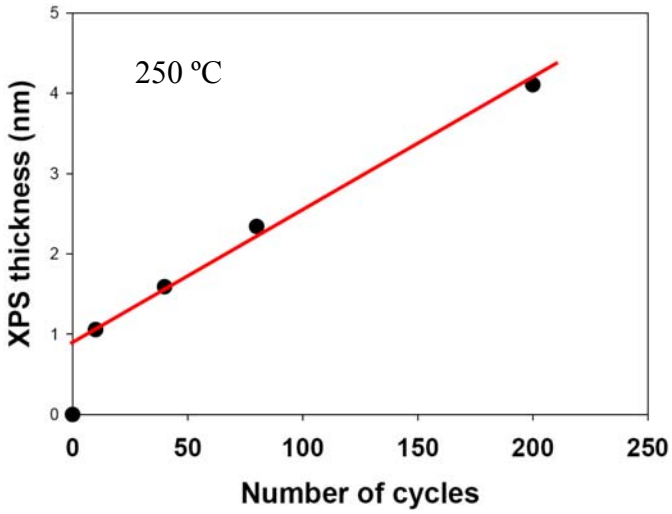

Figure 3-18 Growth of PDMAT ALD tantalum nitride on a hydrophobic OSG surface

The evolution of the chemical states of silicon, carbon, oxygen and nitrogen is presented in Figure 3-19. There are no significant shifts in the silicon (~ -103.2 eV for Si2p) and carbon (~ -284.5 to -285.0 eV for C1s) peaks, indicating no surface reactions involving formation of Si-Ta bonds or Ta-C bonds. Like what is in the pristine OSG film, silicon atoms are still bonded with oxygen and methyl, and carbon atoms are still in the aliphatic bonding environment which is typical in methyl groups. Since there is no obvious disturbance of Si-CH_3 bonds abundantly present on the low k surface, the possibility of additional chemisorption pathways through Si-CH_3 bonds should be excluded. On the other hand, as suggested by the contact angle measurement and the observation of very slow nucleation with $TaCl_5$, the low k surface does not contain a lot

of reactive silanol groups. The much improved deposition with PDMAT must be attributed to a mechanism other than the two surface reaction routes mentioned above.

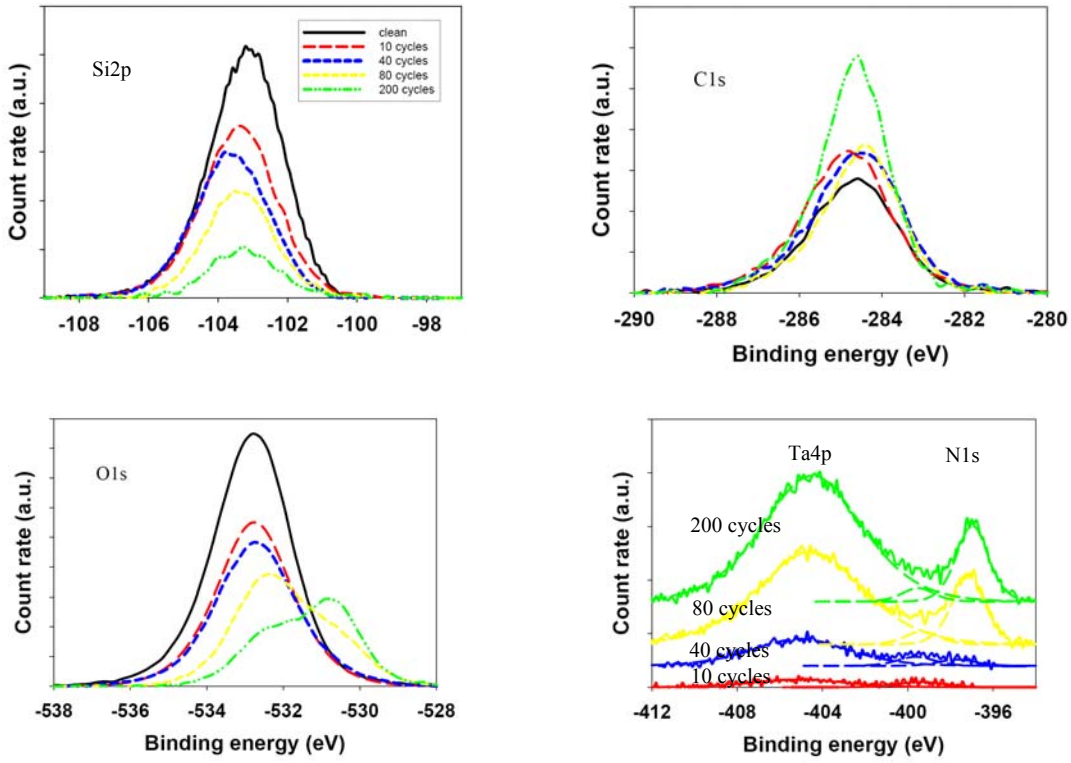

Figure 3-19 Surface chemistry evolution during PDMAT ALD tantalum nitride deposition on a hydrophobic OSG surface

The high ALD process temperature at 250°C and the low decomposition temperature of solid phase PDMAT at 55°C lead to suspicion of the role of the possible CVD component in the apparent fast ALD nucleation. Re-examination of the saturation curve on SiO_2 revealed that the tantalum amount indicative of deposition in fact never saturated. It always increased with the precursor pulse time per cycle. A plot of Ta signal after 80 cycles against the precursor pulse time used per cycle is presented in Figure 3-20. No plateau is present, which suggests a significant amount of deposition was due to self-decomposition which increased linearly with total time of exposure to the precursor.

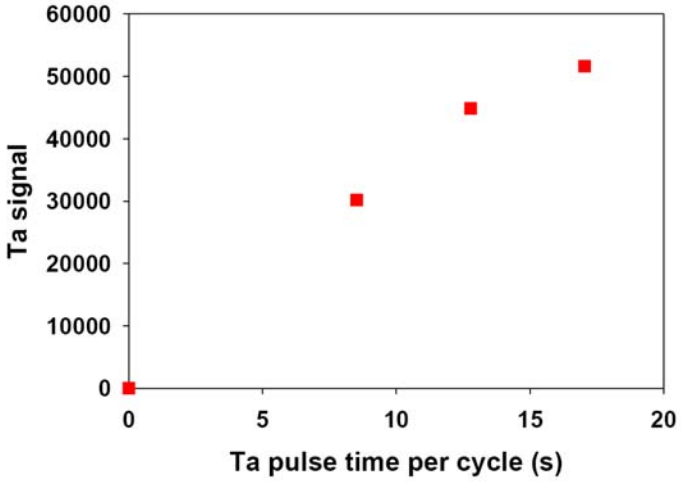

Figure 3-20 PDMAT saturation curve on SiO_2

The standard ALD chemistry for PDMAT precursor produces dimethylamine through a transammination process in Eqn. 3-1.

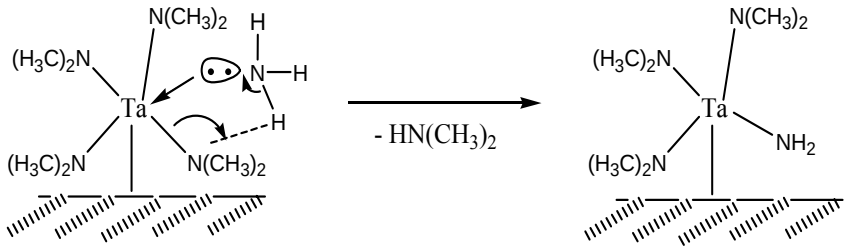

(3-1)

In this standard reaction, carbon can only be incorporated as a result of incomplete reaction, steric hindrance (ligands inaccessible to ammonia) [76], or readsorption of dimethylamine products. According to a quantum chemistry calculation on ALD hafnium precursors, [197] the bond strength of transition metal-alkylamine bonds is about 20% lower than that of metal-chloride bonds. Metal-alkylamines supposedly react with ammonia much more completely and rapidly than metal-chlorides. Since in $TaCl_5$ ALD processes there is only little amount of chlorine residue due to partial reaction, even less carbon residue should be expected in PDMAT process due to incomplete reaction or steric hindrance. This leaves re-adsorption of dimethylamine

products to be the main contribution to the carbon impurities. The dimethylamine residue can also explain the small secondary peak at -399.0eV for N1s. Nevertheless, significant amount of non-carbidic carbon residue in the form of dimethylamine is not imaginable as dimethylamines are very volatile at the process temperature. It is difficult to re-adsorb that much dimethylamine to explain the final carbon to nitrogen ratio about 1:1.

Self-decomposition of PDMAT remains another suspect for carbon impurity incorporation. Absence of carbide formation suggested that any reaction mechanism must be involving non-carbidic carbon. One such reaction pathway is through the formation of an imine ligand which is bonded to a metal center via the nitrogen end (i.e., the Ta←N=C configuration) as illustrated in Eqn. 3-2. Many organometallic imine complexes contain a similar metal-N bonding configuration as reported in the literature. [197]-[199]

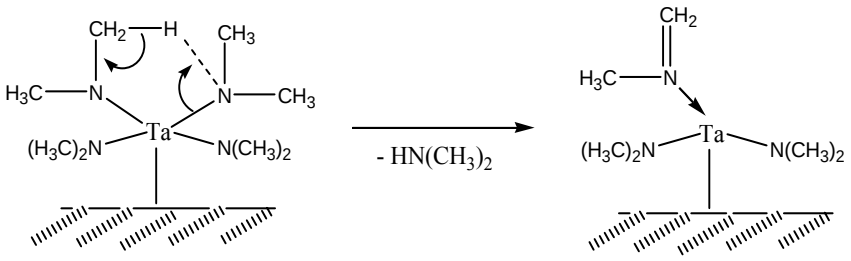

(3-2)

It is suspected that the CVD component as a result of PDMAT self-decomposition could have generated a thin layer over-coating on the substrate surface regardless of the surface chemistry. And this newly formed thin overlayer provides additional chemisorptive sites for more efficient ALD nucleation. It has to be realized though, that this CVD coating is of weaker bonding to the substrate, which may adversely affect the adhesion to the substrate.

In summary, ready ALD nucleation was observed on SiLK™ films. Comparison with previous studies on e-beam Ta and Ta(N) processes on SiLK™ suggested that a mild chemical reaction, formation of charge transfer complexes could be the chemisorption mechanism for the initiation of ALD process on SiLK™ films.

In contrast, varying results were observed on silica-based films, from immediate nucleation on dense SiO_2 to nearly no nucleation on a hydrophobic porous OSG low k film. The ALD nucleation on OSG films was found to be closely correlated to the silanol groups on the low k surfaces. More surface methyl termination, or more hydrophobic a surface, less or slower nucleation was observed on the surface.

The apparently much improved nucleation process with PDMAT could not be attributed to better reaction energetics or any additional chemisorption pathways involving the other terminal groups on the surface, $Si\text{-}CH_3$ groups. Most likely, it was the benefits of the initial self-decomposition of PDMAT precursor under the surface temperature gradient.

Chapter 4: Surface Activation with Radical Beams

4.0 Overview

As discussed in Chapter 3, the surface inactivity of organosilicate low k dielectrics in ALD nucleation is due to inadequate surface density of the only reactive silanol groups. In spite of the critical importance of the initial chemical reactions in controlling the barrier uniformity and morphology, no help is expected from the materials engineering of low k dielectrics, for the inactive organic termination is incorporated for k reduction and surface hydrophobicity which both are more fundamentally essential properties to the successful integration of low k dielectrics. The surface inactivity characteristic of OSG low k dielectrics can only be overcome with a remedy of additional surface activation process.

Plasma pre-treatments with O_2, N_2 and H_2 have been applied to various low k dielectrics for atomic layer deposition of nitride barrier layers. [75],[83],[200] In addition to the enhanced ALD nucleation and growth, a surface sealing effect was also observed when plasmas were applied to microporous (pore size less than 2 nm) low k dielectrics. [86],[126] O_2 and N_2 plasma treatments on CVD organosilicates (OSG) were generally successful in enhancing chemisorption by activation of the low k surfaces with low energy ions and atomic species, but only for some special cases, the underlying low k film retained its dielectric property. While these studies have generated interest in applying plasma induced atomic species for surface modification, the effects on barrier formation on low k surfaces are not well understood, particularly regarding the surface bonds and chemical reaction for initial barrier formation.

In this chapter, application of atomic hydrogen and amine radical beams in activating low k dielectric surface was studied with *in-situ* XPS analysis. Radical beams were intentionally chosen to avoid the physical damage normally caused by more energetic ions and to separate the chemical effects from the physical effects in a corresponding plasma process. Only pretreatment was used in order to focus on the surface activation effect. Other process enhancement effects when applying radical beams during ALD deposition are to be discussed in the next chapter. Although primarily aimed at activating OSG surfaces, radical beam pretreatment was also applied to SiLK™ surface to examine the interactions of radical beams with the surface benzene groups and to provide better understanding of the reactive nature of the radical beams.

4.1 Surface activation with amine radicals

As generally understood and indicated by previous studies of low energy ion mediated nitridation process on orgnaosilicate low k films, [129],[153] the chemical effects during a plasma surface treatment, i.e., formation of nitrogen containing reactive moieties as a result of collisions of impinging gas molecules, nitrogen or ammonia, are able to alter the surface reactivity of OSG films. Based upon these observations, amine radicals obtained from cracking ammonia have been used in this study to activate OSG surfaces. The purpose is to form surface amino groups which are reactive with Ta precursors as they are in fact the chemisorptive groups for the precursor molecules on the evolving ALD tantalum nitride surface.

This surface activation pretreatment was first demonstrated with $TaCl_5$ ALD tantalum nitride process on the dense OSG film. There was preexisting nitrogen in the film most likely incorporated during the plasma enhanced CVD deposition process with

the use of nitrous oxide (N_2O) as one of the mild oxidizers. Samples from the dense OSG were examined with XPS prior to any pretreatments and after each of the beam treatment. The effect of the radical beam pretreatments on ALD nucleation was examined by comparing tantalum nitride deposition after 30 identical ALD cycles on the pristine film and the film after radical beam pretreatments.

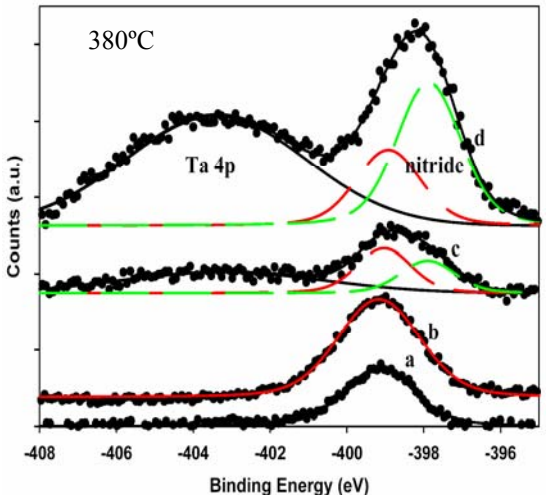

Figure 4-1. Effects of radical pretreatments on ALD tantalum nitride growth on dense OSG low k. N1s spectra
a) of clean surface;
b) after pretreatments;
c) 30 ALD cycles on untreated film; and
d) 30 ALD cycles on pretreated film.

Since two elements characteristic of tantalum nitride, Ta and N, have XPS peaks Ta4p and N1s adjacent to each other around -400eV, it is very convenient to demonstrate the deposited amount of tantalum nitride by presenting the XPS signal intensities of Ta4p and N1s in one graph. Certainly, it involves a lot of deconvolution based on previous knowledge of Ta4p and N1s peaks. [129],[153] The observed evolution of Ta4p and N1s spectra is presented in Figure 4-1. The low k surface had been carefully cleaned with acetone and deionized water followed by outgassing at 350°C for at least 4 hours at low 10^{-7} torr. As indicated by curve 4-1a, there was pre-existing nitrogen in the

original film with a binding energy at -399.0eV, which corresponds to nitrogen in O-Si-N bonding environment. [156] After the film was exposed to 30 ALD cycles, only a small Ta4p peak developed at -403.5eV as a nitride peak appeared at -397.7 eV (curve 4-1c). After the low k film was pre-treated with atomic hydrogen and amine radical beams, its surface was observed to have incorporated a larger nitrogen concentration (curve 4-1b). When the pretreated film was exposed to 30 identical ALD cycles, the tantalum signal was almost tripled (compare curves 4-1c and 4-1d). At this point, the ratio between Ta and Si signals increased from 0.11 to 0.25, indicating that a significant amount of tantalum nitride was already formed.

The surface modifications by the radical beams were quantified by spectral analysis of the XPS peak intensities. The changes of the surface chemical compositions are tabulated in Table 4-1. The slightly different carbon and oxygen concentrations obtained by "surface" (30° exit angle) and "bulk" (90° exit angle) scans of the pristine film indicated a thin overlayer of carbonaceous contaminants existing on the low k surface after the normal cleaning procedure. Atomic hydrogen pre-treatment to the dense OSG low k surface did not cause much surface modifications except removal of the slight compositional inhomogeneity. After additional amine radical and atomic hydrogen were both applied by cracking NH_3, the surface carbon concentration was further reduced to appreciably below the bulk carbon concentration, suggesting depletion of methyl groups from the surface region. Nitrogen enrichment following the beam treatments was observed as expected, since the pretreatments were intended to alter the film surface chemistry by creating more amino surface functional groups to react with the incoming

$TaCl_5$ precursors with an aim to promoting nitride formation. As a result, enhanced nitride formation was clearly confirmed as depicted in curve 4-1d.

Table 4-1: Evolution of Surface Chemical Composition

	Before beam treatments		After H treatment		After N and H treatments ("Surface")
	"Surface"	"Bulk"	"Surface"	"Bulk"	
O	42.7%	40.7%	44.1%	43.7%	44.1%
C	23.6%	25.0%	21.2%	21.0%	16.0%
Si	30.2%	30.7%	30.6%	31.1%	31.6%
N	3.4%	3.6%	4.0%	4.1%	7.0%

Note: The "surface" angle is 30° from the sample surface and the "bulk" angle is normal to the sample surface.

More complete ALD tantalum nitride growth curves on the pristine OSG film and the pretreated OSG surface are compared in Figure 4-2. The growth rate on the pristine film surface was so slow that only one data point was collected to save the precursor. The rest of the growth was simply a linear projection. In contrast, on the pre-treated OSG surface, the growth curve demonstrated typical ALD growth features. It is evident that there existed an initial transient growth region where part or all of the incoming precursor molecules adsorbed directly onto the low k dielectric surface to form one saturated "monolayer" coverage. In this initial transient growth region, radical beam pre-treatments significantly enhanced tantalum nitride formation. However, even with the surface pre-treatments, the growth rate was still lower than that in the subsequent linear growth region. Most likely, this is because the surface density of the added nitrogen-containing moieties did not reach the density of silanol groups on cleaned SiO_2 due to the low material density of low k materials and non-optimized pre-treatment conditions. In the linear growth region, precursor chemisorption occurred on the newly formed nitride

surface. Denser and reactive nitride surface led to an increased ALD growth rate. The linear growth behaviour was a result of constant nitride surface chemistry in the subsequent reaction cycles.

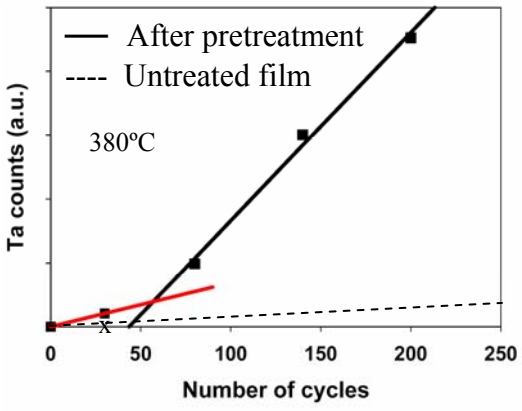

Figure 4-2. Growth curves on pristine and pretreated dense OSG.
Symbol x represents the deposition amount after 30 ALD cycles on the pristine film and the dashed line is the projected growth.

The decay of the substrate Si2p signal can be used to estimate the thickness of the overlayer and the growth rate in the linear growth region. Using a simple exponential decay model described in Chapter 2, assuming a "complete" surface coverage at saturation and taking 3.5 nm as the effective attenuation length for Si2p photoelectrons in a tantalum nitride overlayer, the growth rate was estimated to be 0.019 nm per cycle. This is close to the growth rates previously reported in ALD tantalum nitride processes on SiO_2, [77] but still 40% below the growth rate of 0.032nm/cycle obtained in this work on atomic hydrogen cleaned SiO_2 surface. Nevertheless, this suggested a much improved ALD nucleation on the low k surface resulting from the radical beam treatments.

The close correlation between the amine radical treatment and the enhanced ALD nucleation was further demonstrated by comparing the deposition amount from 80 identical ALD cycles with varying amine pre-treatment time on the dense OSG film. The

curve in Figure 4-3 indicated that ALD nucleation improved with NHx treatment time, and eventually levelled off as the surface was maximally activated.

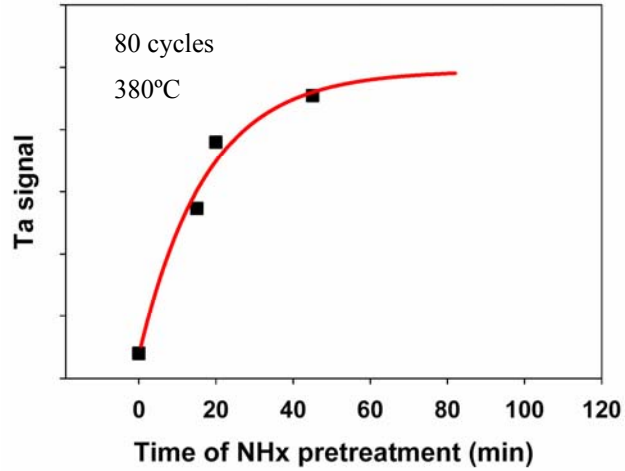

Figure 4-3. Surface activation as a direct result of amine radical pre-treatment.

To investigate the different roles of atomic hydrogen and amine radicals in ALD nucleation enhancement, the amount of deposition from 80 identical ALD cycles was again compared on OSG films pre-treated with atomic hydrogen only and OSG films pretreated with atomic hydrogen followed by amine radical beam. The corresponding Ta4p and N1s spectra are presented in Fig. 4-4. On films pretreated with atomic hydrogen only, 80 identical ALD cycles saw various amount of tantalum nitride deposition, varying from nearly nothing on a porous hydrophobic OSG film in Fig. 4-4a to small amount of deposition on another less hydrophobic OSG film in Fig. 4-4b. Whereas 80 identical ALD cycles produced similar amount of tantalum nitride deposition on all OSG films with additional identical amine radical beam pre-treatment as presented in Figs. 4-4c and 4-4d.

It can thus be concluded that the pre-treatment with atomic hydrogen beam itself did not provide all the surface activation observed, and it was the amine radical beam that made the OSG low k surfaces more reactive with Ta precursor.

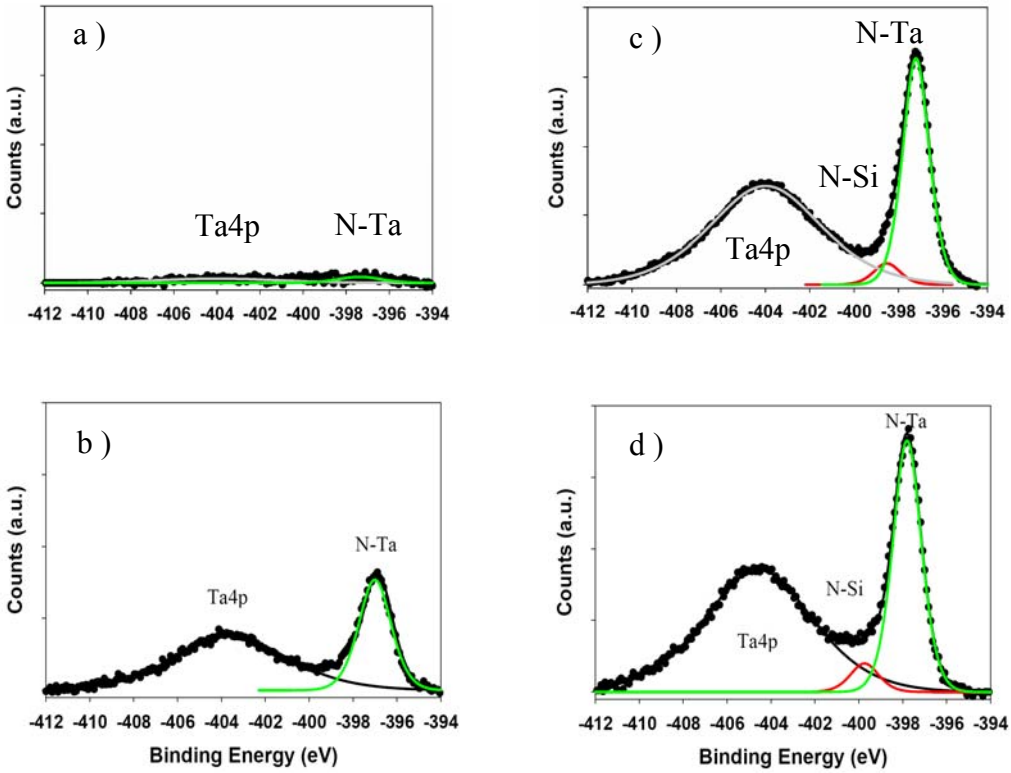

Figure 4-4. Comparison of atomic hydrogen and amine radical pretreatments. a) and c) were on a hydrophobic surface; and b) and d) were on another OSG surface. a) and b) were obtained after 80 ALD cycles with atomic hydrogen pre-treatment, and c) and d) were obtained after 80 ALD cycles with additional amine radical pre-treatment.

While the role of atomic hydrogen in activating the low k surfaces will be discussed further in the following section, the apparent lack of reactions between atomic hydrogen species and the surface groups on the OSG low k films can be explained by the fact that Si-O bonds (~ 800 kJ/mol) [201] are much stronger than Si-H (~ 300 kJ/mol) [201] and Si-CH_3 (~300 kJ/mol) [202] bonds. The only possible reaction with atomic hydrogen is to replace methyl groups with Si-H bonds. However, the newly formed Si-H bonds are not very reactive with Ta precursor either, as the formation of Si-Ta bonding has a much smaller driving force in chemical potential reduction, compared with the formation of O-Ta bonding. [203],[204]

Modification of the OSG low k surfaces by amine radicals is better understood. A possible mechanism is amine radicals replacing methyl groups since the formation of Si-N bond (~ 470 kJ/mol) [201] is energetically preferred. Si-NHx and Si-OH bonds can serve as effective adsorption sites for $TaCl_5$ precursor. As a result, the density of surface adsorption sites was increased, and so was the growth rate.

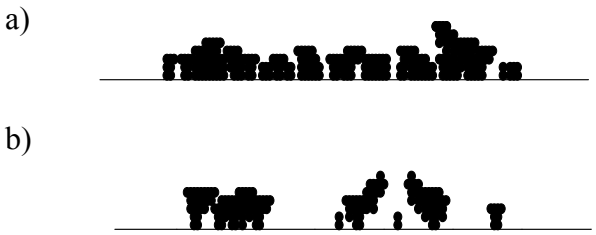

Figure 4-5. Monte Carlo simulation of the effect of surface activation on ALD growth. a) Growth on surface with 50% functionality and b) growth on surface with 10% functionality. (Courtesy of Junjing Bao)

To illustrate the effect of surface activation on ALD growth, a simple Monte Carlo simulation of the initial growth was carried out by Junjing Bao. [205] It is a one dimensional layer of 100 sites, out of which 10% were assumed to be chemisorptive. Of course, the surface functionality varies from film to film. The 10% functionality was assumed on pristine OSG surfaces to account for the number of cycles, normally more than 100 cycles, needed to form a complete coverage on pristine OSG surfaces. 10% reaction probability between $TaCl_5$ and NH_3 was estimated from a more typical growth rate of 0.24 Å/cycle at higher temperature, [77] or 10% of coverage per cycle, and 2.5Å was assumed to be the covalent radius of ALD Ta_3N_5. As shown in Figure 4-5, after the first 10 cycles, clusters were formed around the 10 chemisorptive sites. Suppose surface activation can increase the surface reactive sites to 50%, 10 identical cycles can deposit much more molecules, leading to interconnected clusters, close to a layer-by-layer growth behaviour.

4.2 Surface cleaning with atomic hydrogen

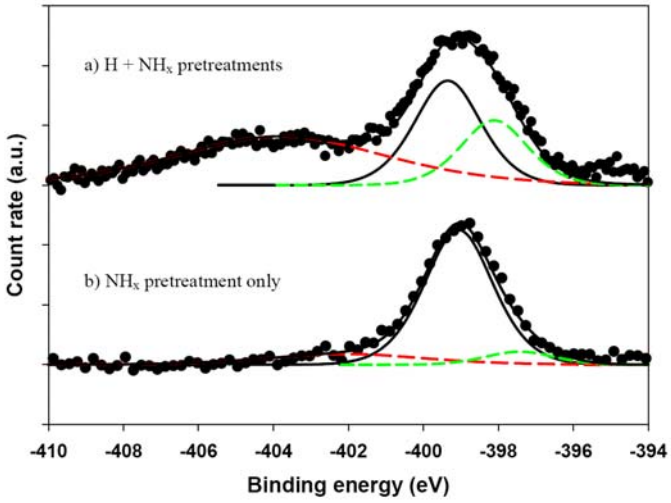

Figure 4-6. Effect of *in-situ* atomic hydrogen surface cleaning.

Before the adoption of atomic hydrogen surface treatment as an *in-situ* low temperature surface cleaning technique, ALD barrier deposition was observed to have shown large sample to sample variation even on samples cleaved from the same wafer. And the deposition rate varied with the shelf time of films. In the worst case, comparing two wafer pieces cleaved from the dense OSG wafer one year apart, identical ALD recipes produced significant deposition on one wafer piece pretreated only with amine radical beam, while not so much deposition on the piece cleaved one year later. Only after insertion of atomic hydrogen pretreatment prior to the amine radical beam pretreatment, was large amount of tantalum nitride observed to form on the pretreated OSG surface. The resulting XPS Ta4p and N1s spectra are compared in Figure 4-6. It is clear that atomic hydrogen pretreatment could remove whichever residues or contaminants accumulated on the surface and what had prevented effective surface activation.

The apparent variation in the surface chemistry from sample to sample can be attributed to surface carbonaceous contamination. And the surface chemistry certainly varied with shelf time and surface cleaning history. Due to the strong sensitivity of ALD barrier process to the substrate surface chemistry, such variation can introduce a lot of uncertainties that are undesirable for the surface chemical analysis of ALD processes and industry-level process development.

During *in-situ* atomic hydrogen pretreatment, the reactive hydrogen atoms can seek unpaired electrons in organic groups with unsaturated carbon bonds. This surface hydrogenation process can produce more volatile organic groups which can be evaporated at relatively low temperature. In fact, hydrogenation of SiLK™ surface during atomic hydrogen pre-treatment has provided an example to illustrate such a mechanism.

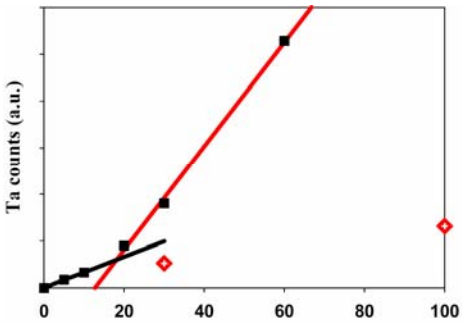

Figure 4-7. ALD growth curves on SiLK™ (red diamonds represent data points with atomic hydrogen step)

It has been observed that radical beam treatments had a very adverse effect on the interfacial adhesion between ALD TiN barrier on aromatic low k films. [75] In this study, without the capability to make adhesion testing samples, the effect of atomic hydrogen beam on the ALD growth rate was examined by inserting an atomic hydrogen step into the ALD process sequence prior to the ammonia step in each cycle. The growth

rate dropped dramatically. The growth curve is compared with that on the pristine SiLK™ film in Figure 4-7.

Table 4-2: Profilometry measurements of SiLK

Exposure time	Film thickness
0	1 kÅ
150 min (H)	0
3 min(H) × 100	0.5 kÅ
12 hours (H2)	1 kÅ

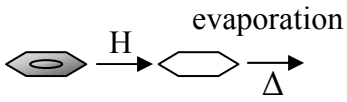

Figure 4-8. Hydrogenation of SiLK™.

The reason for this apparent surface deactivation of SiLK™ by atomic hydrogen was investigated by profilometric measurements taken on films exposed to different dose of atomic hydrogen irradiation. The results are listed in Table 4-2. It is obvious that atomic hydrogen beam can easily etch SiLK™ film away at our process temperature. The film thickness decreased with exposure time to the atomic hydrogen beam. The dramatic reduction in the growth rate is due to either evaporation of the underlying SiLK™ film or loss of surface benzene structures as a result of hydrogenation. According to a previous study by Y. Zhou *et al.*, [75] hydrogenation of aromatics into volatile cycloalkanes (Figure 4-8) is a well known reaction pathway due to the unsaturated π electrons. [206] Based upon these observations in this study and previous studies by other researchers, it can be inferred that surface alkane side groups are inactive in precursor chemisorption and can eventually hurt the interfacial adhesion between ALD barriers and the underlying pristine low k dielectric. In addition, this observation also serves as an evidence of presence of atomic hydrogen since SiLK™ film can remain intact in hydrogen gas ambient.

In spite of the apparent lack of reactions between atomic hydrogen species and the surface groups on the dense OSG film, and its limited role in activating OSG low k dielectric surfaces, atomic hydrogen beam provides a good method for surface cleaning at low temperature. After all, a clean surface is essential for successful chemisorption. [207]

4.3 Radical beam damage on OSG low k dielectrics

Beam induced damage has become a concern for low k process in general and one of the top issues for porous low k integration. Even though much less damage of OSG low k dielectrics is expected from the radical beam pretreatments, the beam damage was investigated with XPS and FT-IR.

The beam damage on the low k films was first evaluated with the ratios between XPS C1s and Si2p signal intensities. Silicon is chosen as the baseline signal because it is the skeleton of the low k structure, and there is no known chemistry for silicon to react with the radicals used in this study. C/Si ratio was used to eliminate any fluctuation in x-ray power output and the multiplier function of the electron analyzer.

The percentage of relative change in C/Si ratio with respect to what is in the pristine films is plotted in Figure 4-9 against atomic hydrogen exposure. The corresponding evolution of C1s spectra is presented along in Figure 4-10. Carbon depletion is very obvious, especially on the hydrophobic porous OSG film. 20 minute exposure to atomic hydrogen beam removed 40% of the methyl groups from the surface. Whereas the dense OSG film demonstrated much stronger resistance against atomic hydrogen irradiation, 50 minute exposure only removed about 18% of the methyl groups. The gradual leveling-off of the damage rate is an indication of the short penetration path of atomic hydrogen, possibly due to fast recombination of atomic hydrogen with one

another. The rapid carbon depletion of the porous OSG may also be correlated to its looser molecular structure. Atomic hydrogen certainly can have a longer diffusion path in it as well.

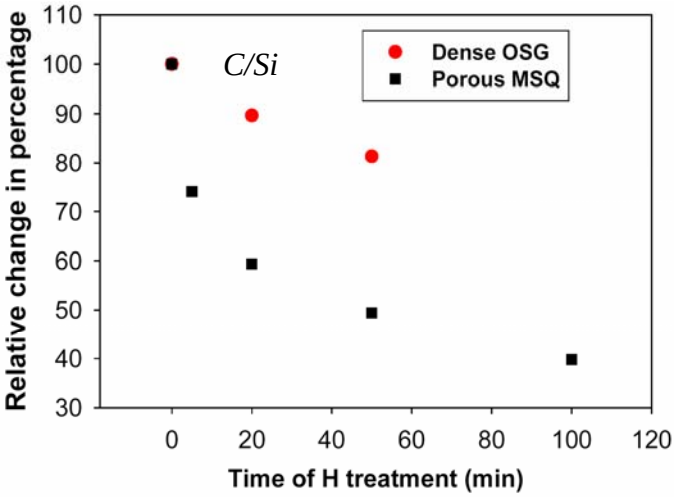

Figure 4-9. Carbon depletion as a result of atomic hydrogen treatment on dense and porous OSG low k films.

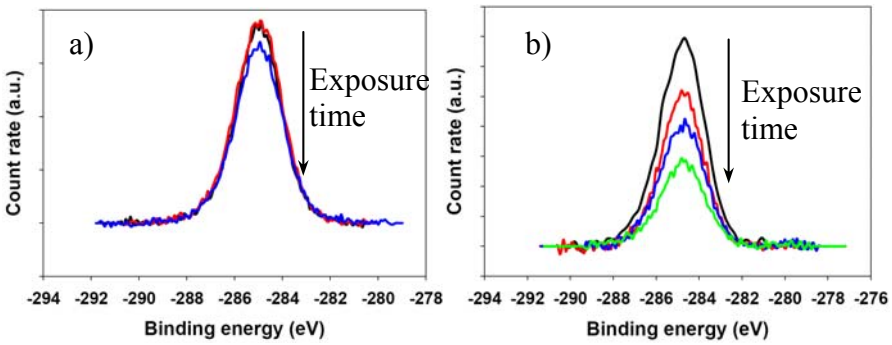

Figure 4-10. Evolution of C1s during exposure to atomic hydrogen. a) dense OSG and b) porous OSG.

Even with so much carbon depletion, there was not much distortion, such as peak broadening and significant peak shifting, on the C1s spectra presented in Figure 4-10. This suggests that atomic hydrogen irradiation is a mild carbon depletion process, which does not involve so much physical impact as to generate many dangling bonds or charged moieties as may be expected from low energy ion bombardment in a plasma process.

Based on these observations, our standard atomic hydrogen clean process runs only for 10 to 15 minutes. And these observations of damage do not limit the potential of applying atomic hydrogen as a surface cleaning technique, firstly because the beam damage is local at the surface region due to the short diffusion path of atomic hydrogen and, secondly, because application of atomic hydrogen will run in tens of seconds in a real process and the resulting damage will not be so severe as presented here.

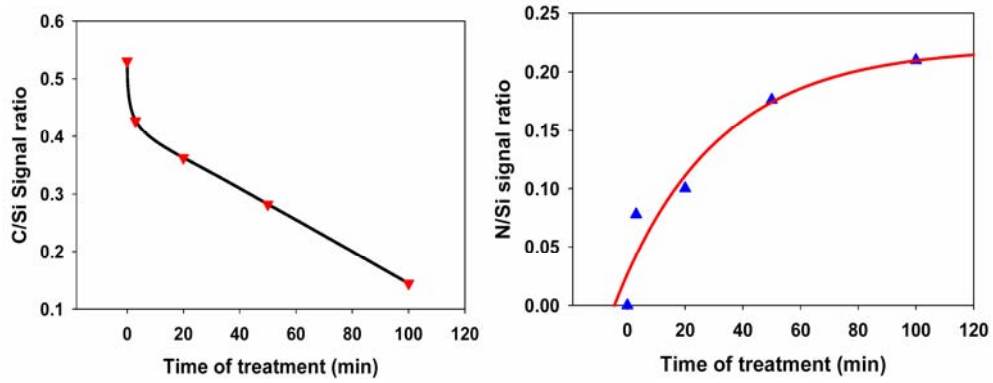

Figure 4-11. Carbon depletion as a result of amine radical treatment on porous OSG low k films.

However, beam damage appears accelerated by the presence of an amine radical. Again, porous OSG films were exposed to amine radical beam for different time periods, and carbon to silicon ratios are plotted against amine exposure in Figure 4-11. With incorporation of nitrogen, carbon concentration dropped very rapidly. In contrast with the gradual leveling-off with H exposure, the carbon depletion resulting from amine treatment seemed to linearly increase with exposure. After a 100 minute exposure, only a very small amount of carbon was left. This could be due to longer diffusion path for amine radicals in the low k films and the stronger attack of amine radicals on Si-CH_3 bonds. The longer diffusion path could be explained as a result of atomic hydrogen recombination. Even though more atomic hydrogen species are generated during the plasma cracking of ammonia, hydrogen atoms tend to recombine with hydrogen atoms,

which could have left the extra amine radicals no other reaction pathway for relaxation but reactions with Si-CH_3 bonds in the low k.

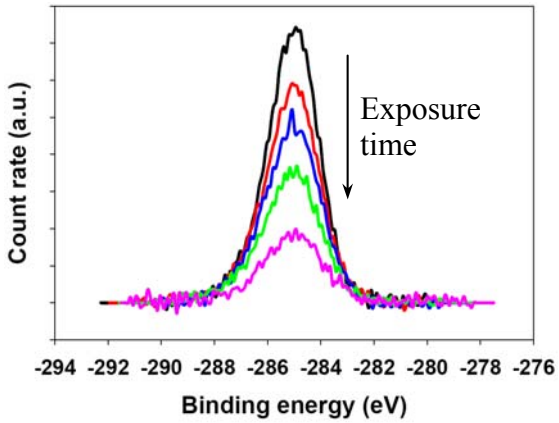

Figure 4-12. Evolution of C1s spectra during amine radical irradiation on porous OSG films.

Again, despite of the aggravated beam damage, the evolution of C1s spectra presented in Figure 4-12 did not show much distortion of the peak shape and much peak shifting. This suggested that the radical beam pre-treatments, even the very reactive amine radical beam pre-treatment, were in fact a much milder surface treatment technique than the corresponding plasma processes.

4.4 Potentials in promoting pore sealing with radical beam pretreatments

As illustrated by a similar Monte Carlo simulation done by J. Bao which is reproduced in Figure 4-13a to compare the initial growths of ALD films on porous inactive surface and activated surface, [208] the pore openings in a sense can be treated as additional inactive areas, and ALD nucleation on the more sparsely distributed chemisorptive sites becomes more difficult deeper into the pores. Consequently, large island growth mode and discontinuous initial coverage are expected, and it takes really large agglomerates of deposited molecules to eventually bridge the inactive areas, or in other words, to seal the porous surface. Even if the pore openings are sealed, the rough

surface resulting from the initial formation of large islands naturally becomes problematic in a subsequent PVD Cu seed process. Resistivity considerations mean that too thick an ALD barrier is not acceptable, so the "valleys" with thin barrier coverage become the weak spots that may crack under stressing and provide pathways for Cu out-diffusion.

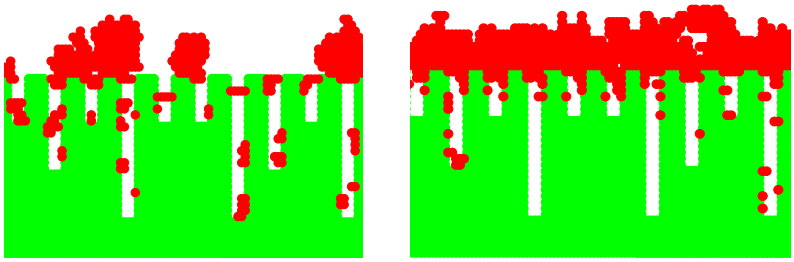

a) 20 cycles of deposition on untreated porous OSG surface

b) 20 cycles of deposition on activated porous OSG surface

Figure 4-13. Monte Carlo simulation of initial ALD growth on porous OSG surfaces, assuming 10% surface functionality for untreated surface a) and 50% for activated surface b) and 2.5 molecule size for the dimension of pore openings. (Courtesy of J. Bao)

The need for pore sealing comes as no surprise as conformal deposition tends to magnify the features underlying a deposition surface. For a super-conformal technique such as ALD, the rough topography caused by big interconnected pores can not be smoothened out during ALD deposition. Worse yet, ALD deposition may magnify the roughness resulting from the substrate chemical topography. It is thus imperative to reduce the dead regions for ALD nucleation, pore openings and other inactive regions. There come two approaches: reduction of the size of openings and activation of the top surface of the matrix material.

The best solution to reduction of the size of pore openings, of course, is through materials engineering. There are reports of new types of low k materials engineered to

have periodic molecular porosity. [209] However, before the pore size distribution can be made sufficiently tight and the mean pore size of uniformly molecular dimensions, it is still up to process engineering to come up with more economical solutions. It was reported that plasma treatments of microporous OSG surface could seal the porous surface against the subsequent ALD deposition. The mechanism behind the pore sealing was often attributed to "good" physical damage to the porous surface such as densification. The bombardment of the low k surface with low energy ions can break the weak organic terminal groups from the silicon skeleton and enhance crosslinking, thus reduce the molecular free volume intentionally incorporated in the low k materials to lower the mass and bond density. So it has to be done very carefully at certain optimal conditions on relative low porosity materials to avoid damage deep into the materials. Considering the possible insertion point for ALD, such materials also require a lot of materials engineering effort.

The above observations of the inactivity of surface alkane groups and the reactivity of silanol and amino groups in precursor chemisorption also suggest to us the potential of using radical beam pretreatments for pore sealing. With radical beam pretreatments, the "benefits" of physical densification are definitely lost. However, the chemically enhanced reactivity of the surface region provides another mechanism for fast closure of the pore openings against further precursor diffusion.

As compared in Figure 4-13, enhanced surface reactivity in the surface region can considerably increase the nucleation sites and the initial growth rate on the exposed matrix material and on the sidewalls of the pores alike. Fast growth from the two

activated sidewalls opposite to each other at the openings can certainly close the openings much faster, leaving a much smoother surface for the subsequent seed process.

The search for experimental evidences of such a speculation was unsuccessful and inconclusive, due to difficulties in procuring proper porous low k materials and failure to perform electron energy loss spectroscopy (EELS) analysis or other electrical testing.

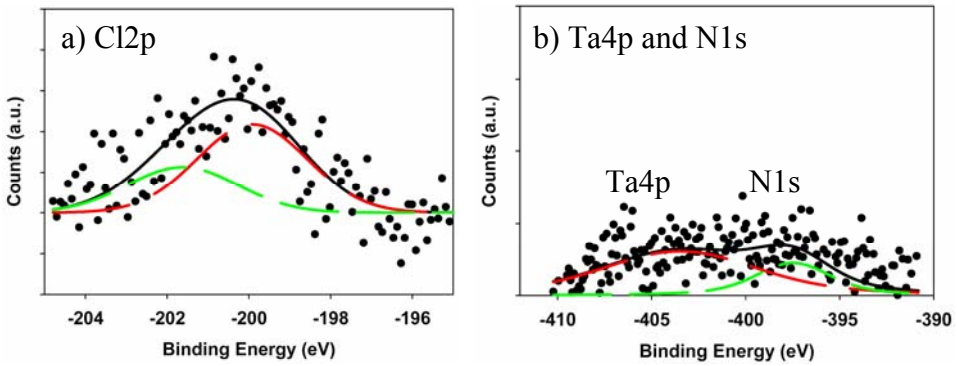

Figure 4-14. No deposition on hydrophobic porous OSG surface after 80 ALD cycles.

Nevertheless, *in-situ* XPS analysis has generated many useful results demonstrating that radical beam pretreatments are promoting pore sealing, if they have not already sealed the pores. As presented in Figure 4-14, on the hydrophobic porous OSG film without any pretreatments, not much chlorine and tantalum nitride signals were observed no matter for how long the ALD process had been performed. It is understandable since most of the surface area and the pore openings are inactive during precursor chemisorption. It was so slow a nucleation process that the precursor penetration was not observed. It also suggested that for the precursor penetration to have any effect in the form of deposition, a significant number of chemisorptive sites have to be present on the sidewalls of pores.

After atomic hydrogen and amine radical beam pretreatments, significant amount of deposition was observed on the film as expected from the surface activation effect. When examining the angular dependence of the ratios between those XPS signals supposedly only present in the over-layer and silicon signal from the substrate film, it was observed that it followed the theoretical model for a uniform over-layer on top of a substrate with clean interface. [151] The results are presented in Figure 4-15. The over-layer signal to substrate signal ratios almost doubled as the photoelectron exit angle went from 90° to 30°. When only a very thin layer is formed uniformly on a substrate, except for common geometrical factors, the over-layer signals do not attenuate much in itself while the substrate signal changes with the sine of the electron exit angle. Island formation or large amount of intermixing usually causes the surface scan ratios to increase much less proportional to $1/\sin\theta$. The good agreement observed with the theoretical model suggested not only a uniform coverage but also absence of significant intermixing between tantalum nitride over-layer and the low k substrate film. This could only have been achieved by suppressed precursor penetration.

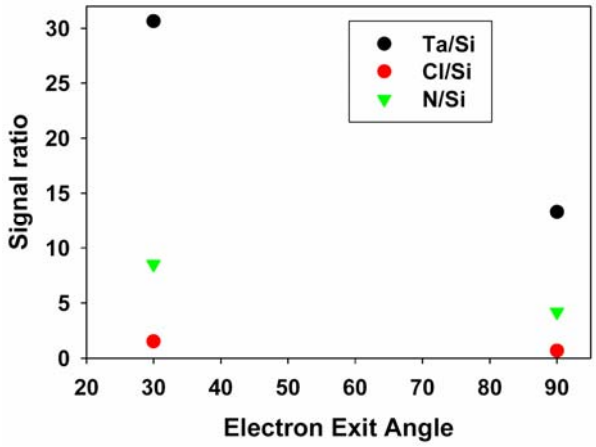

Figure 4-15. Angle-dependent XPS analysis after 80 ALD cycles on the pre-treated porous OSG surface.

The strongest evidence so far obtained for the role of radical beam pretreatments in promoting pore sealing on porous OSG surfaces actually came from in-*situ* observations of PDMAT ALD processes. As compared in Figure 4-16, radical beam pretreatments on the originally hydrophobic OSG film was found to reduce the amount of ALD deposition instead of enhancing it. As discussed in the previous chapter, PDMAT process most likely has a CVD component in the initial nucleation region. This CVD component would leave behind deposition wherever PDMAT precursor was able to penetrate into the film regardless of the surface reactivity or inactivity. Large amount of deposition on the pristine film could be a good evidence of precursor penetration which was already observed on this type of films by E.T. Ryan *et al.*. [126] The reduced deposition as a result of radical beam pretreatments may well be the expected evidence for some degree of pore sealing by surface activation.

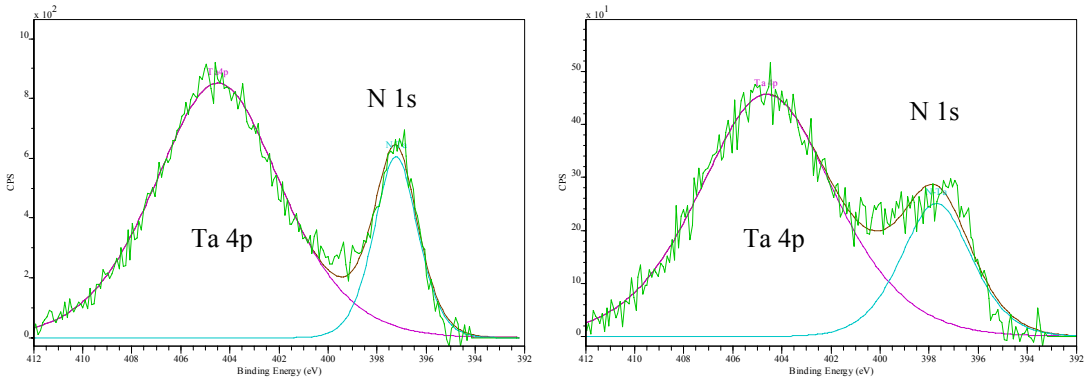

a) On untreated OSG. b) On pre-treated OSG.

Figure 4-16. Comparison of deposition by 80 cycle PDMAT ALD processes on the originally hydrophobic OSG surface

It is understood that such claims require more hard physical evidences other than XPS analysis, such as TEM/EELS [104],[126] or cyclic voltametry [210] to quantify the amount of penetration; and there could be effects of radical beam pretreatments other

than surface activation which are also beneficial to pore sealing, such as improved crosslinking at the process temperature after the terminal methyl groups are partially removed. However, the resources and efforts required for a conclusive understanding of the mechanisms are far beyond what is available for university research.

In summary, radical beams, amine radical beam in particular, can be used for activation of otherwise inactive organosilicate low k dielectric surfaces to enhance ALD nucleation and growth. It has been determined that the enhancement is through methyl depletion from the surface followed by formation of amine moieties on the surface. The replacement can create more chemisorptive sites for ALD nucleation. This also explains the apparent contradictory observations that ALD barrier process is found to be difficult to nucleate on blanket OSG films but never has any difficulties on patterned structures, because the surface treatment involved in the plasma patterning processes has activated the originally inactive surfaces. However, plasma induced damage in porous low k processing has already become a serious concern.

Atomic hydrogen provides an effective in-situ low temperature surface cleaning technique. Pretreatments with atomic hydrogen beam were observed to expose the real substrate surface through hydrogenation of the carbonaceous contaminants which have been observed to be detrimental to ALD nucleation.

Radical beams, atomic hydrogen and amine radicals alike can cause severe damage on porous OSG films when irradiated with an overdose. Dense organosilicates, on the other hand, showed sufficient resistance against such chemical attack.

As reported elsewhere, SiLK™ low k films can not sustain radical beam irradiation without damage, as free radicals were observed to disrupt the benzene structures and form more volatile saturated cyclic alkanes. Atomic hydrogen beam irradiation etched SiLK™ films while at the same time greatly reducing the surface nucleation rate. This is not surprising because that we know that these reaction pathways are indeed etching recipes for SiLK™. The adverse effects of surface hydrogenation of SiLK™ films have provided further evidence for the inactivity of saturated alkanes in ALD nucleation.

In principle, radical beam irradiation selectively enhances nucleation rate in the surface region, as illustrate by simple Monte Carlo (MC) simulation, fast growth at the pore opening can supposedly close the pore openings. This speculation found some support in *in-situ* XPS analysis of PDMAT ALD process on the porous OSG surface. However, lack of electron energy loss spectroscopy (EELS) and metal plating capabilities did not allow further investigation of any physical evidence of such potential in promoting pore sealing in this work.

Chapter 5: Process Enhancements with Radical Beams

5.0 Overview

Plasma enhanced ALD barrier processes were extensively studied in order to achieve deposition at lower process temperature and to achieve better film properties. [96], [210]-[213], [77]-[79] It is understood that the enhancements are primarily due to the chemical reactivity of the highly reactive radicals generated continuously in the plasma processes. Compared with plasma processes, pure radical beams are chemically very reactive while physically less destructive and electrically neutral. This distinct property has generated significant interest in applying radical beams instead of plasma in thin film deposition and for process enhancements. [214]-[218]

Besides the initial surface treatments examined in the previous chapter, other roles of radical beams in process enhancements of ALD tantalum barrier processes also need to be investigated. This chapter presents investigative work on the roles of atomic hydrogen and amine radicals in process enhancements of ALD tantalum barrier processes, including formation of Ta/Ta_3N_5 bi-layer structure with atomic hydrogen, radical beam assisted ALD nitride deposition, chlorine reduction by atomic hydrogen and protection against film oxidation with atomic hydrogen.

5.1 Ta ALD process with atomic hydrogen as the reagent

Although metallic Ta/Ta(N) is the most desirable film stack for copper barrier, low electrical resistivity of the underlying tantalum nitride is not an essential film property. The overall effective Cu resistivity is affected more by the barrier thickness than the barrier resistivity when the barrier resistivity is anyway about 20-100 times (60-200 μΩ·cm[40]) higher than the Cu resistivity (3.5μΩ·cm at 32nm technology node[3]). For

via contact resistance, an anisotropic etch can also be inserted to remove the dielectric barrier at the via bottom on top of the Cu of the underlying metal level. There were process innovations reported to implement PVD Ta flash on ALD dielectric nitride. [64],[91],[100] Despite the harsh reality that a conformal CVD or ALD nitride process produces dielectric nitride film, a lot of effort has been dedicated to reducing the valence state of tantalum in ALD tantalum nitride films from the dielectric valence state (+5) to a more metallic (+3) valence state. The reason to form the dielectric phase in the conventional thermal ALD process is believed to be that ammonia does not have the reducing power to reduce the Ta (+5) in $TaCl_5$ to the metallic Ta (+3) in the cubic[96] or hexagonal[219] TaN. [76] To form any conductive phase of Ta(N) or pure elemental Ta, atomic hydrogen must be provided as the reducing agent, either in the form of silane (SiH_4), [82] methylized hydrazine (N_2H_4) derivatives, [92] neutrals in plasma enhanced process, [96] or in our case, pure atomic hydrogen beam.

Since PDMAT ALD tantalum nitride process contains a CVD self-decomposition component, the resulting carbon impurities make it impossible to obtain metallic tantalum. Most of the attempts to grow more conductive tantalum nitride and elemental tantalum have been focused upon halide ALD chemistry with $TaCl_5$ precursor in particular. Figure 5-1 demonstrates the possibility of using atomic hydrogen beam to reduce Ta in $TaCl_5$ precursor to a metallic valence state and thus grow a Ta/Ta_3N_5 bilayer on the dense OSG film.

In this demonstration, metallic Ta was formed with an atomic hydrogen pulse of 25 seconds taking the place of the ammonia pulse in each cycle. To avoid reactions of tantalum with the OSG substrate film, 200 cycles of thermal ALD Ta_3N_5 was first grown

on the dense OSG film which was cleaned with atomic hydrogen and activated with amine radicals (curve 5-1a). This Ta_3N_5 layer provides not only a good substrate to the formation of metallic tantalum but also a baseline Ta4f spectrum for comparison.

On top of the Ta_3N_5 layer, 200 cycles of radical ALD process was then added where in each cycle, a 25 second pulse of atomic hydrogen took the place of ammonia as the reagent. The resulting Ta4f spectrum is presented in Figure 5-1b. The peak shift was obvious. The primary Ta4f 7/2 peak apparently shifted from -25.3 eV in curve 5-1a to a much lower -22.4 eV in curve 5-1b. After deconvolution, the peak at -25.3 eV which corresponds to Ta-N bonding in Ta_3N_5 actually decreased in intensity and another peak developed at -22.4 eV which corresponds to metallic β-Ta bonding. [153],[165],[40] Lower binding energy of Ta4f photoelectrons suggests that more outer shell electrons have not been lost to other atoms in ionic bonding. Or in other words, the newly formed overlayer has more conductive electrons than the underlying Ta_3N_5 film.

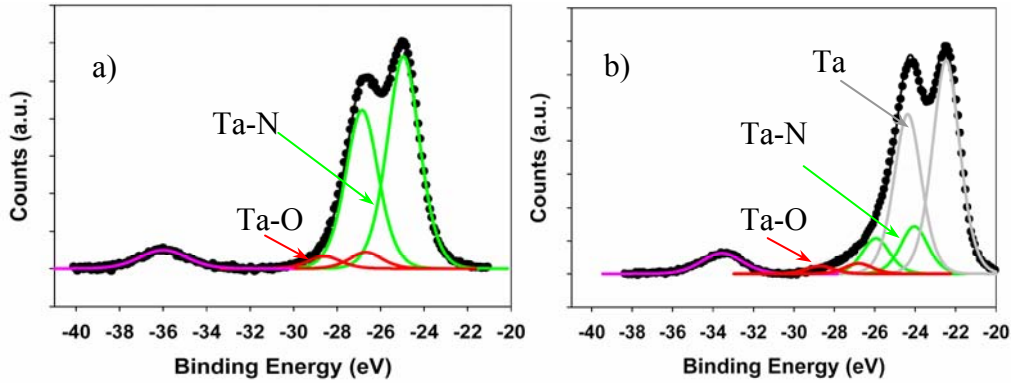

Figure 5-1. Formation of Ta/Ta_3N_5 bilayer on the dense OSG.

Stoichiometric analysis of the surface chemical composition found that excluding tantalum oxide, the tantalum to nitrogen ratio increased from 0.57 after 200 cycle thermal ALD Ta_3N_5 to 1.45 after additional 200 cycle radical ALD Ta process with atomic hydrogen. This observation was better illustrated by the evolution of Ta4p and

N1s spectra which is presented in Figure 5-2. During the additional 200 cycles of radical ALD process, Ta4p signal intensity increased a lot, and like the Ta4f peaks, Ta4p shifted to much lower binding energy, from -404.0 eV to -401.6eV. N1s peak only showed slight decrease in intensity due to decay in the additional overlayer. Obviously, much more tantalum in a more conductive state was formed above the originally dielectric Ta_3N_5 film surface. Besides nitride, there were only small amounts of oxide and chloride impurities present in the film. As confirmed in Figure 5-3, the oxide amount did not increase during the radical ALD process. Therefore, it was elemental tantalum that was formed during the radical ALD process.

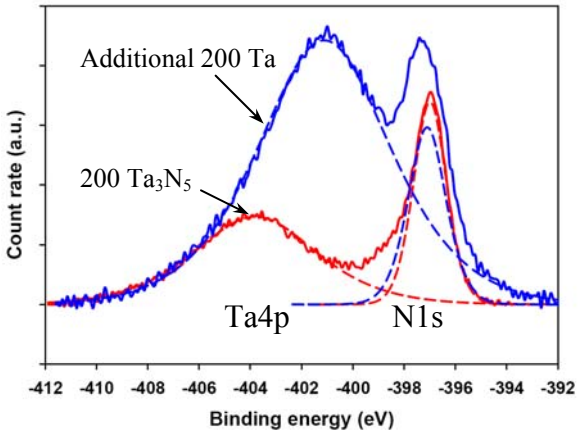

Figure 5-2. Evolution of Ta4p and N1s. Red curve was obtained after 200 cycle thermal ALD process and blue curve after additional radical ALD process.

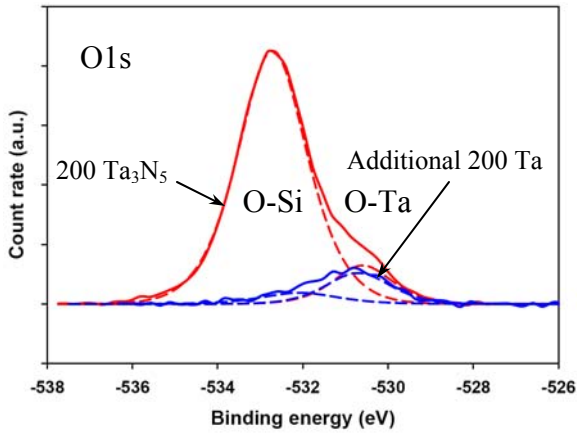

Figure 5-3. Comparison of oxide formation

The resistivity of the ultra-thin barriers as deposited was then checked with 4-point sheet resistance measurement. The sheet resistance dropped from infinity on films deposited by 400 cycles of thermal ALD Ta_3N_5, to 2.25 kΩ/□ on the bilayer structure formed in the above process. This correlated well with the XPS observations. The corresponding resistivity number was not available because the conductive film thickness was less than 5 nm due to surface oxidization.

The above processes were carried out at 330°C. At this temperature, there was no known reaction between $TaCl_5$ and H_2. Ta CVD process involving $TaCl_5$ and H_2 was reported to only occur above 900°C. [210] So the reaction to form metallic Ta naturally involved species far more reactive than molecular hydrogen. Since the only reagents present in our process were atomic and molecular hydrogen, the reagent involved in the observed Ta ALD process must have been atomic hydrogen, and the reaction can be simply:

$$TaCl_5 + H \rightarrow Ta + HCl \qquad (5\text{-}1)$$

It can thus be concluded that atomic hydrogen can be used to produce metallic Ta forming ALD Ta/Ta_3N_5 bi-layer barrier stack. This agrees well with the reports on H_2 plasma enhanced CVD Ta process using $TaBr_5$ at 450°C, [211] and H_2 plasma enhanced ALD Ta processes using $TaCl_5$ at less than 300°C. [222] However, applications of halide ALD chemistries are facing severe process compatibility issues. HF by-products from TaF_5 may etch the underlying OSG low k and HCl by-products may cause Cu cross contamination by forming volatile $CuCl_2$. [76] With so many overwhelming materials issues involved in Cu/low k integration, the industry is rightly conservative against halide ALD chemistries. It is safe to claim there is no Cu-compatible ALD Ta process so far.

5.2 Radical beam-assisted ALD tantalum nitride process

Radical beam as reagents have many benefits. The high chemical reactivity of radicals can improve the reaction energetics as much as a corresponding plasma process will do. The exclusion of energetic ions from radical beam prevents impact-induced dangling bonds deep in the bulk of the film deposited. And in the case of porous low k substrate films, it also avoids plasma damage to the substrate low k films.

Using a radical beam obtained from cracking ammonia gas in ECR plasma, a radical-enhanced ALD (RE-ALD) Ta_3N_5 process was demonstrated and compared with the thermal ALD process at 300°C.

Compared with the thermal ALD process, there was not much difference in the experimental conditions except that a 10 second radical beam pulse took the place of 5 second ammonia pulse in each cycle. So the new pulse sequence in each cycle became 2 second argon purge, 14 second $TaCl_5$, 3 second argon purge, 5 second evacuation followed by 10 second radical beam.

Note the fluence of ammonia in the thermal process was different from the fluence of amine radical beam in the RE-ALD process. It was not well quantified due to the lack of a mass spectrometer. The process pressure for the RE-ALD process was maintained at 2 mtorr while it was 20 mtorr for the thermal ALD processes. So the exposure dose to amine radical beam 20 mtorr·second was supposed to be comparable but smaller than the exposure dose to ammonia which was 100 mtorr·second. Also, there was ammonia neutrals present in the beam coming out of the plasma chamber as a result of either incomplete dissociation or self-recombination. The RE-ALD process actually may always contain a thermal ALD component. In addition, atomic hydrogen species were

present resulting from cracking ammonia into amine radicals and atomic hydrogen. A certain portion of reaction involving atomic hydrogen species was expected. Accurate analysis of such complex reaction mechanisms was impeded by the lack of reliable quantification method of the beam composition.

Nevertheless, difference between two such processes can still tell us whether RE-ALD process is possible with such process conditions, and the comparison between the two processes can demonstrate the process enhancements expected of amine radical and atomic hydrogen reagent.

To focus on the process enhancements due to an improved reaction energetics, the processes were carried out on SiO_2 substrate which was cleaned with atomic hydrogen to eliminate any other effect due to surface activation. And 80 cycles of ALD Ta_3N_5 process were put down first to further exclude any substrate surface chemistry effect. On this newly formed ALD Ta_3N_5 film, deposition by 120 cycle ALD process using radical beam as the reagent is compared with that by 120 cycle thermal ALD process. The resulting growth curves are presented in Figure 5-4.

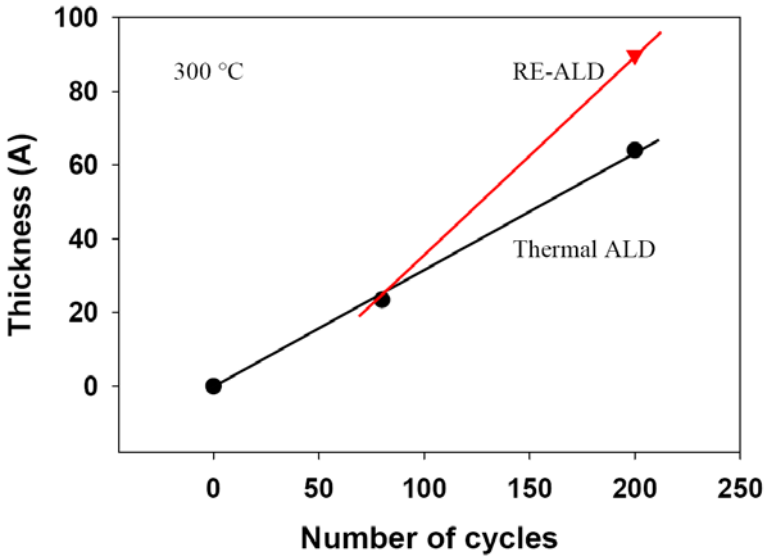

Figure 5-4. Comparison of RE-ALD and thermal ALD Ta_3N_5 processes

In the graph above, higher growth rate was observed in the RE-ALD segment. Compared with about 0.32Å/cycle in the thermal ALD process, the growth rate increased to 0.54Å/cycle with amine radicals as the reagent. Consequently, the substrate signals, O1s in O-Si bonding and Si2p decayed more in the thicker film deposited by the RE-ALD process as shown in Figure 5-5. This was expected since the amine radicals and atomic hydrogen species are more reactive than ammonia.

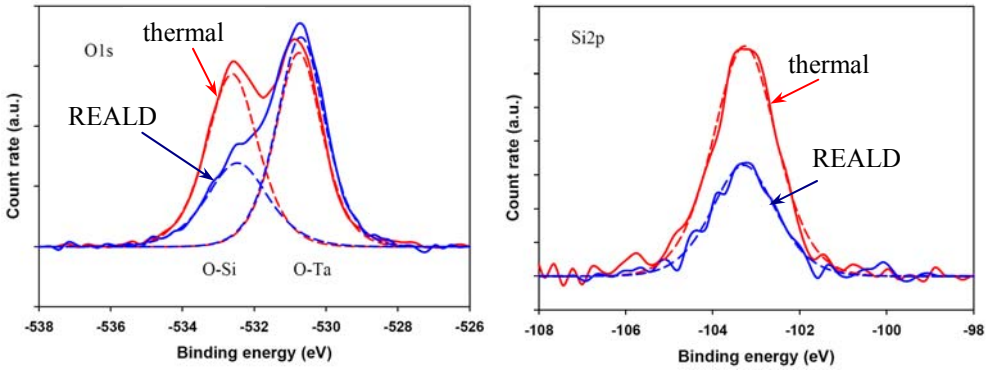

Figure 5-5. Comparison of O1s and Si2p signals in thermal ALD and RE-ALD processes.

Ta4f spectra obtained after 80 cycle thermal ALD process, additional 120 cycle thermal ALD process and additional 120 cycle RE-ALD process are compared in Figure 5-6a and 5-6b. In the thermal processes from 80 cycles to 200 cycles, $Ta4f_{7/2}$ peak of the Ta4f doublet in Ta-N bonding environment remained at -25.2eV, and the atomic ratio between tantalum atoms in such bonding to nitrogen atoms was found to be 0.59 which was very close to the theoretical ratio of 0.60 in Ta_3N_5. In contrast, after the 120 cycle RE-ALD process, the Ta4f doublets in Ta-N bonding environment can be deconvoluted into two pairs of doublets. One pair has $Ta4f_{7/2}$ at -25.2eV and the other has $Ta4f_{7/2}$ at -24.2eV. The atomic ratio between tantalum atoms in such bonding environment and nitrogen atoms was found to have increased to 0.68. The deviation from the stoichiometric tantalum to nitrogen ratio in the deposited nitride film and the lower Ta4f

binding energy indicated that a slightly more conductive nitride phase Ta(N) was formed in the RE-ALD process and less nitrogen content was incorporated than in Ta_3N_5.

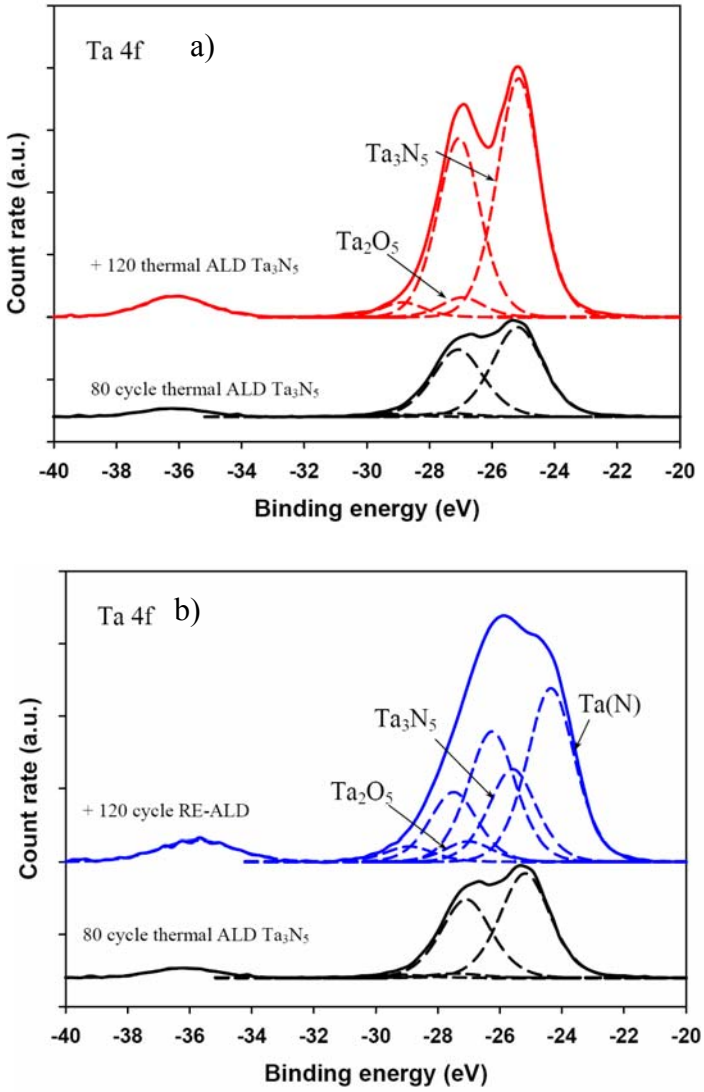

Figure 5-6. Evolution of Ta4f spectra in thermal ALD and RE-ALD processes.

Besides the standard ALD chemistry with ammonia which produces Ta_3N_5, the other possible reactions could have involved amine radicals and atomic hydrogen:

$$TaCl_5 + NH_x \rightarrow Ta(N) + HCl \quad (5\text{-}2)$$

$$TaCl_5 + H + NH_x \rightarrow Ta(N) + HCl \quad (5\text{-}3)$$

In the Ta4f spectrum obtained on the film deposited in the above RE-ALD process, the Ta4f doublets with $Ta4f_{7/2}$ at -25.2eV can be attributed to the standard thermal ALD chemistry with ammonia while the Ta4f doublets with $Ta4f_{7/2}$ at -24.2eV can be attributed to the reactions involving amine radicals and atomic hydrogen species.

5.3 Reduction of chlorine content with atomic hydrogen

It has been observed that the chlorine impurities came from incomplete reaction between NH_3 with $TaCl_5$ in one ALD cycle. As presented in Section 3.1, the chlorine impurities were present in the form of Ta-Cl bonding. Its amount increased with the number of cycles and eventually saturated at a certain level depending upon the process conditions. The bulk chlorine impurity content was far less than what was present on the evolving nitride surface. All these observations are pointing to the incomplete reaction of ammonia with $TaCl_5$ as the origin of chlorine with negligible steric hindrance effect. Steric hindrance can not be a main factor because the chlorine impurities were much richer on the surface which was supposed to be easier to access for the incoming ammonia molecules.

According to the thermodynamics that governs chemical reactions, given sufficient time, unlimited supply of reactants and constant removal of by-products can push the chemical equilibrium as close to completion as possible. For ALD processes under such circumstances, volatile by-products can be removed very efficiently and proper reactant gas partial pressures can be maintained. The reaction will keep going until one of the residual reactants is used up. In the case of $TaCl_5$ ALD chemistry, fresh ammonia molecules can keep reacting with residual $TaCl_5$ until no $TaCl_5$ is left. Practically however, the pulse duration for ammonia can not be very long for economical

reasons. Because the reaction for halide ALD chemistry is not favourable, and is endothermic at typical process temperatures, and because the reaction rate can not be further increased with increasing the process temperature for its compatibility with the low k processes, a certain number of unbroken Ta-Cl ligands will remain in the film deposited. As residual surface chlorine impurities may hurt adhesion, additional finishing treatments or process enhancements are needed to remove or reduce the chlorine impurities.

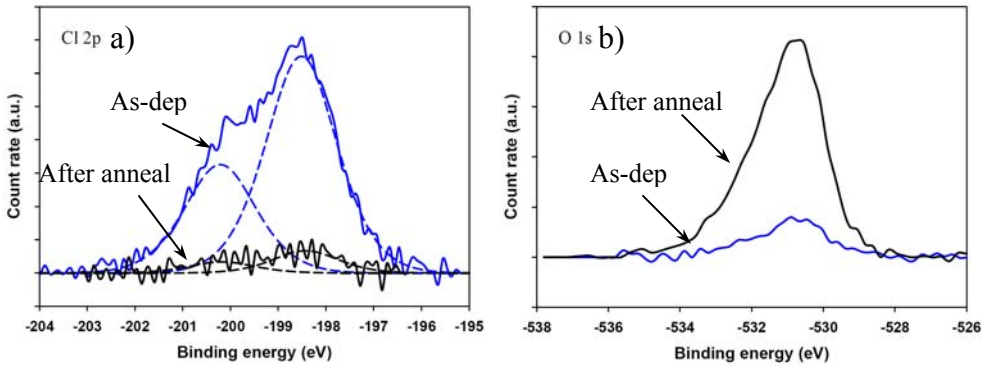

Figure 5-7 Removal of chlorine impurities with thermal anneal.

A natural solution will be annealing in ammonia or nitrogen ambient. It has also been noticed that oxidation during anneal can easily remove most of the chlorine impurities. One example was presented in Figure 5-7. When 400 cycles of ALD Ta_3N_5 were put down on the dense OSG film, which was cleaned and activated with the radical beams, significant amount of chlorine in the form of Ta-Cl was incorporated (Fig. 5-7a). After annealing at 300°C for 60 minutes in H_2 ambient, chlorine content dropped to trace amounts (Fig. 5-7a). While at the same time, Ta-O amount increased significantly (Fig. 5-7b). Quantitative analysis found that O-Ta signal intensity increased from 1561 counts per second (cps) to 7738 cps while Cl-Ta signal intensity dropped from 3867cps to 361cps. Considering the ratio between the atomic sensitivities of O1s and Cl2p core

level electrons 0.90/0.72, the increase of oxygen in O-Ta bonding was comparable to the loss of chlorine in Cl-Ta bonding, indicating oxidation of Ta-Cl bonds as the mechanism. However, thermal anneal may not be the best solution to the removal of chlorine impurities for fear of the additional thermal budget involved and possible surface oxidation hurting the microstructure of subsequent metallic Ta deposition. Given the high reactivity of atomic hydrogen with Ta-Cl bonds, atomic hydrogen was investigated as an alternative to reduce chlorine residue.

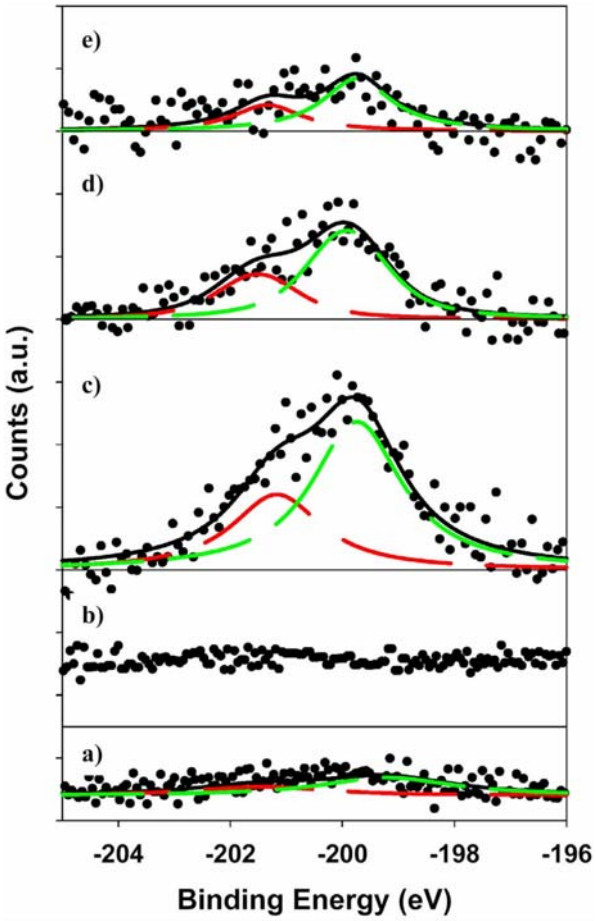

Figure 5-8 Evolution of Cl2p during an ALD cycle with atomic hydrogen being introduced to reduce Cl content.
a) after exposure to $TaCl_5$ and purge with Ar; b) after reaction with atomic H and with NH_3; c) after additional exposure to $TaCl_5$; d) after 10 min treatment with atomic H; and e) after additional 4 hour 390°C anneal in a H_2 ambient.

The effect of atomic hydrogen in reducing chlorine residue, as well as the step-by-step nature of ALD reactions, was demonstrated by the evolution of Cl2p spectra in one ALD cycle with intentionally increased $TaCl_5$ pulse duration and additional exposure to atomic hydrogen prior to the ammonia step. The spectral evolution is presented in Figure 5-8.

After exposing a SiO_2 sample to $TaCl_5$ precursor, a small Cl2p peak started to show up in Fig. 5-8a, indicating chemisorption of the precursor molecules. After being treated with atomic hydrogen and then exposed to NH_3 reagent, the Cl2p peak was hardly discernable from the background (Fig. 5-8b), indicating a complete reaction between the precursor, atomic hydrogen and ammonia.

The possibility of the chlorine reduction as a result of reactions with hydrogen molecules or even with any residual oxygen molecules can be ruled out by monitoring the Cl2p evolution following two different treatments of a SiO_2 sample overexposed to $TaCl_5$ precursor (Fig. 5-8c). The chlorine content was almost halved (Fig. 5-8d) when the sample was treated with atomic hydrogen for only 10 minutes at 350 ºC, whereas the chlorine content remained clearly visible (Fig. 5-8e) after additional 4 hour anneal at 390ºC in a H_2 ambient.

Based on the above observation of reduction of chlorine impurities with additional atomic hydrogen step in one ALD cycle, similar beam application was demonstrated on low k films. An atomic hydrogen step was inserted prior to the introduction of ammonia in each ALD cycle. In one optimized process of 30 ALD cycles, the chlorine signal was reduced to beyond detection limit. The difference of Cl2p spectra between such a process and its thermal counterpart effect is compared in Figure 5-9.

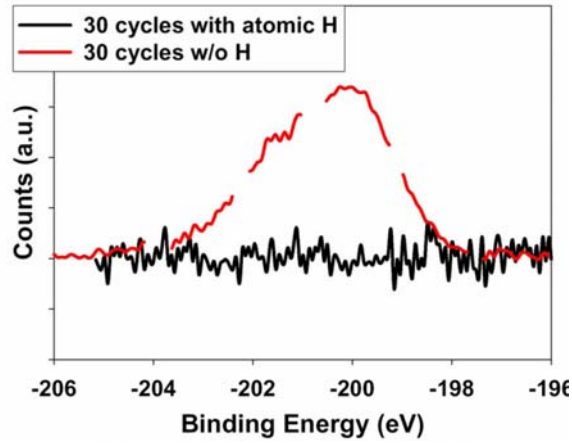

Figure 5-9. Comparison of Cl2p spectra. The Cl count rates have been normalized to Ta counts.

This is believed to be because in the following possible reactions of $TaCl_5 + H \rightarrow Ta + HCl$ and $TaCl_5 + N + H \rightarrow Ta(N) + HCl$, the reaction energy barrier between atomic species and $TaCl_5$ precursors are considerably lower than that between NH_3 gas molecules and $TaCl_5$, as suggested by the high dissociation energies of NH_3 and H_2. As the reactions became more complete, there were not so many partially reacted precursor ligands left in the film.

5.4 Prevention of oxidation by atomic hydrogen

The capability of forming metallic Ta also provided a chance to look into the origin of oxidation in the ALD processes. Angle-dependent XPS already revealed that there was always much more oxide on the surface than in the bulk, indicating surface oxidation during sample transfer after deposition even in the ultra-high vacuum.

Besides surface oxidation, there could also be oxide formation due to oxygen impurities in ammonia and argon purge gas and oxygen outgassing from the tubing sidewall and the chamber sidewall. To investigate this possibility, O1s spectra on the dense OSG are compared in Figure 5-10 with barriers deposited with three different processes: 80 cycles of thermal ALD Ta_3N_5 (Fig. 5-10a), 80 cycle similar process but

with prolonged purging pulse (Fig. 5-10b), and 200 cycles of metallic Ta (Fig. 5-10c). It is clear that the metal oxide peak at -530.7 eV binding energy increased with process time in Fig. 5-10a and Fig. 5-10b, indicating oxygen incorporation during the processes as another source of oxide impurities.

Interestingly, much less oxide was shown in Figure 5-10c to have formed in the metallic Ta process even though metallic Ta was more prone to surface oxidation. Since the longer process time in the metallic Ta process did not result in more oxide formation, the oxide formed in the metallic Ta process should be attributed mainly to surface oxidation after deposition.

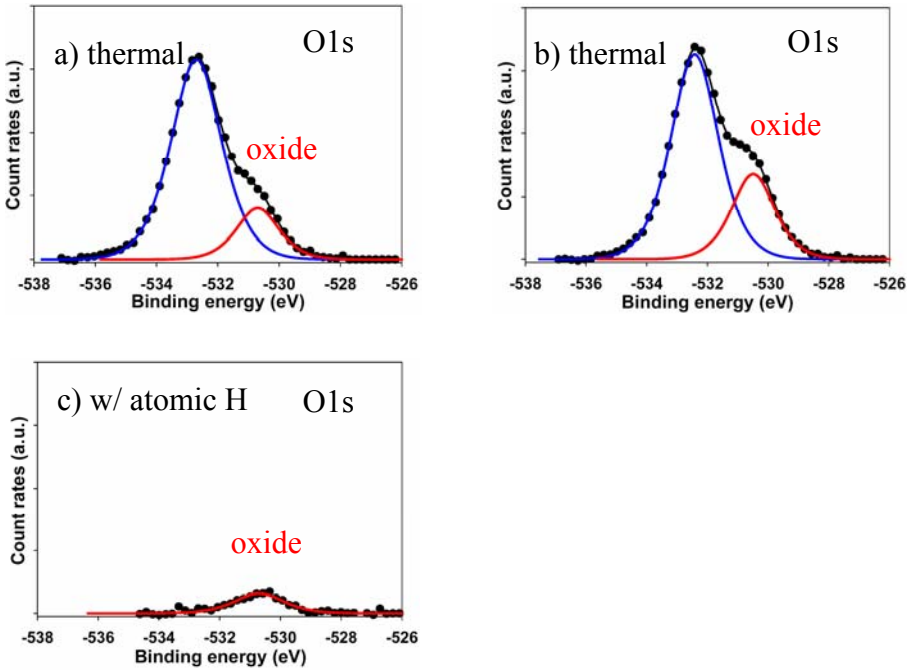

Figure 5-10 Origin of oxidation. O1s spectra after a) 16 sec × 80 cycles; b) 29 sec × 80 cycles; and c) 28 sec × 200 cycles

Oxidation was suppressed during the deposition process involving atomic hydrogen. The reduced oxygen incorporation could be attributed to either less oxygen partial pressure in the chamber or preferred reaction with atomic hydrogen by oxygen.

Since atomic hydrogen was not found to reduce tantalum oxide to metallic tantalum in our experiments, the observed less oxide incorporation should be due to lower oxygen partial pressure in the chamber in the presence of atomic hydrogen. In the above process, atomic hydrogen step was only an additional step prior to the ammonia pulse, and the deposition process sequence contained as much, if not more exposure time to ammonia and argon as in the thermal ALD processes. The oxygen impurities that were reduced must have come from sources other than ammonia reagent and argon gas, or otherwise, similar amount of oxide should have formed in the metallic Ta process. A natural source of oxygen is oxygen outgassing from the sidewalls. With the tendency to react with any oxidant forming water, atomic hydrogen was able to extract oxygen from the chamber, creating a protective ambient against film oxidation during the ALD processes.

In summary, several other possible applications of radical beams in enhancing ALD barrier processes were examined in this chapter. Insertion of an atomic hydrogen step into the conventional thermal ALD process cycle was found to considerably reduce chlorine impurity and oxygen content in the Ta_3N_5 film. Atomic hydrogen was also demonstrated as a reducing agent to be used to form metallic Ta on ALD Ta_3N_5 barrier without much oxygen, chlorine and carbon impurities. These applications of atomic hydrogen take advantage of the high reactivity of atomic hydrogen with halide and oxidants. Similarly, amine radical beam was demonstrated to improve the ALD reaction energetics. This suggested that a wider process window could be achieved with the use of radical beams. Although the supply of reactive radicals by thermal cracking or plasma cracking still faces technical difficulties caused by low dissociation efficiency and fast

self-recombination rate, there is growing interest in applying radicals in thin film deposition to utilize the chemical reactivity while at the same time avoiding undesired substrate damage and film defects in plasma processes.

Chapter 6: Surface Silylation and Its Impact on ALD Nucleation

6.0 Overview

Another route for surface modification is to utilize molecules reactive with the surface functional groups. Through a self-assembly process, a monolayer of these molecules can be selectively assembled on surface reactive sites and create a surface of new chemical functionality. To avoid using any exotic chemicals, silicon-based agents are the natural choice for such self-assembled monolayer (SAM) applications for surface and interface modifications in silicon processing technologies.

Silylation, i.e., incorporation of silicon atoms, is a widely used technique to modify a chemical compound to more volatile derivatives for detection in gas chromatography and mass spectroscopy. [223] In semiconductor manufacturing, silylation agents, such as hexamethyldisilazane (HMDS), trimethylsilyldiethylamine (TMSDEA) and etc., have been used as primer in the lithographic process to modify the surface chemistry for adhesion promotion and surface tension reduction. [224]-[226] Recently, surface silylation is being actively investigated for dielectric repair after plasma processing of porous ultra low k dielectrics. [138]-[141] From an integration point of view, given the strong sensitivity of ALD barrier process to substrate surface chemistry, its impact on the subsequent ALD barrier process has to be carefully evaluated.

This chapter presents preliminary work on surface silylation for dielectric recovery and silylation-based CVD deposition of organosilicate pore sealant for pore sealing of plasma damaged porous ultra low k dielectrics. The emphasis is still placed on the modification of the low k surface chemistry and its subsequent effects on the ALD nucleation process.

6.1 Introduction of surface silylation and pore sealing

The interest in silylation of low k surfaces does not arise from barrier formation but rather from the limitations imposed by plasma-induced sidewall damage on further dimensional scaling. It is understood that porous ultra low dielectric constant dielectrics may be implemented at or beyond 45nm technology node. [3] Integration of porous ultra low dielectric constant dielectrics is a very challenging task due to their poor mechanical strength and poor resistance against chemical and plasma damage. The plasma damage induced during the etch/ashing/clean processes can result in degradation of the dielectric and electrical properties and aggravated surface roughness. [105],[109],[135],[227]-[233] These issues can lead to severe yield and reliability concerns.

As plasmas densify a porous medium and embed charged ions and dangling bonds, a damaged "skin" layer very much silica-like is formed. [228],[234] When patterning a trench structure, all the sidewalls of the trench are affected by the plasma patterning processes. Even without considering the dielectric degradation due to moisture adsorption, the presence of such a silica-like damaged "skin" layer can significantly increase the effective dielectric constant if the damaging process is not self-limiting. A simple parallel-plate capacitor model shows that the increase of the effective dielectric constant due to a skin layer of thickness δ on the two sides of a dielectric line with a spacing w is $\frac{2\delta}{w}\cdot(k^{SiO_2}-k_0)\approx 4\frac{\delta}{w}$. Following the low-k roadmap, [3] when k_0=2.2 ultra-low k (ULK) materials are to be implemented at 32nm technology node in 2x pitched levels, while maintaining k_{eff} lower than 2.5, the thickness of the damaged layer δ has to be at the most less than $\frac{(2.5-2.2)}{(k^{SiO_2}-2.2)}\times 2\times 32\times\frac{k^{SiO_2}}{2.5}\times\frac{1}{2}\approx 8.5nm$. This has not taken into account

the contributions from other surrounding dielectrics with higher dielectric constants, such as the cap layer, etch stop and hard mask residues, which all add to the effective dielectric constant. All together, it is not hard to imagine that less than 3nm thick damaged layer will be required on future generation low k patterning processes.

Unfortunately, current low k patterning technologies usually leave behind damage more than 10 nm deep into the available ULKs. If there are no quick breakthroughs in either patterning processes or ULK property enhancement, the dielectric degradation may limit further scaling of the low k dielectrics. Several simulation models have given out a very pessimistic picture that beyond 32nm, as plasma damaged layers take up a greater portion of the patterned feature width, the benefits of using a lower k dielectric will be completely lost. [110]

Much effort is being dedicated to minimizing such damage in the first place; as a second choice, post-patterning remedies are also being explored as a second choice. Surface silylation of damaged ULK dielectrics is one of such remedies intended for dielectric recovery and surface planarization/pore sealing which have become essential for the successful implementation of porous ULK dielectrics.

As a result of plasma processing, methyl bonds are depleted from the organosilicate (OSG) based low k surfaces; consequently, large amount of surface silanol groups (Si-OH) are present which can be utilized as the reactive sites to form self-assembled layers. Attacking these silanol sites to form Si-O-Si bonds, silylation agents are chemisorbed onto the film surface and modify the surface chemistry.

It has been generally understood that the dielectric degradation is caused by depletion of the weakly polar Si-CH_3 bonds, generation of polar Si-OH bonds, additional

moisture adsorption on these polar sites, and film densification due to the collapse of pore structure. [104],[135],[234]-[235] Among these factors, silylation is aimed at passivating Si-OH bonds to prevent moisture adsorption. [237] For this reason, hydrophobic alkyl side groups are to be incorporated into silylation agents to give the final surface a hydrophobic finish.

Increased leakage is another aspect of plasma damage. Under the physical impact of energetic ions, a large number of broken bonds and charged ions can be left deep inside the bulk of porous low k dielectrics after plasma processes. These defective and electrically active sites can provide additional conduction mechanisms in the presence of electric field. With this in mind, small molecules of silylation agents can be very helpful by going deep into the damaged low k and passivating the dangling bonds.

The last but not the least concern is pore sealing. Failure to form a continuous barrier layer on the porous low k dielectric surfaces is a severe reliability concern if there is not so much room left for material engineering to achieve more desirable pore size distribution in the porous low k dielectrics. When the pore size is about 1nm small and tightly distributed as in the case of CVD microporous materials with relatively low porosity, plasma processing involved in the patterning processes was observed to be able to seal or partially seal the porous surface. [86],[126],[234],[235] This can be attributed to the physical densification effect and the chemical activation effect discussed in Chapter 4. The need for pore sealing by itself does not necessarily justify an additional process step in the future process flows for implementation of ultra low k dielectrics. Nevertheless, it has been realized that it would be beneficial to barrier formation if an additional sealant layer can be deposited as a low k surface finish to planarize porous low k surfaces, which may possibly be further roughened during plasma processing. Although any cross-linking

material deposited on top of a porous low k surface can have some sort of surface planarization effect, a silylation based CVD process is more desirable for its process compatibility, process simplicity and interfacial integrity.

One approach of surface silylation for dielectric recovery is to use tri-alkyl-substituted disilazanes or chlorosilanes, such as hexamethyldisilazane (HMDS) and trimethyl chlorosilane (TCMS), and so on. [138]-[141] While these silylation agents have been confirmed to recover part of the dielectric damage, they are inadequate for surface planarization/pore sealing due to only monolayer coverage. And they are also detrimental to the subsequent barrier processes with atomic layer deposition (ALD), because the final surface after silylation is terminated with methyl bonds which are inactive in ALD nucleation process as discussed in previous chapters. The adverse effect on ALD nucleation by HMDS surface silylation has been experimentally confirmed with *in-situ* XPS studies which will be presented in the last section of this chapter.

If atomic layer deposition (ALD) of Cu barriers is ever to be inserted into the back-end-of-line (BEOL) process sequence, it will be a process step following the aforementioned low k dielectric recovery and pore sealing processes. Due to its sensitivity to the substrate surface chemistry, strong interactions with the dielectric recovery and pore sealing processes are expected. These interactions have to be considered when developing a dielectric recovery and pore sealing process. Extensive studies on dielectric recovery, pore sealing, and ALD barrier process have been reported. However, few of the studies have tried to manage these issues from an integration point of view. Most of them attempted to manage these issues separately.

In this work, a novel silylation process has been attempted with the chemistry expertise of Dr. Woon-chun Kim to tackle these issues from an integration point of view. Based upon the concept of surface silylation to selectively attack the silanol bonds induced in plasma processing, while at the same time introducing cross-linking bonds for pore sealing and surface planarization, and also attempting to provide surface nucleation sites for ALD barrier process, a two-step silylation process has been developed: deposition of crosslinked organosilicate sealant layer with alkylsilsesquioxanes for pore sealing and surface planarization, followed by a surface finish with phenyl containing tri-substituted silylation agents, such as phenyldimethylchlorosilane (PDMCS) and diphenyltetramethyldisilazane (DPTMDS), for dielectric recovery and to introduce benzene groups at the surface as the ALD nucleation sites and to passivate the surface silanol groups against moisture uptake.

6.2 Surface silylation for dielectric recovery

6.2.1 Evidence of silylation

The generic reaction mechanisms for silylation are given as follows,

a) $Si\text{-}OH + R_2SiR'\text{-}NH\text{-}R'SiR_2 \rightarrow Si\text{-}O\text{-}R_2SiR' + NH_2 - R'SiR_2$ (6-1)

b) $Si\text{-}OH + R_2SiR'\text{-}Cl \rightarrow Si\text{-}O\text{-}R_2SiR' + HCl$ (6-2)

Most of the experimental details can be found in Section 2.4. As a preliminary study, all the surface silylation experiments were carried out with wet chemistry in a ventilated hood. Novel dielectric recovery agents, such as phenyldimethylchlorosilane (PDMCS) and diphenyltetramethyldisilazane (DPTMDS) and etc., were obtained from Gelest. Other silylation agents more commonly used, such as trimethylchlorosilane (TMCS), hexamethyldisilazane (HMDS) and etc., were obtained from Sigma-Aldrich.

Because the silylation processes are very sensitive to moisture, moisture has been carefully controlled in all the experiments. Damaged low k samples were baked at 120°C for more than 2 hours before silylation. The samples were then put in a stirred solution of silylation agents maintained at 80°C for various time periods. They were removed from the solution and rinsed with corresponding solvents to remove residues of the silylation agents. Some of the samples were post-baked at 200°C to achieve better dielectric recovery results.

The dielectric recovery and pore sealing process was demonstrated on the mesoporous organosilicate low k film with a mean pore size of 2.4 nm, a thickness of 3000Å and a dielectric constant of 2.2. This low k film was first damaged with a low power (100W) Ar/O_2 plasma process to simulate the plasma damage that may occur during etch/ashing/clean processes.

The chemical change was monitored with FT-IR and the surface hydrophobicity was studied with contact angle measurements. Contact angle measurements were done with three liquids: water, glycerol and diiodomethane in order to separate the polar and non-polar surface energies. The change in the dielectric property was studied with metal-oxide-semiconductor (MOS) capacitors formed by shadow masked Al(Cu) sputtering. Capacitance-voltage and leakage-voltage data were collected on these MOS capacitor structures.

Chemical modifications induced by plasma processing and the subsequent silylation were monitored with FT-IR and XPS. Since FT-IR is not a surface sensitive technique, the Ar/O_2 plasma damaging process was intentionally overdone up to 10 minutes to illustrate the changes in the IR absorbance characteristics.

As shown in Figure 6-1 and 6-2, plasma induced damage were evidenced by the decreases in Si-CH_3 deformation at 1276 cm^{-1} and aliphatic C-Hx stretches at 2800-3000 cm^{-1} and the increase in silanol groups (960 cm^{-1}) and the associated broad free hydroxyl band around 3600 cm^{-1} due to moisture absorption on the silanol sites. It is expected as plasma normally damage low k films through depleting methyl groups bonded with silicon and creating more dangling Si bonds. In the presence of moisture, these dangling bonds form silanol groups. And moisture can be physisorbed on the polar silanol groups. The adsorbed moisture and the increased silanol termination both contribute significantly to the dielectric loss. The shift in Si-O-Si asymmetric stretches at 980-1260 cm^{-1} is usually interpreted as a plasma densification effect: [238] transformation of low bond angle suboxide around 1035 cm^{-1} to higher bond angle Si-O-Si network at 1070 cm^{-1}. IR spectrum after silylation of the damaged ULK film with diphenyltetramethyldisilazane (DPTMDS) catalyzed with phenyldimethylchlorosilane (PDMCS) showed higher Si-O-Si absorbance and slightly higher amount of aliphatic C-Hx stretches at 2800-3000 cm^{-1} possibly as a result of formation of more Si-O-Si bonds in the silylation process.

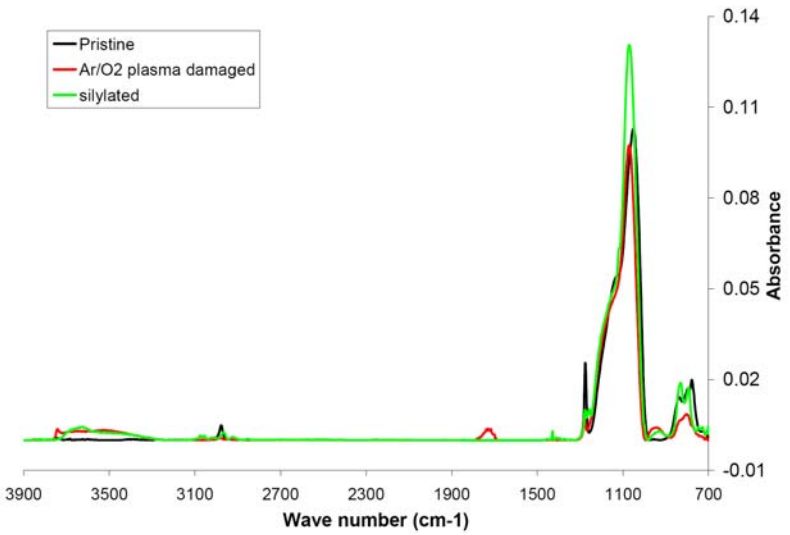

Figure 6-1. Evolution of IR spectra of porous OSG film.

The evidence for incorporation of benzene structures on the surface was not very obvious due to low concentration and overlapping with other absorption bands. Nevertheless, the observed additional IR absorption bands at 3020-3080 cm^{-1} may be interpreted as C-H stretches in the phenyl (Ph) group bonded with silicon [239] and the two little kinks at 1255 cm^{-1} and 1120 cm^{-1} can be interpreted as Si-CH_3 deformation in $PhSi(CH_3)_2$ and Si-Ph stretch respectively. [239] The slight increase in absorption at 730 cm^{-1} may also be interpreted as out-of-plane ring vibration in Si-Ph bonds. [239] This is accompanied by an increase of Si-C stretch in $Si(CH_3)_2$ bonds at 800 cm^{-1}. [238] In the corresponding XPS C1s evolution presented in Figure 6-3, small peaks which can be interpreted as π-π* shake-ups started to appear at -290 ~ -292eV after silylation.

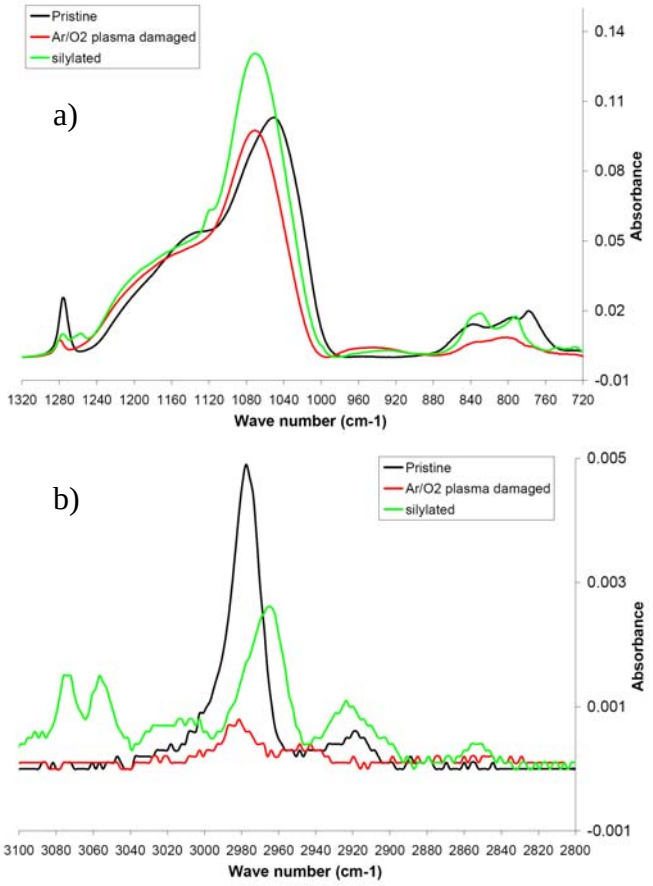

Figure 6-2. Detailed evolution of IR spectra during silylation experiments.

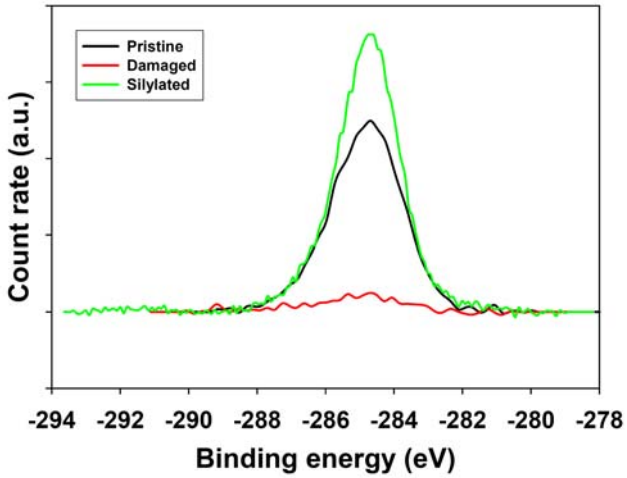

Figure 6-3. Evolution of XPS C1s spectra during silylation experiments.

Surface silylation was more conclusively shown with the surface energy measurements. Using three liquids, the contact angles were measured on the pristine film, film after the plasma process and film after the subsequent silylation process. Applying Young-Dupré equation, the polar and dispersive surface energy terms were extracted. The results are tabulated in the following table:

Table 6-1: Results of contact angle measurements

Contact angle	H_2O	Glycerol	Diiodomethane	γ^p(erg/cm^2)	γ^{Dis}(erg/cm^2)
Pristine film	83.8	85.1	54.5	4.7	26.9
Damaged	5.7	13.7	23.9	23.2	35.6
Silylated film	79.3	80.6	33.5	8.3	36.8

The recovery of surface hydrophobicity is very clear with the changes in the contact angle of water on the pristine surface, the plasma damaged surface and the silylated surface. The contact angle was more than 80° on the original film as it was very hydrophobic. As a result of the plasma process, more polar silanol groups and dangling

bonds were generated on the surface, so the contract angle decreased dramatically to a value beyond the detection limit. After the silylation process, the contact angle was almost completely recovered. Correspondingly, the polar surface energy increased considerably from 4.7 erg/cm^2 of the pristine film to 23.2 erg/cm^2 due to the plasma damage and was reduced significantly back to 8.3 erg/cm^2 resulting from the surface silylation. Consequently, surface hydrophobicity was expected from the silylated film.

Silylation attempts to address specifically the root cause of dielectric degradation: methyl depletion and induced hydrophilicity. With addition of hydrophobic methyl termination, surface hydrophobicity can be recovered. However, only slight decrease of free hydroxyl groups was observed in our preliminary experiments. This can be attributed to water absorption before or after silylation. Similar observations were reported by other researchers. [237] Surface hydrophobicity only prevents moisture adsorption on the surface but does not guarantee elimination of pathways for moisture. [240],[241] The loose molecular structure of porous low k, in general, and the interconnected pore structure of this mesoporous material in particular have provided more than enough such pathways for moisture penetration. As long as there are polar sites present in the bulk of the damaged low k film, moisture can eventually penetrate through the hydrophobic surface region and get adsorbed anyway despite of surface hydrophobicity after silylation.

Although there have been attempts to repair plasma damage deep in the bulk of porous low k's, [138],[140],[141] it is not really practical to completely remove these deep bulk damage considering the long time which would be required first to drive out the adsorbed moisture. The bulk damage has to be first mitigated by optimized plasma

processes. In case of severely damaged porous low k films as in this study, a mere monolayer coating simply could not block the moisture pathways formed during the plasma processes. Moreover, because these silylation agents themselves are very sensitive to moisture, without a deep dehydration pre-bake to drive out water molecules adsorbed on silanol sites in the bulk, silylation might not have been as effective to react with bulk silanol sites as it is supposed to be. It is not hard to imagine that a complete dielectric recovery process in real applications will involve a certain thickness of densified layer either by tweaking the plasma processes or adding blocking sealant layer before a hydrophobic finish with surface silylation or vice versa. That being said, as will be demonstrated in the next section, surface silylation by itself has been found to improve significantly the dielectric and electrical properties of the damaged porous low k film.

6.2.2 Evaluation of dielectric recovery effects

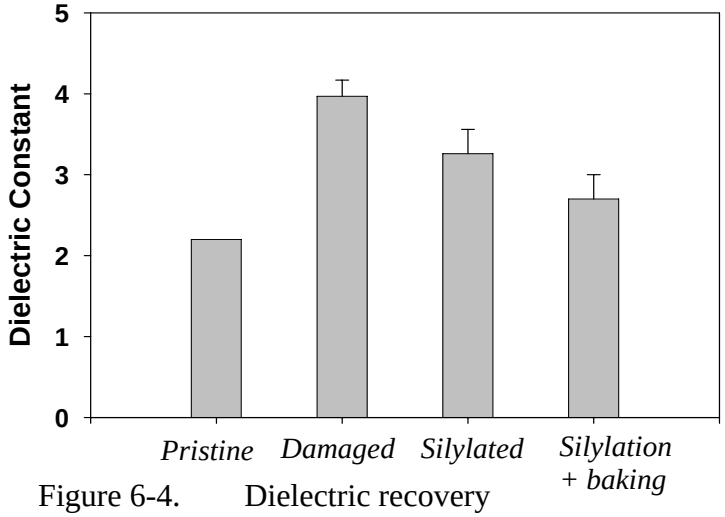

Figure 6-4. Dielectric recovery

The effects of surface silylation on the dielectric constant and the leakage current were evaluated using standard metal-insulator-semiconductor (MIS) capacitors. The dielectric constants obtained were presented in Figure 6-4. Because the films are highly porous and the film thickness was only around 3000Å, plasma damage-induced

leakage made these capacitors very leaky. Most of the C-V measurements failed due to degraded dielectric break down before arriving at the flat band voltage which was normally as high as -15V or 0.5MV/cm in terms of the electrical field. Only a few capacitors survived. The error bars given in the chart are conservatively estimated to be 10% based on historical data.

As shown in the chart above, the dielectric constant increased from 2.2 to 3.9 after a plasma process with 85/15 Ar/O_2 ratio for 10 minutes. With dehydration bake, the dielectric constant could drop to 3.5 on the damaged film, indicating that the dielectric degradation was partly caused by moisture adsorption. After silylation of the damaged film in DPTMDS solution catalyzed with small amount of PDMCS, the dielectric constant decreased to 3.2. After additional dehydration bake at 200°C, further decrease in the dielectric constant was observed. The final k value was 2.7 on the repaired surface indicating some degree of dielectric recovery.

In fact, the repair of plasma-induced damage was more remarkable in the leakage current measurements. On the plasma damaged film, all the MOS capacitors became very leaky. Measured at -1.0V from the transition point or at an electrical field of 0.03 MV/cm, the leakage current jumped from 0.1nAmp/cm^2 to μAmp/cm^2 in the worst case. At bias higher than -1.0V, the leakage current on some samples ran away, showing dielectric breakdown. Due to the large experimental scatter, only I-V curves on a good sample are presented in Figure 6-5. The plasma condition was 85/15 Ar/O2 ratio at 100W for 5 minutes. The leakage jumped to 88nAmp/cm^2 due to plasma damage. After silylation, the leakage current was reduced by orders of magnitude to 0.26nAmp/cm^2. Dehydration bake alone was able to reduce considerably the leakage current on the

damaged sample to 23nAmp/cm^2. However, only with silylation was the leakage current remarkably reduced to a level similar to what was on the pristine film. And additional dehydration bake had no significant effect on the reduced leakage current.

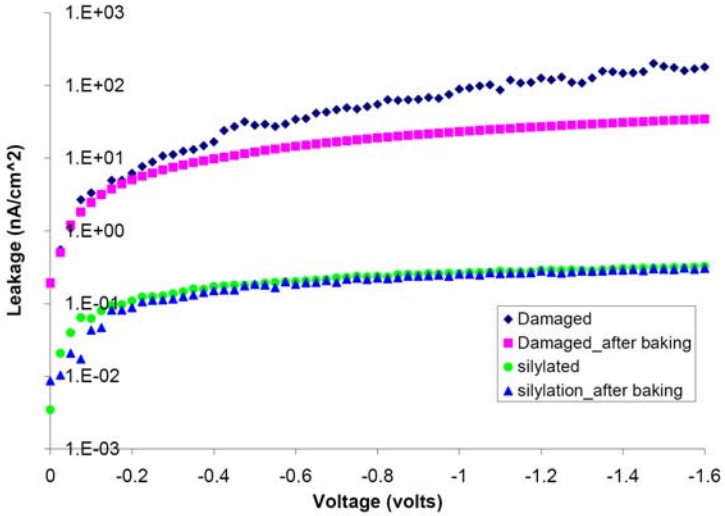

Figure 6-5. Examples of leakage current measurements.

To further investigate the dependence of the leakage current on the plasma conditions, four different plasma processes were performed on the same porous OSG film, followed by an identical silylation process and dehydration bake. The leakage currents measured at -1.0V from the transition were charted in Figure 6-6.

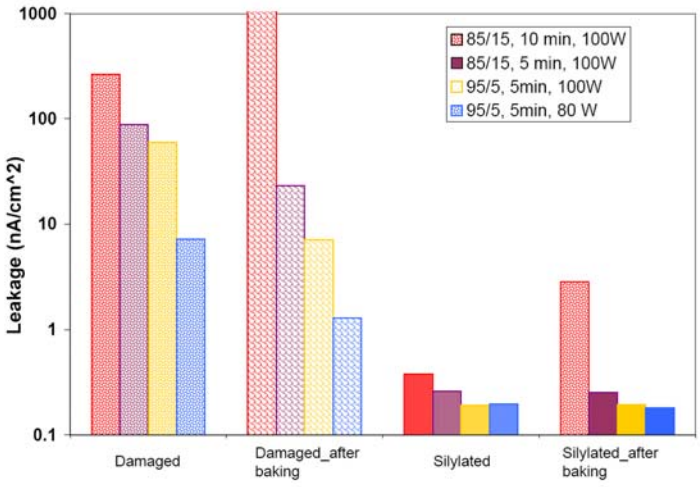

Figure 6-6. Reduction of the leakage current by silylation.

When using the leakage current as a measure of damage, the plasma induced damage increased with O_2 partial pressure, DC bias (related to DC plasma power output) and process time. It was expected because the chemical effect by oxygen radicals and the physical impacts by energetic ions, especially the heavy argon ions, are regarded as the main factors causing the damage.

On all the samples damaged in different plasma conditions, silylation reduced the leakage current by orders of magnitude. Dehydration bake helped reduce a little the leakage in the damaged films, but did not help much in further reducing the leakage in the silylated films. This observation revealed another important if not the more important role of silylation: passivation of dangling bonds on the surface and in the bulk. In most cases, the dielectric degradation is partly caused by moisture adsorption on the damaged sites while the increased leakage current is directly associated with the damaged sites themselves. This is the reason that dehydration bake was very effective in dielectric recovery but not so effective in reducing the leakage current.

Another evidence of the effect of silylation in repairing the dangling bonds came from reduction of C-V hysteresis after silylation. The hysteresis in the capacitance-voltage sweep is indicative of charge trapping at the metal electrode/dielectric interface and in the bulk. [242]-[246] The reduction of CV hysteresis suggests that silylation agents may passivate dangling bonds deep in the bulk at the same time, depending upon the molecular size of the silylation agents and the pore interconnectivity. In this study, all silylated samples showed some degree of reduction in the CV hysteresis. The best example was shown in Figure 6-7, where the CV hysteresis was completely eliminated.

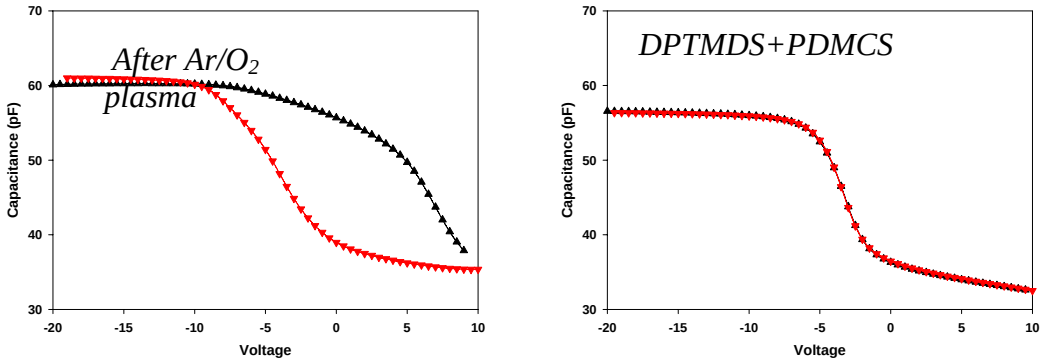

Figure 6-7. Elimination of CV hysteresis

Capacitance and leakage measurements both appear very sensitive to plasma induced damage and the subsequent silylation process. But the capacitance measurements are complicated by its sensitivity to moisture adsorption in the bulk of the damaged dielectric even after capping with the metal electrode. Based on the results above, it can be concluded that the silylation effect in recovering the dielectric constant is limited by the pre-existing plasma induced damage, mostly the newly formed strong polar silanol bonds, and silylation can only help passivate these bonds and other dangling bonds but not to remove them.

6.3 Silylation based CVD organosilicate pore sealant

It was clear from the CV measurements that a monolayer silylation was not able to block moisture penetration into the bulk of the damaged mesoporous dielectric. Additional sealant is then required for both hermetic sealing and surface planarization.

Pore sealing was attempted by Dr. W. Kim using certain alkylsilsesquioxanes on the damaged OSG films. These molecules can react with the surface silanol bonds to form Si-O-Si bonding with volatile alcohol byproducts. They can also cross-link among themselves through formation of Si-O-Si bonding with volatile ether byproducts. The alkyl side groups act as cross-linking terminators, preventing formation of complete silica

network. In this way, anchoring on the plasma damage induced surface silanol groups, a thin low k coating can be deposited and gradually bridge the pore openings. As the coating thickness increases, porous surface can be planarized and eventually sealed against precursor and moisture penetration. The mechanism is illustrated in Figure 6-8.

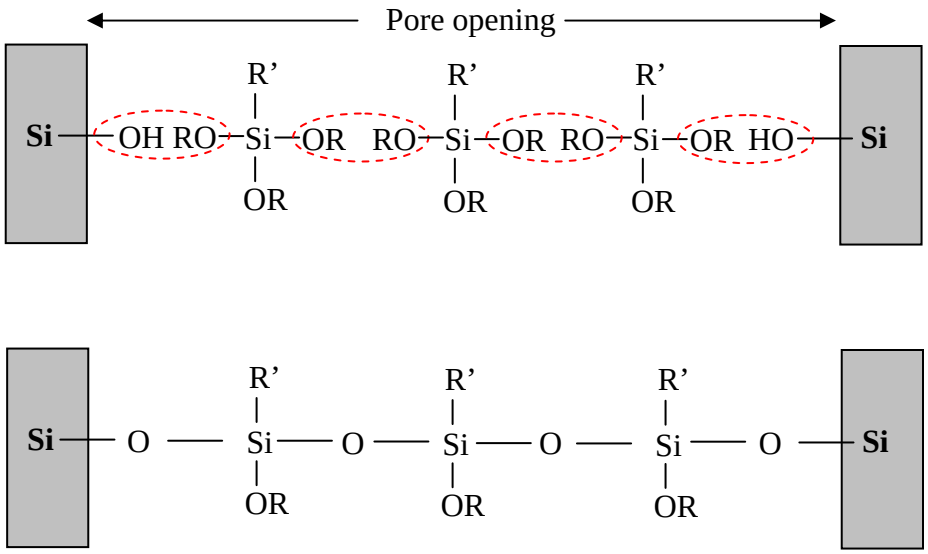

Figure 6-8. Pore sealing with organosilicate sealant

The effect of pore sealing was examined with cross section TEM. A sample of the porous organosilicate film after the plasma process and a sample after the organosilicate sealant deposition were capped with ALD Ta_3N_5 barrier. Then the samples were coated with either photo-resist or Cr to make cross section TEM specimens. Cross section TEM specimens were made out of these two samples following a recipe developed by Won-chong Baek. The wafer pieces were diced to form 50 to 100 μm thick fin structures. The fin structures were picked out and glued to copper holders made out of standard TEM copper meshes. TEM specimens were made after cutting and milling with focused ion beam (FIB). Because our porous low k film can not take high intensity focused electron beam, electron energy loss spectroscopy (EELS) was not successful on

these TEM specimens. Only cross section TEM and STEM images are presented in Figure 6-9.

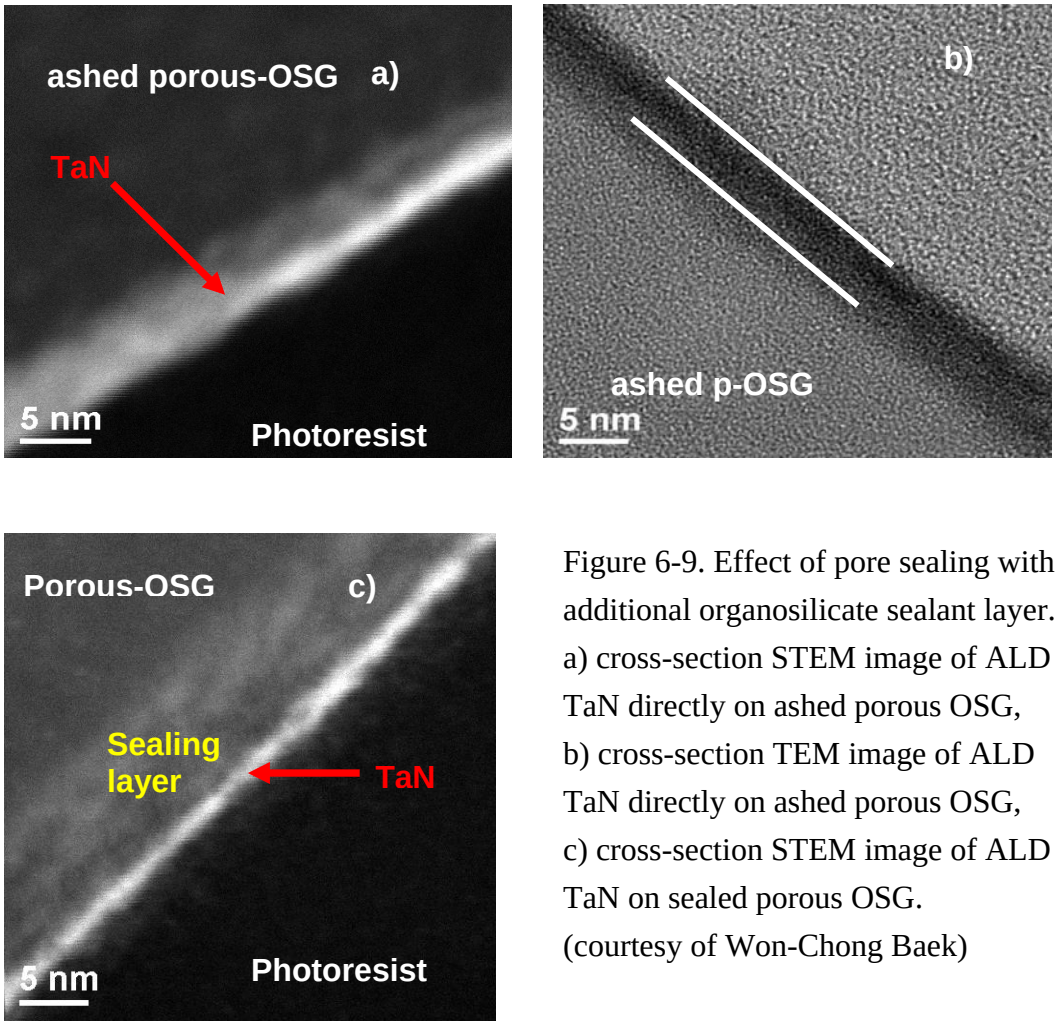

Figure 6-9. Effect of pore sealing with additional organosilicate sealant layer. a) cross-section STEM image of ALD TaN directly on ashed porous OSG, b) cross-section TEM image of ALD TaN directly on ashed porous OSG, c) cross-section STEM image of ALD TaN on sealed porous OSG. (courtesy of Won-Chong Baek)

Direct ALD Ta_3N_5 barrier deposition on the Ar/O_2 plasma damaged porous OSG sample had a diffuse interface, which could be attributed to precursor penetration and intermixing due to the surface roughness. From the TEM cross-section image in Figure 6-9b, the diffuse interface thickness is about 5 nm, only two pore sizes thick. This could actually suggest that the plasma damaged surface was already partially sealed. The penetration of Ta_3N_5 barrier was not very severe. With the additional sealant layer, a much better defined interface was observed between the sealant layer and the ALD Ta_3N_5

barrier (comparing Figs. 6-9a and 6-9c). The improved interface is an indication of much less intermixing or penetration.

By varying deposition time, sealant layers of various thicknesses can be deposited. So far, pore sealing has been achieved with sealant of a thickness less than 10 nm. The impact of the sealant layer on the dielectric property of the porous low k was not evaluated though. Since the sealant thickness is only a very small portion of the whole film thickness and the sealing agents themselves are monomers used in OSG low k synthesis, the film deposited at the low processing temperature should not have affected much the overall film dielectric constant.

The following is a rough estimation of the impact of a 10nm additional sealant layer on the overall film dielectric constant. Assuming a k value of 2.2 for future porous ultra low k and a serial parallel capacitor model for the contribution of the sealant layer, the maximum increase in the dielectric constant due to the additional 10nm sealant layer on a 100nm porous low k can be estimated to be:

$$\Delta k = \frac{d_{total}}{\frac{d_{ULK}}{k_{ULK}} + \frac{d_{sealant}}{k_{sealant}}} - k_{ULK} = \frac{110}{\frac{100}{2.2} + \frac{10}{2.8}} - 2.2 = 0.044 \qquad (6\text{-}1)$$

$$\frac{\Delta k}{k} \approx \frac{0.044}{2.2} = 2.0\% \qquad (6\text{-}2)$$

It is clear from the reaction chemistry that the sealing agents can not remove the plasma induced silanol groups, but the incorporation of additional methoxyl or ethoxyl groups and alkyl side groups may help passivate the damaged sites in the bulk. When moisture is driven out before the pore sealing process, the sealant layer can also serve as a blocking layer against moisture penetration. But the final surface contains plenty of

siloxane groups which may turn into silanol groups through hydrolysis. Additional surface finish may then be needed to achieve surface hydrophobicity.

6.4 Impact on ALD barrier process

Based on the results and discussion presented in Section 6.2 and 6.3, surface silylation and pore sealing processes can be complementary in achieving desired surface hydrophobicity and resistance against precursor and moisture penetration. A complete pore sealing and dielectric recovery process was thus proposed with silylation based CVD deposition of an organosilicate sealant layer followed by surface silylation with phenyl-containing agents as a surface hydrophobic finish.

Study of this proposed finishing process for porous low k patterning was focused upon its impact on the subsequent ALD barrier deposition. The improvements in the dielectric and electrical properties of the damaged porous low k were presumed according to the experimental results and theoretical analysis in the previous sections. Two surface finish processes after a pore sealing process were compared, one with trimethylchlorosilane (TMCS), and the other with phenyldimethylchlorosilane (PDMCS). These chemicals were generally regarded as incompatible with OSG low k processes for fear of the possible etching effect by the hydrochloride byproducts. They were used here rather than the more process compatible HMDS and DPTMDS only for better reaction rates. The difference of the final silylated film surface lies in that the film surface silylated with TMCS has much more methyl termination than that silylated with PDMCS. The growth behaviors of ALD Ta_3N_5 on these two types of surface chemistry were examined to illustrate the impacts of surface silylation on ALD barrier process.

ALD nucleation process was studied with the integrated system for *in-situ* XPS study of ALD process presented in previous chapters. 150 identical ALD Ta_3N_5 cycles were deposited on three repaired plasma damaged porous OSG samples: one with only sealant deposition, one with sealant and TMCS finish and one with sealant and PDMCS finish. The corresponding XPS Ta4p and N1s spectra were presented in Figure 6-10.

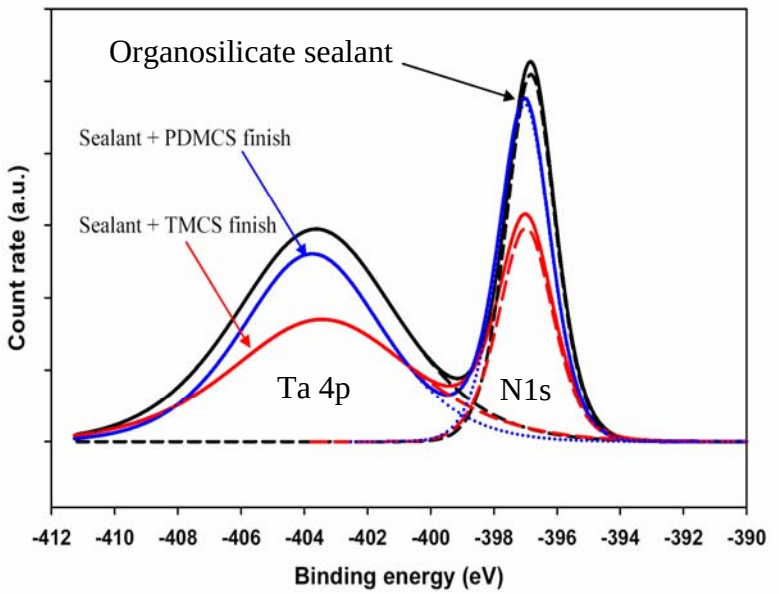

Figure 6-10. Impact of surface silylation on ALD nucleation.

As evidenced by the decrease of Ta4p and N1s peak heights, the ALD growth rate was almost halved after surface silylation with trimethylchlorosilane (TMCS). In contrast, the deposition was maintained at a similar level after surface silylation with phenyldimethylchlorosilane (PDMCS). This contrast was intended to demonstrate the capability of our proposed silylation agents in incorporating benzene rings for ALD nucleation sites. The observation again highlighted the strong surface chemistry sensitivity of ALD barrier processes. If the silylation agents are not engineered properly, the additional surface finish following the pore sealing step intended for dielectric recovery can adversely affect the subsequent ALD barrier process.

In this chapter, a novel surface treatment based upon surface silylation was investigated for pore sealing, dielectric recovery and its impact on ALD Ta_3N_5 barrier process. This process involved use of organosilsesquioxanes for pore sealing followed by surface finish with phenyl-containing silylation agents.

As a preliminary study, the effects of the proposed process on dielectric recovery and pore sealing were only examined in two separate unit process steps: surface silylation and pore sealing. On porous organosilicate (OSG) surfaces damaged with various Ar/O_2 plasma processes, surface silylation has been demonstrated to be possible with diphenyltetramethyldisilazane (DPTMDS) catalyzed with phenyldimethylchlorosilane (PDMCS) as evidenced by the changes to the surface chemistry and the surface energy. The silylation process was observed to significantly reduce the dielectric constant and considerably reduce the leakage. On the same plasma-damaged porous OSG film, less than 10nm thick organosilicate sealant layer had a clearly defined interface with ALD Ta_3N_5 barrier showing no intermixing in cross-section TEM images. After the two unit process steps were confirmed with experimental observations, additional theoretical analysis was included to illustrate the negligible side effect of the sealant layer on the overall film dielectric constant.

Effects of dehydration bake on the dielectric and electric properties of the plasma damaged porous OSG samples and silylated samples were also studied. Since the dehydration bake usually has a positive effect on the damaged samples while not very effective on the silylated samples, the role of silylation is most likely to passivate the damage-induced polar sites and broken bonds on the surface and in the bulk and recover

surface hydrophobicity. Even though there is no way to remove the damage-induced polar silanol groups, passivation of these moisture adsorptive sites is one of the best remedies we can have. Because monolayer coverage can not serve as a hermetic sealant when the mean pore size is large, surface hermeticity may have to be approached through a silylation-based CVD sealant followed by hydrophobic surface finish as proposed.

However, a hydrophobic surface is often not a proper surface chemistry for ALD barrier processes. Too much methyl termination as in the case of HMDS silylation process is detrimental to ALD barrier nucleation. To overcome this difficulty, surface finish with phenyl containing silylation agents has been used instead. It was confirmed to be able to recover surface hydrophobicity, passivate interface dangling bonds, and retain the surface activity for ALD nucleation. Such a surface treatment method is believed to help form a continuous Cu barrier with ALD at a minimal thickness.

Chapter 7: Summary and Future Work

This dissertation has been focused upon understanding the importance of the substrate surface chemistry in ALD barrier formation processes and investigating possible surface modification solutions to engineering the low k/barrier interface and the barrier stack as part of the grand task of Cu/low k interface engineering.

For this purpose, an ultra-high vacuum system has been designed and built up for *in-situ* x-ray photoelectron spectroscopy analysis of ALD barrier formation processes. With this setup, ALD Ta_3N_5 processes with both $TaCl_5$ and PDMAT precursors have been implemented with success and carefully examined. The system has been able to deposit high quality ALD barrier films in a quite reliable, controllable and repeatable way, without major accidents.

Addition of an ECR plasma induced atom/ion hybrid source to the system has further expanded its capacities. This allows utilization of pure low energy reactive radicals for versatile surface modifications and process enhancements. Coupled with *in-situ* XPS analysis, it provides a good opportunity to study the fundamental aspects of surface modification and surface engineering in these deposition processes and process enhancements.

Initial chemisorption of the two types of precursors, $TaCl_5$ and PDMAT, has been examined with this setup on SiO_2 and two main types of low k dielectrics, Organosilicates (OSGs) and SiLK™, porous version as well as dense version. Depending on the surface density of the exposed reactive silanol or amino groups, $TaCl_5$ nucleation rates differed from material to material. Baseline process was first established on SiO2. From the growth curve, the linear growth behavior started right away. No incubation time

was observed. In contrast, on both SiLK™ and OSG films, a linear growth region was always preceded by a nucleation region. The incubation time varied from a low k surface to another. On SiLK™, it was a matter of 20 to 30 ALD cycles while on pristine OSG films it could take almost forever to have appreciable deposition on some films with extremely hydrophobic surface.

The absence of carbide formation or silicide formation during the chemisorption processes suggested that Ta precursors couldn't disrupt and react with Si-CH_3 bonds. Extrapolation of metal oxide formation on SiO_2 to the beginning of ALD tantalum nitride process revealed that reaction of tantalum precursors with surface silanol groups to form Si-O-Ta bonding was the pathway for chemisorption of the precursors on SiO_2 and organosilicate low k films. Variation in the surface density of silanol groups could explain the observed variation in the nucleation behaviors on OSG low k surfaces.

Compared with e-beam Ta and Ta(N) processes studied previously on SiLK™, atomic layer deposition produced much sharper barrier/low k interface without much intermixing. During $TaCl_5$ chemisorption process, benzene structures on SiLK™ were disturbed but, again, without any indication of the formation of metal carbides. This has been attributed to charge transfer complex formation, a known chemical reaction pathway between transition metals and aromatics where the benzene structures are thus attacked without immediate appearance of metal carbide. The presence of abundant benzene rings in SiLK™ can easily explain the observed ready nucleation of $TaCl_5$ ALD process.

Examination of the initial chemisorption process in PDMAT ALD process has revealed that there is no additional reaction pathway for PDMAT chemisorption on OSG low k surfaces. The apparent improvement of chemisorption process with PDMAT on

highly hydrophobic surface can not be explained with the improved reaction energetics by using weakly bonded dimethylamino ligands. It is suspected that a self-decomposition CVD component at the process temperature of 250°C has been helpful to the ALD nucleation process. This speculation has been partially confirmed by the observation that PDMAT ALD growth does not saturate with the precursor pulse duration.

Surface modification of the inactive OSG low k dielectric surfaces has been successful using atomic hydrogen and amine radical beams. Atomic hydrogen beam pretreatment has been proved to provide a useful low temperature surface cleaning technique to remove the carbonaceous surface contaminants and reveal the real substrate surface chemistry. Amine radical beam, on the other hand, can replace the inactive surface methyl groups and form amino moieties on the surface which are very reactive in precursor chemisorption. Consisting of radicals of only thermal energies, these surface activation pretreatments are effective in modifying surface chemistry without too much physical damage as normally seen in plasma processes. This has become very important when it comes to porous low k processing, which is supposed to be the type of low k dielectrics ALD barriers will ever be deposited on.

Radical beam enhanced ALD process has been implemented with amine radical beams taking the place of ammonia as the reactive agent. Using atomic hydrogen as the regent, metallic tantalum has been deposited on ALD Ta_3N_5 layer at a low k compatible temperature. This proves the concept of ALD Ta/Ta_3N_5 film stack is possible with $TaCl_5$ being the precursor. However, incompatibility with the current Cu processes remains a show-stopping issue for any halide ALD chemistry to be adopted in Cu metallization. In addition, other process enhancements with atomic hydrogen have also been investigated,

such as chlorine extraction and ambient oxygen suppression. Atomic hydrogen beam has been found to be effective in reducing chlorine and oxygen impurities in the deposited film owing to the high reactivity of the atomic species.

The need for dielectric recovery and pore sealing process to implement porous low k dielectrics has caused new concerns about the impacts of this additional process on the subsequent ALD barrier process. As one of the approaches to dielectric recovery and pore sealing of plasma damaged porous low k dielectrics, surface silylation aims at passivating plasma-induced dangling bonds against moisture penetration. The recovered surface hydrophobicity has been shown experimentally to be detrimental to ALD barrier nucleation. There is a fine trade-off between surface hydrophobicity and ALD barrier nucleation. Taking advantage of the observed ready nucleation of precursors on SiLK™, a novel silylation-based pore sealing and dielectric recovery approach has been proposed to use alkylsilsesquioxanes to form an organosilicate sealant layer followed by surface finish with phenyl-containing silylation agents, such as diphenyltetramethyldisilazane (DPTMDS) and phenyldimethylchlorosilane (PDMCS). This process has been confirmed with cross section TEM and other electrical characterization measurements to be able to form sharp barrier/low k interface with a sealant layer less than 10 nm thick, and partially recover the dielectric constant. With this finishing process for porous low k patterning, the ALD barrier nucleation process has not been adversely affected.

Surface modifications with radical beams and silylation and the corresponding changes in ALD barrier nucleation behavior and growth have once again confirmed the strong sensitivity of ALD process to the substrate surface chemistry. Methyl termination is inhibitive to precursor chemisorption while silanol or amino moieties are excellent

chemisorptive sites for precursor molecules. The trade-off between surface hydrophobicity and ALD barrier nucleation will become an integration concern in porous low k implementation.

It has to be realized that the system thus designed and constructed has far more capabilities than demonstrated in this work. In this sense, the whole dissertation work can be regarded as a preliminary study for further in-depth investigations of many integration issues in Cu/low k interconnects of next technological generations. It can be extended in two directions as follows:

In ALD deposition, new barrier candidates with atomic layer deposition can be studied with new precursors. For instance, ALD Ruthenium. To extend it even further, high dielectric constant oxide can also be studied using this system. Besides the surface chemical analysis, more measurements of macroscopic properties should be set up to better evaluate the effects of surface modifications on macroscopic properties, such as interfacial adhesion and barrier effectiveness against Cu diffusion.

In low k patterning, with a residual gas analyzer (RGA) being added to the system, the versatility of feed gases in the atom/ion hybrid source makes it a perfect setup to study the damage mechanisms of porous low k in a remote plasma process. With controls over the beam species and ion energy, a variety of low integration issues can be investigated, such as surface treatments of porous low k with low energy ions or radicals for hermetic sealing and surface planarization.

Apendix A: UHV system for *in-situ* XPS study of ALD barrier process

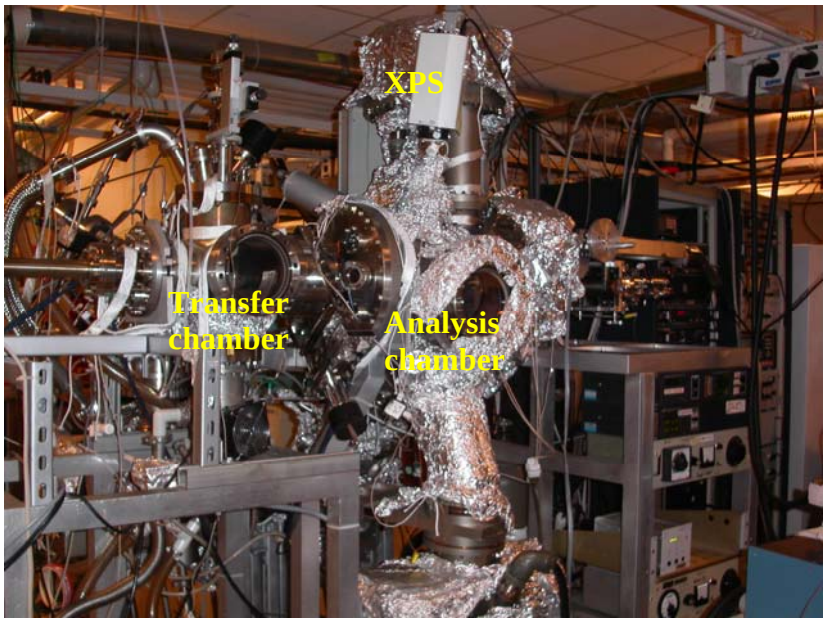

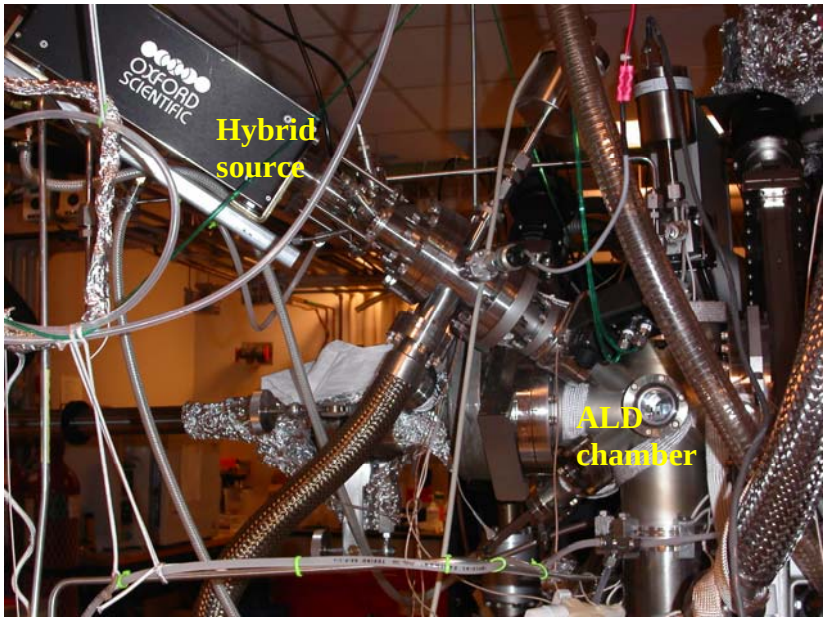


Gas cabinet


Ampoule
box


Control


manifold

Appendix B: Diagrams for gas flow control

B-1: Master control plan

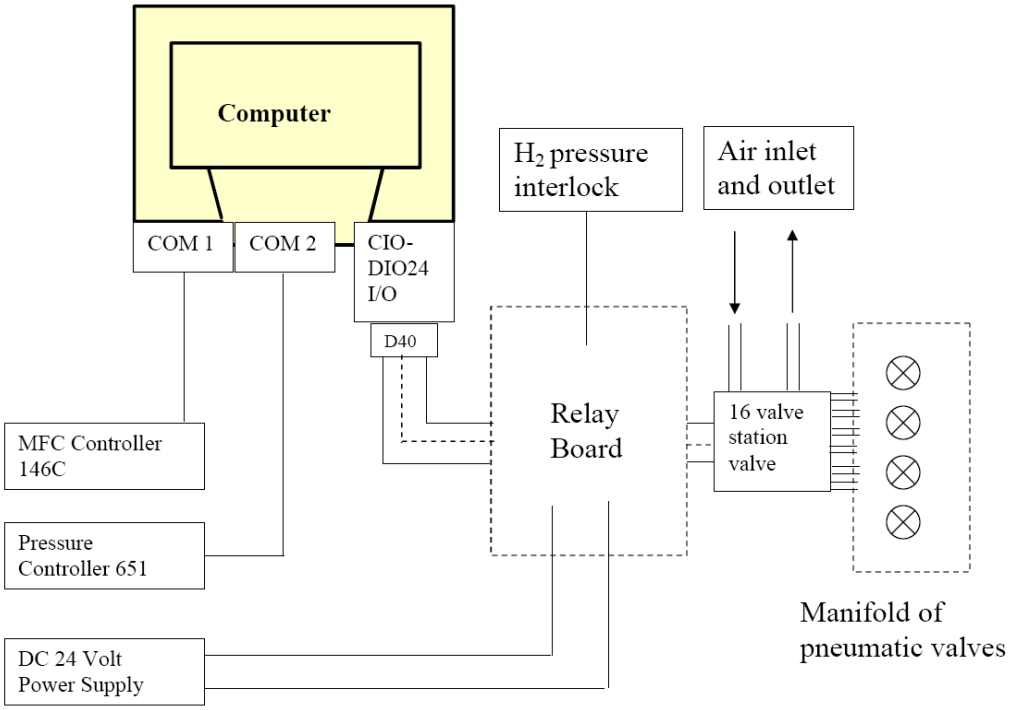

B-2: Station valve (manifold control)

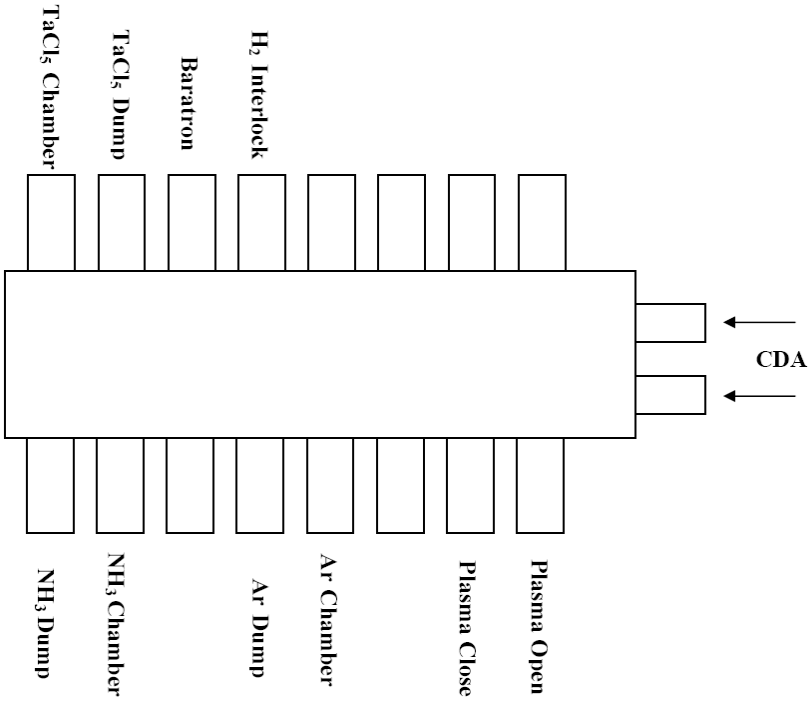

B-3: Valve control

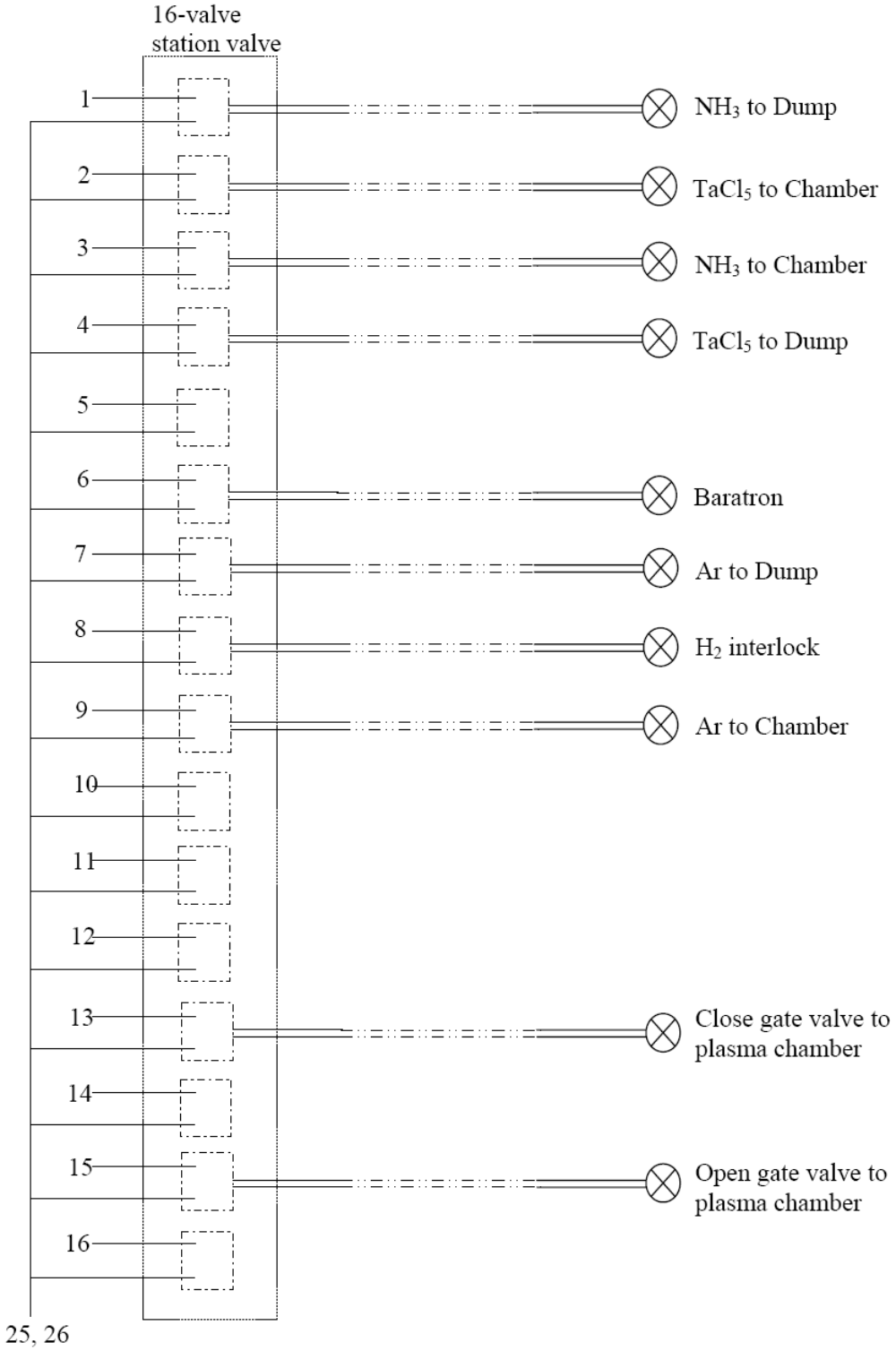

B-4: Circuit map for the relay board

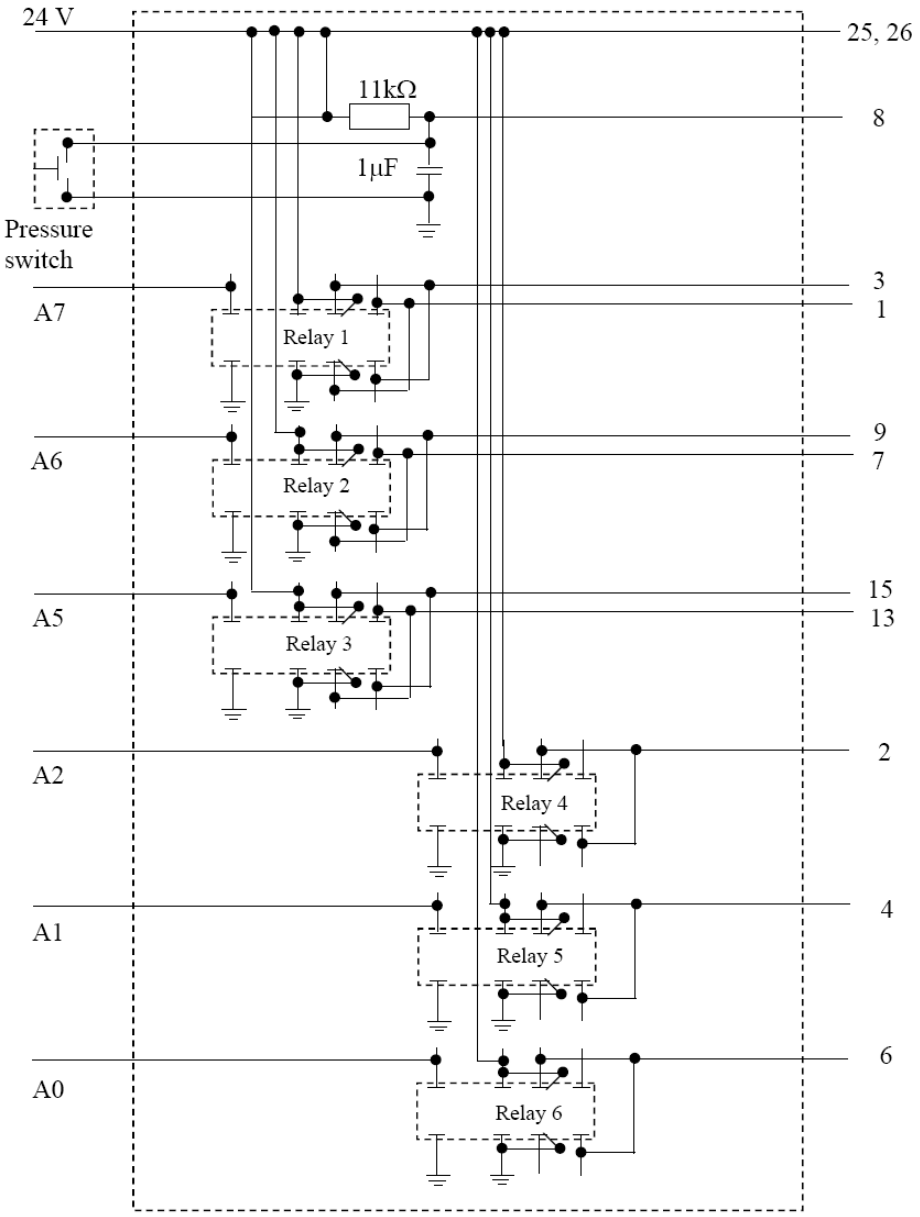

B-5: Circuitry for the relay module and hydrogen interlock

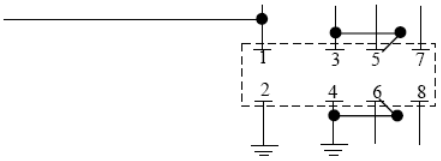

NTE R40-1102-5 relay module has 8 terminals. Digital input is applied on pin 1 and 2. Signal for output (24V DC as in the experiment) is applied on pin 3 and 4. Output is switched from pin 5 and 6 to pin 7 and 8 when the input signal changes from "low" to "high". The relay module is employed to use a computer digital I/O signal (5V) to switch on and off a DC 24V output, which in turn is applied on the control line of a station valve.

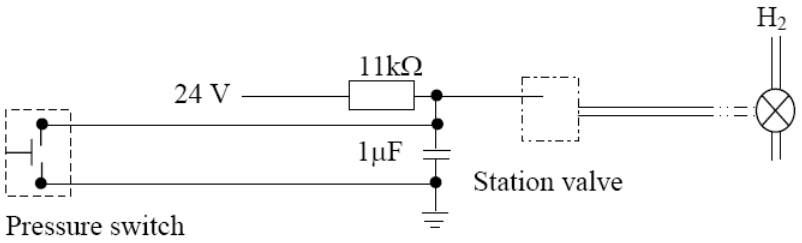

Independent hydrogen interlock is to prevent hydrogen from being mistakenly flowed into the plasma chamber when the chamber is vented. It is made up of a pressure switch, a pneumatic single way valve on the hydrogen gas line, an 11kΩ resistor and a 1μF capacitor. The pressure switch is normally open at pressure higher than the threshold pressure which is adjustable and set at 30 torr in the experiment. The circuitry is designed to send a 24V DC signal to the station valve when the plasma chamber is at high pressure. (Note: the station valve operates with the differential voltage between the control line and the common 24V DC power line. So a "high" signal, 24V on the control line actually closes the station valve.)

Bibliography

[1] G. Moore, Electronics, Vol.38, No. 8, April (1965)
[2] M. Bohr, Intel Developer Forum, Aug. (2005)
[3] International Technology Roadmap for Semiconductors, 2004 update, SEMATECH (2004)
[4] B.J. Lin, Session 3.1, Int. Elect. Dev. Meet. (2005)
[5] M. Okuno *et al.*, Session 3.2, Int. Elect. Dev. Meet. (2005)
[6] W-H. Lee *et al.*, Session 3.3, Int. Elect. Dev. Meet. (2005)
[7] C.-H. Jan *et al.*, Session 3.4, Int. Elect. Dev. Meet. (2005)
[8] Chow, M. Melanie, Cronin, E. John, Guthrie, L. William, Kaanta, W. Carter, Luther, Barbara, Patrick, J. William, Perry, A. Kathleen, Standley, and L. Charles, US patent 4,789,648 (1988)
[9] J. Paraszczak, D. Edelstein, S. Cohen, E. Babich, and J. Hummel, p261, Int. Elect. Dev. Meet. Tech. Dig. (1993)
[10] J. Ida, Y. Yoshimaru, A. Ohtomo, K. Shimokawa, A. Kita and M. Ino, p59, Proc. Symp. VLSI Technol. (1994)
[11] S.P. Jeng, M.C. Chang, T. Kroger, P. McAnally, and R.H. Havemann, p73-74, Dig. Tech. papers, Symp. on VLSI Technology (1994)
[12] M.A. Fury, Vol. 260, p703, Mat. Res. Soc. Symp. Proc. (1992)
[13] P. Singer, Vol. 17, No. 13, p52-4, 56, Semi. Int. (1994)
[14] J. Torres, Vol. 91, p112-123, Appl. Surf. Sci. (1995)
[15] M. Bohr, p241-244, Int. Elect. Dev. Meet. Tech. Dig. (1995)
[16] W.C. Elmore, Vol. 19, p55-63, J. Appl. Phys. (1948)
[17] D.A.B. Miller, Vol. 88, No. 6, p728-749, Proc. IEEE, June (2000)
[18] J.A.Davis, R. Venkatesan, A. Kaloyeros, M. Beylansky, S.J. Souri, K. Banerjee, K.C. Saraswat, A. Rahman, R. Reif and J.D. Meindl, Vol. 89, No. 3, p305-324, Proc. IEEE, March (2001)
[19] J.N. Sun, D.W. Gidley, T.L. Dull, W.E. Frieze, A.F.Yee, E.T. Ryan, S. Lin and J. Wetzel, Vol. 89, No. 9, p5138-5144, J. Appl. Phys., May (2001)
[20] M. Tada, H. Ohtake, J. Kawahara and Y. Hayashi, Vol. 51, No. 11, p1867-1876, IEEE Trans. Elect. Dev. (2004)
[21] Z. Chen, K. Prasad, N. Jiang, N. Babu, S. Balakumar and C.Y. Li, p478-482, Proc. 43rd Int. Reliab. Phys. Symp. (2005)
[22] Z. Tokei, J. Van Aelst, C. Waldfried, O. Escorcia, P. Roussel, O. Richard, Y. Travaly, G.P. Beyer and K. Maex, p495-500, Proc. 43rd Int. Reliab. Phys. Symp. (2005)
[23] J.F. Guillaumond, L. Arnaud, C. Guedj, W.F.A. Besling, G. Reimbold, M. Dupeux, and J. Torres, p660-661, Proc. 43rd Int. Reliab. Phys. Symp. (2005)
[24] C.-C. Yang *et al*., p213-220, Adv. Metal. Conf. 2004 (2005)
[25] X. Lu, J.W. Pyun, B. Li, N. Henis, K. Neuman, K. Pfeifer, and P.S. Ho, p33-35, Proc. of IEEE 2005 Int. Inter. Technol. Conf. (2005)
[26] J.W. Pyun, X. Lu, J. Chung, S. Yoon, P.S. Ho, N. Henis, K. Neuman, L. Smith and K. Pfeifer, Vol. 87, No. 6, p61907-1-3, Aug. (2005)

[27] T.N. Theis, p1-11, Proc. Symp. on Electrochemical Processing in ULSI Fabrication and Interconnect and Contact Metallization: Materials, Processes and Reliability (1999)
[28] R.D. Mikkola, Q.-T. Jiang, R. Carpio, and B. Carpenter, p235-241, Vol. 562, Polycrystalline Metal and Magnetic Thin Films, Mat. Res. Soc. Symp. Proc. (1999)
[29] R.J. Gutmann, T.P. Chow, W.N. Grill, A.E. Kaloyeros, W.A. Lanford, and S.P. Murarka, p41-57, Advanced Metallization for Devices and Circuits—Science, Technology and Manufacturability Symposium, Mat. Res. Soc. (1994)
[30] J. Li, S. Hong, S. Russell, and J.W. Mayer, p305-320, Crucial Issues in Semiconductor Materials and Processing Technologies, Proc. NATO Adv. Study Inst. On Semi. Mat. Proc. Technol. (1992)
[31] S.Q. Wang, Vol. 19, No. 8, p30-40, Mat. Res. Soc. Bulletin, Aug.(1994)
[32] C.-K. Hu, M.B. Small and P.S. Ho, p171-176, Materials in Microelectronics II Symposium, Mat. Res. Soc. (1992)
[33] C.-K. Hu, S. Chang, M.B. Small and J.E. Lewis, p181-187, Proc. VLSI Mutlilevel Interconnect Conf. (1986)
[34] K. Holloway and P.M. Fryer, Appl. Phys. Lett., Vol. 57, No. 17, p1737-1739, Oct. (1990)
[35] Cabral Jr., Cyril, Dehaven, P. William, D. Edelstein, Klaus, D. Peter, Pollard III, J. Manley, Stanis, L. Carol, Uzoh, and C. Emeka, US patent 6,291,885 (1997)
[36] E. Kolawa, J.S. Chen, J.S. Reid, P.J. Pokela and M.-A. Nicolet, J. Appl. Phys., Vol. 70, No.3, p1369-1373, Aug. (1991)
[37] K. Holloway, P.M. Fryer, C. Cabral Jr., J.M.E. Harper, P.J. Bailey, and K.H. Kelleher, J. Appl. Phys., Vol. 71, No. 11, p5433-5444, June (1992)
[38] P. Catania, J.P. Doyle and J.J. Cuomo, J. Vac. Sci. Technol. A, Vol. 10, No. 5, p3318-3321, Sept-Oct (1992)
[39] J.O. Olowolafe, C.J. Mogab, R.B. Gregory and M. Kottke, J. Appl. Phys., Vol. 72, No.9, p4099-4103, Nov. (1992)
[40] D. Edelstein, C. Uzoh, C. Cabral Jr., P. DeHaven, P. Buchwalter, A. Simon, E. Cooney, S. Malhotra, D. Klaus, H. Rathore, B. Agarwala, and D. Nguyen, p9-11, Proc. 2001 Int. Inter. Tech. Conf. (2001)
[41] S.S. Wong, C. Ryu, H. Lee and K.-W. Kwon, p75-81, Advanced Interconnects and Contact Materials and Processes for Future Integrated Circuits Symposium, Mat. Res. Soc. (1998)
[42] L.G. Feinstein and R.D. Huttermann, Vol. 16, No. 2, p129-145, Thin Solid Films, May (1973)
[43] N. Schwartz and E.D. Feit, Vol. 124, No. 1, p123-131, J. Electrochem. Soc., Jan. (1977)
[44] R. Petrovic, T. Nenadovic, N. Kraljevic, and T. Dimitrijevic, Vol. 57, No.2, p333-336, Thin Solid Films, Mar. (1979)
[45] Colgan, G. Evan, Fryer, and M. Peter, US patent 5,281,485
[46] S. Johnston, D. Feller, V. Dubin, and P. Moon, Adv. Metal. Conf. 2003, p335-340, Mat. Res. Soc. (2004)
[47] S.G. Malhotra, D. Canaperi, S. Chiras, L. Deligianni, G. Johnson, M. Krishnan, M. Lane, F. McFeely, C. Murray, S. Ponoth, A. Simon, T. Spooner, P. Vereecken, and J. Yurkas, Adv. Metal. Conf. 2004, p525-530, Mat. Res. Soc. (2005)

[48] Z.-W. Sun, R.-R. He, and J.O. Dukovic, Adv. Metal. Conf. 2004, p531-537, Mat. Res. Soc. (2005)
[49] S. Johnston, R. Chebiam, H. Simka, P. Fischer, and V. Dubin, Adv. Metal. Conf. 2004, p539-544, Mat. Res. Soc. (2005)
[50] H. Kim, T. Koseki, T. Ohta, Y. Kojima, H. Sato and Y. Shimogaki, J. Electrochem. Soc., Vol. 152, No. 8, pG594-600, Aug. (2005)
[51] T.N. Arunagiri, Y. Zhang, O. Chyan, M. El-Bouanani, M.J. Kim, K.H. Chen, C.T. Wu and L.C. Chen, Appl. Phys. Lett., Vol. 86, No. 8, p83104-1-3, Feb. (2005)
[52] S.D. Ruebush, R.E. Couch, S. Thevuthasan, and C.S. Fadley, Surf. Sci., Vol. 421, p 205-236 (1999)
[53] T.H. Andersen and L. Bech, Surf. Rev. Lett., Vol. 9, No.2, p723-727 (2002)
[54] H. Wolter, K. Meinel, Ch. Ammer, K. Wandelt, and H. Neddermeyer, J. Phys.: Condens. Matter, Vol. 11, p19-37 (1999)
[55] O.-K. Kwon, S.-H. Kwon, H.-S. Park and S.-W. Kang, J. Electrochem. Soc., Vol. 151, No. 12, pC753-756 (2004)
[56] Y. Zhang, L. Huang, T.N. Arunagiri, O. Ojeda, S. Flores, O. Chyan and R.M. Wallace, Electrochem. Solid-state Lett., Vol. 7, No.9, pC107-C110 (2004)
[57] H.J. Barth, J. Bierner, H. Helneder, W. Robl, K. Schober, and M. Schneegans, Proc. SPIE, Vol. 3214, p2-12 (1997)
[58] F. Cerio, J. Drewery, E. Huang, and G. Reynolds, J. Vac. Sci. Technol. A, Vol. 16, No. 3, p1863-1867 (1998)
[59] S.M. Rossnagel, IBM J. Res. Dev., Vol. 43, No.1-2, p163-179, Jan-Mar. (1999)
[60] G. Alers, R.T. Rozbicki, G.J. Harm, S.K. Kailasam, G.W. Ray, and M. Danek, Proc. 2003 Int. Intercon. Technol. Conf., p27-29 (2003)
[61] K.-C. Park, I.-R. Kim, B.-S. Suh, S.-M. Choi, W.-S. Song, Y.-J. Wee, S.-G. Lee, J.-S. Chung, J.-H. Chung, S.-R. Hah, J.-H. Ahn, K.-T. Lee, H.-K. Kang, K.-P. Suh, Proc. 2003 Int. Intercon. Technol. Conf., p165-167 (2003)
[62] C.-C. Yang, Y. Wang, L. Clevenger, A. Simon, S. Greco, K. Chanda, T. Spooner, A. Cowley, and S. Fang, US patent 6,784,105 (2004)
[63] C.E. Uzoh, US patent 5,930,669
[64] C.-C. Yang, D. Edelstein, L. Clevenger, A. Cowley, J. Gill, K. Chanda, A. Simon, T. Dalton, B. Agarwala, E. Cooney III, D. Nguyen, T. Spooner, and A. Stamper, p135-137, Proc. 2005 Int. Inter. Tech. Conf. (2005)
[65] A.M. Shevyakov, G.N. Kuznetsova, V.B. Aleskovskii, Khim. Vysokotemp. Mater., Tr. Vses. Soveshch., 149-55 (1965)
[66] T. Suntola, US pat. 4,058,430 (1977)
[67] T. Suntola and M. Simpson, Atomic Layer Epitaxy, Chapman and Hall, NY (1990)
[68] T. Suntola, Appl. Surf. Sci., Vol. 100-101, p391-398, July (1996)
[69] B. Sang and M. Konagai, Conf. Rec. 25th IEEE Photovoltaic Specialist Conf, p1085-1088 (1996)
[70] J. Aarik, A. Aidla, and T. Uustare, Philosophical Magazine Lett., Vol. 73, No.3, p115-119, Mar. (1996)
[71] E.-L. Lakomaa, A. Root, and T. Suntola, Appl. Surf. Sci., Vol. 107, p107-115, Nov. (1996)

[72] J.-S. Min, Y.-W. Son, W.-G. Kang, and S.-W. Kang, Advanced Interconnects and Contact Materials and Processes for Future Integrated Circuits Symposium, p337-342, Mat. Res. Soc. (1998)
[73] J. Y. Sun, J.S. Kang, M.C. Paek and K.-S. Nam, J. Korean Phys. Soc., Vol. 33, suppl. Issue, pS170-S174, Nov. (1998)
[74] H.S. Nalwa (ed.), Handbook of thin film materials, Vol. 1: Deposition and processing of thin films, Academic Press, CA (2002)
[75] Y. Zhou, G. .Xu, T. Scherban, J. Leu, G. Kloster and C. Wu, Proc. Int. Conf. Char. Metro. ULSI Technol. (2003)
[76] M. Leskela and M. Ritala, Thin Solid Films, Vol. 409, p138-146 (2002)
[77] H. Kim, J. Vac. Sci. Technol. B, Vol. 21, No. 6, p2231-2261, Nov.-Dec. (2003)
[78] S.M. Rossnagel, A. Sherman, and F. Turner, J. Vac. Sci. Technol. B, Vol. 18, No.4, p2016-2020, July (2000)
[79] H. Kim, C. Cabral Jr., C. Lavoie, and S.M. Rossnagel, Silicon Materials-Processing, Characterization and Reliability Symposium, Mat. Res. Soc. Proc. Vol. 716, p 407-412 (2002)
[80] P. Alen, M. Juppo, M. Ritala, T. Sajavaara, J. Keinonen, and M. Leskela, J. Electrochem. Soc., Vol. 148, No. 10, p G566-571, Oct. (2001)
[81] A.M. Lemonds, J.M. White and J.G. Ekerdt, Surf. Sci., Vol. 538, No.3, p191-203, July (2003)
[82] A. M. Lemonds, Atomic layer deposition and properties of refractory transition metal-based copper diffusion barriers for ULSI interconnects, PhD dissertation, the University of Texas at Austin (2003)
[83] W. Besling, A. Satta, J. Schuhmacher, T. Abell, V. Sutcliffe, A. Hoyas, G. Beyer, D. Gravesteijn, and K. Maex, p288-291, Proc. Int. Interconn. Technol. Conf. (2002)
[84] J.-S. Park, H.-S. Park, and S.-W. Kang, J. Electrochem. Soc., Vol. 149, No. 1, pC28-C32 (2002)
[85] A. Furuya, N. Ohtsuka, K. Misawa and S. Ogawa, J. Appl. Phys., Vol. 98, No.9, p94902-1-6, Nov. (2005)
[86] S.M. Rossnagel and H. Kim, presentation at 2003 Am. Vac. Soc. Annual meeting, (2003)
[87] K.-I. Choi, B.-H. Kim, S.-W. Lee, and J.-M. Lee, Proc. IEEE Int. Interconn. Technol. Conf., p129-131 (2003)
[88] J.-W. Hong, K.-I. Choi, Y.-K. Lee,S.-G. Park, S.-W. Lee, J.-M. Lee, S.-B. Kang, G.-H. Choi, S.-T. Kim, U.-I. Chung, and J.-T. Moon, Proc. IEEE Int. Interconn. Technol. Conf., p9-11 (2004)
[89] C.B. Musgrave, presentation at NSF/SRC Engineering Research Center for Environmentally Benign Semiconductor Manufacturing (2003)
[90] N. Kumar, S. Chu, D.L. Diehl, T. Tanimoto, A. Ohkura, K. Maekawa, K. Mori, K. Kobayashi, and M. Yoneda, Adv. Metall. Conf. 2004, p 247-252, Mat. Res. Soc. (2005)
[91] D. Edelstein *et al*., IEEE Int. Reliability Physics Symp., p316-319 (2005)
[92] M. Juppo, M. Ritala, and M. Laskelä, J. Electrochem. Soc., Vol. 147, No. 9, p3377-3381 (2000)
[93] P. Alén, M. Juppo, M. Ritala, M. Laskelä, T. Sajavaara, J. Keinonen, J.C. Hooker, and J.W. Maes, J. Electrochem. Soc., Vol. 148, No.10, pG 566-571 (2001)

[94] P. Alén, M. Juppo, M. Ritala, T. Sajavaara, J. Keinonen, and M. Laskelä, J. Electrochem. Soc., Vol. 151, pG 523-527 (2004)
[95] P. Alén, Atomic Layer Deposition of TaN, NbN and MoN Films for Cu Metallization, PhD dissertation, University of Helsinki, Finland, June (2005)
[96] H. Kim, A.H. Kellock, and S. M. Rossnagel, J. Appl. Phys., Vol. 92, No. 12, p7080-7085, 2002
[97] C. Chaneliere, J.L. Autran, R.A.B. Devine, and B. Balland, Mat. Sci. Eng. R: Reports, Vol. R22, No. 6, p269-322, May (1998)
[98] D.-G. Park, K.-Y. Lim, H.-J. Cho, T.-H. Cha, J.-J. Kim, J.-K. Ko, I.-S. Yeo, and J.-W. Park, 2001 Symp. VLSI Technol., Dig. Tech. Papers, p65-66 (2001)
[99] S. Pidin, Y. Morisaki, Y. Sugita, T. Aoyama, K. Irino, T. Nakamura, and T. Sugii, 2002 Symp. VLSI Technol., Dig. Tech. Papers, p28-29 (2002)
[100] S.M. Rossnagel, R. Wisnieff, D. Edelstein, and T.S. Kuan, Session 4.4, Int. Elect. Dev. Meet. (2005)
[101] C.-K. Ryu, S.-B. Kim, S.-D. Kim and C.-T. Kim, p 343-347, Adv. Metal. Conf. 1999, Mat. Res. Soc. (2000)
[102] S. Ma, M. Dahimene, C. Bjorkman, H. Shan, and R. Ramanathan, 2000 5th Inter. Symp. Plasma Process-induced Damage, p113-116 (2000)
[103] N. Nakamura, K. Higashi, N. Matsunaga, H. Miyajima, S. Sato, and H. Shibata, 2002 7th Inter. Symp. Plasma Process-induced Damage, p162-165 (2002)
[104] T.J. Dalton, N. Fuller, C. Tweedie, D. Dunn, C. Labelle, S. Gates, M. Colburn, S.T. Chen, T. Lai, R. Dellaguardia, K. Petrarca, C. Dziobkowski, K. Kumar, and S. Siddiqui, Proc. IEEE Int. Interconn. Technol. Conf., p154-156 (2004)
[105] M.R. Baklanov, Q.T. Le, E. Kesters, F. Iacopi, J. van Aelst, H. Struyf, W. Boullart, S. Vanhaelemeersch, and K. Maex, Proc. IEEE Int. Interconn. Technol. Conf., p187-189 (2004)
[106] W. Chen, Q. Han, R. Most, C. Waldfried, O. Escorcia, and I. Berry, J. Electrochem. Soc., Vol. 151, No. 8, p F182-188 (2004)
[107] Y. Furukawa, R. Wolters, H. Roosen, J.H.M. Snijders, and R. Hoofman, Microelectronic Engineering, Vol. 76, No. 1-4, p 25-31, Oct. (2004)
[108] N. Kobayashi, presentation at SELETE Symposium 2004, May (2004)
[109] M.A. Worsley, S.F. Bent, S.M. Gates, N.C.M. Fuller, W. Volksen, M. Steen and T. Dalton, J. Vac. Sci. Technol. B, Vol. 23, No. 2, p395-405 Mar./Apr. (2005)
[110] K. Monnig, presentation at the Univ. of Texas at Austin (2004)
[111] N. Hata, C. Negoro, S. Takada, X. Xiao, K. Yamada and T. Kikkawa, Proc. IEEE Int. Interconn. Technol. Conf., p51-53 (2003)
[112] A.C. Diebold, Solid State Technol., Vol. 45, No.1, p48-50 Jan. (2001)
[113] J. Xu, J. Moxom, R. Suzuki, T. Ohdaira and A.P. Miller Jr., Proc. 3rd Int. Symp. Mat. Chem. Nuc. Environ., p118-126 (2003)
[114] E.T. Ogawa, J. Kim, G.S. Haase, H.C. Mogul and J.W. McPherson, Proc. 2003 IEEE Int. Reliab. Phys. Symp., p166-172 (2003)
[115] E.T. Ogawa, J. Kim, G.S. Haase, H.C. Mogul and J.W. McPherson, presentation at 2003 Tropical Research Conf. on Reliability, Oct. (2003)
[116] S.-Y. Kook and R.H. Dauskardt, J. Appl. Phys., Vol. 91, No. 3, p1293-1303, Feb. (2002)

[117] T.P. Ferguson and J. Qu, 2004 Proc. 54th Elect. Comp. Technol. Conf., Vol. 2, p1752-1758, June (2004)
[118] M.W. Lane, X.H. Liu and T.M. Shaw, IEEE Trans. Dev. Mat. Reliab., Vol. 4, No.2, p 142-147, June (2004)
[119] E.M. Zielinski, S.W. Russell, R.S. List, A.M. Wilson, C. Jin, K.J. Newton, J.P. Lu, T. Hurd, W.Y. Hsu, V. Cordasco, M. Gopikanth, V. Korthuis, W. Lee, G. Cerny, N.M. Russell, P.B. Smith, S. O'Brien, and R.H. Havemann, Int. Elect. Dev. Meet. Tech. Dig., p936-938 (1997)
[120] R.D. Miller, R. Beyers, K.R. Carter, R.F. Cook, M. Harbison, C.H. Hawker, J.L. Hedrick, V. Lee, E. Liniger, C. Nguyen, J. Remenar, M. Sherwood, M. Trollsas, W. Volksen and D.Y. Yoon, Mat. Res. Soc. Symp. Proc. Vol. 565, No.3 (1999)
[121] C.J. Hawker, J.L. Hedrick, R.D. Miller and W. Volksen, Mat. Res. Soc. Symp. Proc., Vol. 25, No.54 (2000)
[122] M. Ikeda, J. Nakahira, Y. Iba, H. Kitada, N. Nishikawa, M. Miyajima, S. Fukuyama, N. Shimizu, K, Ikeda, T. Ohba, I. Sugiura, K. Suzuki, Y. Nakata, S. Doi, N. Awaji, and E. Yano, Proc. IEEE 2003 Int. Interconn. Technol. Conf., p71-73 (2003)
[123] J. Nakahira, I. Sugiura, Y. Nakata, N. Misawa, Y. Iba, A. Hasegawa, H. Kitada, F. Sugimoto, N. Nishikawa, Y. Mizushima, M. Oshima, H. Ehara, N. Shimizu, M. Miyajima, S. Fukuyama, H. Matsuyama, M. Minamizawa, E. Yano, and T. Ohba, Adv. Metall. Conf. 2003, p 477-482 (2003)
[124] Y. Hayashi, F. Itoh, Y. Harada, T. Takeuchi, M. Tada, M. Tagami, H. Ohtake, K. Hijioka, S. Saito, T. Onodera, D. Hara and K. Tokudome, Proc. IEEE 2004 Int. Interconn. Technol. Conf., p225-227 (2004)
[125] T. Mourier, V. Jousseaume, F. Fusalba, C. Lecornec, P. Maury, G. Passemard, P.H. Haumesser, S. Maitrejean, M. Cordeau, R. Pantel, F. Pierre, M. Fayolle, and H. Feldis, Proc. IEEE 2003 Int. Interconn. Technol. Conf., p245-247 (2003)
[126] E.T. Ryan, M. Freeman, L. Svedberg, J.J. Lee, T. Guenther, J. Connor, K. Yu, J. Sun, and D.W. Gidley, Materials, Technology and Reliability for Advanced Interconnects and Low-k Dielectrics, Mat. Res. Soc. Vol. 766, p89-94 (2003)
[127] A. Furuya, E. Soda, Y. Yoneda, T. Yoshie, H. Okamura, M. Shimada, M. Ohtsuka, S. Ogawa, Proc. IEEE 2004 Int. Interconn. Technol. Conf., p39-41 (2004)
[128] J. W. Rabalais (editor), Low Energy Ion-Surface Interactions, Wiley Series in Ion Chemistry and Physics, John Wiley & Sons (1994)
[129] S. Vallon, A. Hofrichter, L. Guyot, B. Drevillon, J.E. Klemberg-Sapieha, L. Martinu, F. Poncin-Epaillard, Thin Solid Films, Vol. 290-291, p68-73, (1996)
[129] P. Abramowitz, Forming Nitrides with Low-energy Ions on Low-k Dielectrics, Ph.D. Dissertation, the University of Texas at Austin (2000)
[130] K.J. Kim, N.-E. Lee, M.C. Kim, J.-H. Boo, Thin Solid Films, Vol. 398-399, p 657-662 (2001)
[131] www.semiconductorglossary.com
[132] D. Nguyen, L. Forester, J. Kennedy, R. Burke, and C.-C. Cheng, 1996 Proc. 13th Int. VLSI Multilevel Inteconn. Conf., p148 (1996)
[133] C.K. Ryu, S.-B. Kim, S.-D. Kim and C.-T. Kim, Adv. Metall. Conf. 1999, p343-347, Mat. Res. Soc (2000)
[134] A.E. Braun, Semiconductor International, Oct. (1999)

[135] D. Shamiryan, M.R. Baklanov, S. Vanhaelemeersch, and K. Maex, J. Vac. Sci. Technol. B Vol. 20, No. 5, p1923-1928, Sep/Oct (2002)
[136] R. Sonnemans, C. Waldfried, A. Rastegar and M. Broekaart, 14th Ann. IEEE/SEMI Adv. Semi. Manu. Conf. Workshop 2003, p36-40 (2003)
[137] S. Satyanarayana, R. McGowan, B. White and S.D. Hosali, Semiconductor International, June (2005)
[138] Y.S.Mor, T.C.Chang, P.T.Liu, T.M.Tsai, C.W.Chen, S.T.Yan, C.J.Chu, W.F.Wu, F.M.Pan, W.Lur and S.M.Sze, J. Vac. Sci. Technol. B20(4), July/Aug (2002)
[139] S. Borthakur, S. Satyanarana, A. Knorr and P.S. Ho, Materials, Technology and Reliability of Advanced Interconnects-2005 symposium, Mat. Res. Soc. Proc. Vol. 863, p 195-200 (2005)
[140] B. Xie and A.J. Muscat, F 1.4, Materials, Technology and Reliability of Advanced Interconnects symposium, Mat. Res. Soc. Spring meeting (2004)
[141] B. Xie and A.J. Muscat, presentation at Materials, Technology and Reliability of Advanced Interconnects-2005 symposium, Mat. Res. Soc. Spring meeting (2005)
[142] J. Liu, J. Bao, M. Scharnberg and P. S. Ho, F2.6, Materials, Technology and Reliability of Advanced Interconnects symposium, Mat. Res. Soc. Spring Meeting (2004)
[143] LabVIEW 7.0, National Instruments (2003)
[144] http://www.oxsci.com/pages/products/micro_plasma/index.htm
[145] F. Glocking, The Chemistry of Germanium, p7, Academic Press, London (1969)
[146] Y.V. Bokshits, L.T. Potapenko, S.V. Serezhkina, and G.P. Shevchenko, abstract in the International Conference on Sol-Gel Materials, Poland, June (2001)
[147] US patent application #20050215034 (2005)
[148] W.P. Bai, N. Lu, J. Liu, A. Ramirez, D.L. Kwong, D. Wristers, A. Ritenour, L. Lee and D. Antoniadis, 2003 Symp. on VLSI Technol., Dig. Tech. Papers, p121-122 (2003)
[149] C.J. Powell and A. Jablonski, NIST Electron Effective Attenuation Length Database, ver 1.0 (2001)
[150] Materials Safety Data Sheet, ATMI (2003)
[151] D. Briggs and M. Seah, Practical Surface Analysis, Wiley, New York (1990)
[152] C.J. Powell and A. Jablonski, NIST electron inelastic-mean-free-path database, ver. 1.1 (2000)
[153] J. Liu, Master's Report, the University of Texas at Austin (2002)
[154] S.J. Martin, J.P. Godschalx, M.E. Mills, E.O. Shaffer II and P.H. Townsend, Adv. Mater., Vol. 12, No.23, p1769 (2000)
[155] D.D. Hawn, Surface Science Spectra, Vol. 9, p1-5 (2002)
[156] C.D. Wagner, A.V. Naumkin, A. Kraut-Vass, J.W. Allison, C.J. Powell, and J.R. Rumble Jr., NIST X-ray Photoelectron Spectroscopy Database, ver. 3.4 (2003)
[157] D.A. Shirley, Physical Review B, Vol. 5, p4709 (1972)
[158] http://www.chemicalforums.com/index.php?op=articles;id=13
[159] M.J. Berger, J.H. Hubbell, S.M. Seltzer, J. Chang, J.S. Coursey, R. Sukumar, and D.S. Zucker, NIST XCOM: Photon Cross Sections Database (1998)
[160] PeakFit™, ver. 4.05, AISN Software Inc., now Systat Software Inc., (1991)
[161] N. Fairley, CasaXPS, ver. 2.2.86, (2004)
[162] J. Aarik, A. Aidla, T. Uustare, M. Ritala, and M. Leskela, Appl. Surf. Sci., Vol. 161, No. 3-4, p385-395 (2000)
[163] T.T. Van and J.P. Chang, Appl. Surf. Sci., Vol. 246, No. 1-3, p250-261 (2005)

[164] S.M. George, F.H. Fabreguette, Z.A. Sechrist, and J.W. Elam, Thin Solid Films, Vol. 488, No. 1-2, p103-110 (2005)
[165] M. Scharnberg, Master's thesis, the University of Texas at Austin, Aug. (2003)
[166] J. Liu and M. Scharnberg, poster at SRC CAIST review of task 1021.001, Oct. (2003)
[167] M.P. Seah and S. J. Spencer, Surf. Interface Anal., Vol. 33, p640-652 (2002)
[168] M.P. Seah and W.A. Dench, Surf. Interface Anal., Vol. 1, No.1, p2-11 (1979)
[169] J. G. Ekerdt, Y. Sun, J.M. White, D.Gay, J. Shin, and Q. Wang, presentation at 2005 ULSI Metrology Conference, (2005)
[170] http://www.kruss.info/index.php?content=http%3A//www.kruss.info/techniques/contact_angle_e.html
[171] http://www.appliedmaterials.com/products/producer_black_diamond.html?menuID=1_3_3
[172] http://www.dow.com/silk/index.htm
[173] R. J. Strittmatter, J. L. Hahnfeld, H. C. Silvis, T.M. Stokich, J.D. Perry, K.B. Quellette, Q.J. Niu, J.P. Godschalx, T.H. Kalantar, E. Mubarekyan, R.E. Hefner, Jr., J.Y. Lyonds, J.M. Dominowski and G.R. Buske, Mat. Technolo. Proc. Adv. Inter. Low-k Diel., Mat. Res. Soc., Symp. 2003, Vol. 766, p265-272 (2003)
[174] R. J. Strittmatter, Q. J. Niu, J. Waeterloos, G. F. Meyers, C. E. Mohler, B. G. Landes, J. W. Lyons, J.-H. Im, J. J. Curphy, J. L. Hahnfeld, and H. C. Silvis, 2003 Adv. Metall. Conf., p159-163, Mat. Res. Soc. (2004)
[175] M.P. Seah and S.J. Spencer, J. Vac. Sci. Technol., **A 21**(2), p345-352 (2003)
[176] A. Satta, A. Vantomme, J. Schuhmacher, C.M. Whelan, V. Sutcliffe, and K. Maex, Appl. Phys. Lett., Vol. 84, No. 22, p4571-4573 (2004)
[177] http://www.cem.msu.edu/~reusch/VirtTxtJml/funcrx1.htm
[178] P.L.Timms, Proc. Royal Soc. London, Series A **1** 396 (1984)
[179] R. Haight, R.C. White, B.D. Silverman and P.S. Ho, J. Vac. Sci. Technol. A **6**(4) p2188 (1988)
[180] D.F. Shriver, P.W. Atkins, and C.H. Langford, *Inorganic Chemistry*, W.H. Freeman and Company, New York (1990)
[181] P. Abramowitz, J. Liu, M. Kiene, P. S. Ho and J. Im, Metallization of Polymers 2, (ed. E. Sacher), Kluwer Academic/Plenum Publishers, New York, p141-51 (2002)
[182] C.J. Uchibori and T. Kimura, J. Vac. Sci. Technol. B **21**(4), p1513-15 (2003)
[183] J.L. Jordan, C.A. Kovac, J.F. Morar and R.A. Pollak, Phys. Rev. B 36 (3), p1369-1377 (1987)
[184] P. Abramowitz, M. Kiene, P. S. Ho, J. Vac. Sci. Technol. A **18**(5), p.2254-61(2000)
[185] P. Abramowitz, M. Kiene, P. S. Ho, Appl. Phys. Lett., Vol.74, No.22, p3293-5 (1999)
[186] P.N. Baker, Thin Solid Films, Vol. 14, p3-25 (1972)
[187] M. Stavrev, D. Fischer, C. Wenzel, K. Drescher, N. Mattern, Thin Solid Films Vol. 307, p79-88 (1997)
[188] G.S. Chen, P.Y. Lee, S.T. Chen, Thin Solid Films, Vol. 353, p.264-273 (1999)
[189] X. Sun, E. Kolawa, J.-S. Chen, J.S. Reid and M.-A. Nicolet, Thin Solid Films, Vol. 236, p347-351 (1993)
[190] C. Argile and G.E. Rhead, Surf. Sci. Report, Vol. 10, p 277 (1989)

[191] E. Bauer, Z. Krist., Vol. 110, p372 (1958)
[192] U. Diebold, J. M. Pan, T. E. Madey, Phys. Rev. B, Vol. 47, No. 7, p3868-3876 (1993)
[193] K.H. Ernst, A. Ludviksson, R. Zhang, J. Yoshihara, and C.T. Campbell, Phys. Rev. B, Vol. 47, no. 20, p13782-13796 (1993)
[194] K. Shepherd, J. Kelber, Appl. Surf. Sci., Vol. 151, p 287-298 (1999)
[195] J. Liu, M. Scharnberg, J. Bao, P.S. Ho, and J. Im, J. Vac. Sci. Technol., B **23**(4), p1422-1427 (2005)
[196] J. Schuhmacher *et al.*, presentation at 51st AVS annual meeting (2004)
[197] J.S. Corneille, P.J. Chen, C.M. Truong, W.S. Oh and D.W. Goodman, J. Vac. Sci. Technol. A, Vol. 13, No. 3, p1116-1120, May/June (1995)
[198] B.S. Lim, A.R. Rahtu, J.-S. Park and R.G. Gordon, Inorg. Chem., Vol. 42, p7951-7958 (2003)
[199] F. Basuli, U.J. Kilgore, D. Brown, J.C. Huffman, and D.J. Mindiola, Organometallics, Vol. 23, p6166-6175 (2004)
[200] A. Satta, M. Baklanov, O. Richard, A. Vantomme, H. Bebder, T. Conard, G. Beyer, K. Maex, W.M. Li, K.E. Elers, and S. Haukka, Micro. Eng., Vol. 60, p59 (2002)
[201] D.R. Lide (editor-in-chief), CRC Handbook of Chemistry and Physics, 84th edition (2003-2004)
[202] Http://chemviz.ncsa.uiuc.edu/content/doc-resources-bond.html
[203] I. Barin and O. Knacke, Thermochemical Data of Pure Substances, third edition, Weinheim, Germany (1995)
[204] I. Barin, O. Knacke and O. Kubaschewski, The thermochemical properties of inorganic substances, supplement, Springer-Verlag, Germany (1977)
[205] J. Bao, J. Liu, H. Shi, W. Kim and P.S. Ho, presentation at Techon Meeting (2005)
[206] R. Sen, R. Sumathy and C.N.R.Rao, THEOCHEM, vol. 361, 211-16 (1996)
[207] D.O. Hayward and B.M.W. Trapnell, Chemisorption, 2nd edition (1964)
[208] J. Liu, J. Bao, W. Kim, H. Shi and P.S. Ho, SRC deliverable for task 1021.001 (2005)
[209] M. Tada, H. Ohtake, M. Narihiro, F. Ito, T. Taiji, M. Tohara, K. Motoyama, Y. Kasama, M. Tagami, M. Abe, T. Takeuchi, K. Arai, S. Saito, N. Furutake, T. Onodera, J. Kawahara, K. Kinoshita, N. Hata, T. Kikkawa, Y. Tsuchiya, K. Fujii, N. Oda, M. Sekine, and Y. Hayashi, 2005 Symp. VLSI Technol. (2005)
[210] S. Arkalgud, presentation at Sematech Symp. Japan, Mar. (2006)
[211] J.-S. Park, M.-J. Lee, C.-S. Lee and S.-W. Kang, Electrochem. Solid-state Lett., Vol. 4, No. 4, pC17-C19 (2001)
[212] J.W. Hong, K.I. Choi, Y.K. Lee, S.G. Park, S.W. Lee, J.M. Lee, S.B. Kang, G.H. Choi, S.T. Kim, U.-I. Chung, and J.T. Moon, Proc. IEEE 2004 Int. Interconn. Technol. Conf., p7-9 (2004)
[213] H. Kim, C. Lavoie, M. Copel, V. Narayanan, D.-G. Park, and S.M. Rossnagel, J. Appl. Phys., Vol. 95, No. 10, p5848-5855 (2004)
[214] H. Wiesmann, US patent 4,237,150
[215] H. Wiesmann, A.K. Ghosh, T. McMahon and M. Strongin, J. Appl. Phys., Vol. 50, No. 5, p3752-3754 (1979)
[216] H. Matsumura, H. Umemoto, and A. Masuda, J. Non-crystalline Solids, Vol. 338-340, p19-26 (2004)

[217] A. Shermann, US patent 5,916,365
[218] F. Greer, D. Fraser, J.W. Coburn, and D.B. Graves, J. Vac. Sci. Technol. A, Vol. 21, No. 1, p96-105 (2003)
[219] C. Cabral Jr., P. Dehaven, D. Edelstein, D. Klaus, J. Pollard III, C. Stanis, and C. Uzoh, US patent 6,437,440
[220] K. Hieber, Thin Solid Films, Vol. 24, p157 (1974)
[221] X. Chen, H.L. Frisch, A.E. Kaloyeros, and B. Arkles, J. Vac. Sci. Technol. B, Vol. 16, No. 5, p2887-2890 (1998)
[222] H. Kim and S.M. Rossnagel, Thin Solid Films, Vol. 441, p311-316 (2003)
[223] http://www.registech.com/gc/silylation.html
[224] W. M. Moreau, Semiconductor Lithography , Plenum, New York (1988)
[225] N. Porfiris, J. Newby, A.M. Gundlach, R. Pethrick, S. Affrissman, and A. Tannahill, Proc. 2nd Int. Symp. Ultra-clean Processing Silicon Surf., p335-338 (1994)
[226] J. Bauer, G. Drescher and M. Illig, J. Vac. Sci. Technol. B, Vol. 14, No. 4, p2485-2492 (1996)
[227] W. Chen, Q. Han, R. Most, C. Waldfried, O. Escorcia, and I. Berry, J. Electrochem. Soc., Vol. 151, No. 8, pF182-188 (2004)
[228] T. Abell, D. Shamiryan, J. Schuhmacher, W. Besling, V. Sutcliffe, and K. Maex, Proc. Adv. Metal. Conf., p717, Mat. Res. Soc. (2002)
[229] H.J. Lee, E.K. Lin, W.L. Wu, B.M. Fanaconi, J.K. Lan, Y.L. Cheng, H.C. Liou, Y.L. Wang, M.S. Feng, and C.G. Chao, J. Electrochem. Soc., Vol. 148, No. 10, pF195-F199 (2001)
[230] T. Furusawa, D. Ryusaki, R. Yoneyama, Y. Homma, and K. Hinode, Electrochem. Solid State Lett. Vol. 4, No. 3, pG31-G34 (2001)
[231] T. Abell, Y. Zhou, Q.T. Le, D. Shamiryan, M. Moinpour, and G. Kloster, presentation at Sematech Ultra-low k Workshp, Burlingame, CA (2002)
[232] N. Kobayashi, presentation at Semi. Leading Edge Technol. Symp. 2004, May (2004)
[233] O. Louveau, C. Bourlot, A. Marfoure, I. Kalinovski, J. Su, G. Hills, and D. Louis, Microelectronic Engineering, Vol. 73-74, p351-356 (2004)
[234] K. Maex, M.R. Baklanov, D. Shamiryan, F. Iacopi, S.H. Brongersma, and Z.S. Yanovitskaya, J. Appl. Phys., Vol. 93, No. 11, p8793-8841 (2002)
[235] M. Moinpour and M.D. Goodner, presentation at 10th Annual Review of SRC/NSF Eng. Res. Cen. for Enviromentally Benign Semiconductor Manufacturing, Feb. (2006)
[236] T. Abell and K. Maex, Microelectronic Engineering, Vol. 76, p16-19 (2004)
[237] D.W. Sindorf and G.E. Maciel, J. Am. Chem. Soc., Vol. 105, No. 12, p3767-3776 (1980)
[238] A. Grill and D.A. Neumayer, J. Appl. Phys., Vol. 94, No. 10, p6697-6707 (2003)
[239] G. Socrates, Infrared and Raman characteristic group frequencies : tables and charts, 3rd edition, Wiley, New York (2001)
[240] A. Mckerrow, presentation at the Univ. Texas at Austin (2004)
[241] J. Liu, D. Gan, C. Hu, M. Kiene, and P.S. Ho, Appl. Phys. Lett., Vol. 81 No. 22, p4180-82, Nov. (2002)
[242] C. Leroux, J. Mitard, G. Ghibaudo, X. Garros, G. Reimbold, B. Guillaumot, and F. Martin, presentation at IEEE Intl. Electron Devices Meeting Tech. Digest (2004)

[243] T. Matsuki, Y. Akasaka, K. Hayashi, M. Noguchi, K. Yamashita, H. Syoji, K. Torii, N. Kasai, and T. Arikado, Integration of Advanced Micro- and Nanoelectronic Devices, Mat. Res. Soc. Proc., Vol. 811, p87-92, D3.13.1-6 (2004)
[244] C.D. Young, presentation at IEEE Elect. Dev. Soc. Meeting, March (2006)
[245] R. A. B. Devine, J. W. Tringe, and J. R. Chavez, IEEE Trans. Nuc. Sci., Vol. 49, No. 6, p2729-2732 (2002)
[246] C.J. Park, K.H. Cho, W.-C. Yang, H.Y. Cho, S.-H. Choi, R.G. Elliman, J.H. Han, and C. Kim, Appl. Phys. Lett., Vol. 88, No. 7, p71916-1-3 (2006)

Vita

Junjun Liu was born in Yidu county, Hubei province of China on March 28, 1971, the second child to Changhai Liu and Linian Shen. He received his Bachelor of Science in Physics in 1992 and Bachelor of Arts in the Oriental Studies in 1994 from Peking University, China.

From 1994 to 1998, he was employed as an economic researcher at the Chinese Academy for International Trade and Economic Cooperation, a research subsidiary of the Ministry of Commerce.

In 1998, he was admitted to the University of Virginia as a graduate student in the physics department. In June 1999, he came to the University of Texas at Austin to be enrolled in the Materials Science and Engineering program. He was awarded the degree of Master of Science in Engineering in May 2002 by the University of Texas at Austin.

Permanent address: Rm. 301 Bldg. 2, Cheng Chang Yi Yuan
28 Sheng Li Si Lu
Yichang, Hubei, 443000
The People's Republic of China

This dissertation was typed by the author.